An Engineering Study of Solid-liquid Suspension in Shaken and Stirred Bioreactors

Ehsan Esbati

Department of Biochemical Engineering

University College London

A thesis submitted for the degree of

Doctor of Philosophy

June 2013

I, Ehsan Esbati confirm that the work presented in this thesis is my own. Where information has been derived from other sources, I confirm that this has been indicated in the thesis.

_____

To my family ...

... and to those ordinary men and women who have lost their lives in pursuit of freedom and justice in Iran and the rest of Middle East.

Acknowledgements

I would like to acknowledge first and foremost my supervisor, Prof. Gary J. Lye, without whose help, inspiration and patience I would not have been able to bring this project to completion. I was also able to draw on the experience and knowledge offered in advice by Dr. Martina Micheletti during the course of this project. I would also like to express my gratitude to Prof. Ian Eames for his willing help whenever my limited knowledge of fundamental fluid mechanics failed me. Last but not least, I would like to mention my peers and colleagues, past and present, in Mechanical Engineering and Biochemical Engineering Departments and across the wider student community in University College London for eight fun and stimulating years.

Abstract

Using shaken microwell and stirred miniature bioreactors in early stage bioprocess development requires understanding such devices from an engineering perspective. One particular area which has not to this date been fully explored is the suspension of solid particles in multi-phase operations in such devices. In order to broaden our understanding of this phenomena, a novel correlation is described for predicting the minimum shaking frequency required to suspend at least 90% of solid particles ($0.81\ gml^{-1} < \rho_p < 1.33\ gml^{-1}$) present in a bioprocess involving shaken microwell operations. It was found that predictions made by this correlation are in good general agreement with empirical data with an uncertainty figure of just $\pm 17\%$. Suitability of Zwietering's correlation for predicting the minimum stirring frequency required to suspend solid particles in a miniature and a laboratory scale stirred tank was examined by comparing its predictions to empirical data. It was found that the correlation overestimates the required agitation rate, sometimes by as much as $\approx$ 70%, for the miniature bioreator. Flow inside the two stirred tank bioreactors were also numerically simulated and the results found to be in general agreement with the empirical data.

The influence of suspension quality on immobilised enzyme biocatalysis was studied for two different enzymes: Transketolase and Protex $6L^2$. The results confirmed that poor suspension can corrupt immobilised enzyme reaction kinetics determination and make it appear lower by $\approx 200\%$.

In order to examine the possibility of scale translation between miniature and laboratory scale bioreactors, engineering characterisation of the miniature turbine impeller returned a Power Number of 3.5, while the laboratory turbine impeller returned a Power Number of 5.7, based on experimental power consumption measurements. Constant power per unit volume was chosen for scale-up criteria. Ethyl-(S)-lactate was hydrolysed using immobilised Protex $6L^2$ at a constant P/V value of $0.74\ kWm^{-3}$ at miniature and laboratory scales and returned an average initial rates of $576\pm30\ \mu molg^{-1}min^{-1}$ and $702\pm27\ \mu molg^{-1}min^{-1}$ respectively.

Contents

List of Figures

List of Tables

Nomenclature

Roman Symbols

A	Area, m^2
a_i	Static gas-liquid interfacial area, m^{-1}
A_{ij}	First image intensity matrix
b_h	Turbine blade height, m
b_i	Turbine blade thickness, m
b_w	Turbine blade width, m
B_{ij}	Second image intensity matrix
Bo	Bond number, dimensionless
C_p	Specific heat capacity, $Jkg^{-1}K^{-1}$
C_D	Drag coefficient, dimensionless
d_f	Shake flask diameter, m
d_i	Turbine diameter, m

d_s	Shaking diameter, m
d_v	Vessel diameter, m
D_w	Microwell depth, m
d_w	Microwell diameter, m
D_{O_2}	Oxygen diffusion tension, $m^2 s^{-1}$
D_{value}	Intensity difference, dimensionless
$\mathbf{F}$	Volume force vector, Nm^{-3}
F	Force, N
F_D	Drag force, N
F_E	Effective particle weight, N
Fr	Froude number, dimensionless
g	Acceleration due to gravity, ms^{-2}
h_L	Liquid height, m
k	Turbulent kinetic energy, Jkg^{-1}
$k_L a$	Gas-liquid transfer coefficient, s^{-1}
N_p	Power number, dimensionless
N_s	Shaking or stirring frequency, s^{-1}
N_{90}	shaking frequency needed to ensure >90% suspension, s^{-1}

P	Power, W
p	Pressure, Pa
P'_O	Modified power number, dimensionless
P_G	Power input at gassed conditions, W
P_{UG}	Power input at ungassed conditions, W
Q	Volumetric gas flow rate, $m^3 s^{-1}$
R	Length of the arm pressing against the force sensor, m
r	Radial position, m
Re	Reynolds number, dimensionless
S_a	Specific enzyme activity, $\mu mol g^{-1} min^{-1}$
S_f	Solid volume fraction
Sc	Schmidt number, dimensionless
T_c	Titrant consumption rate, min^{-1}
T_m	Titrant molarity, $molL^{-1}$, mixing time, s
$\mathbf{u}$	Velocity vector, ms^{-1}
u_i	Mean velocity component, ms^{-1}
U_t	Impeller tip speed, ms^{-1}
U_{js}	Just suspension frequency, ms^{-1}

V Volume, m^3

V_L Liquid volume, m^3

V_S Solid volume, m^3

V_s Superficial gas velocity, ms^{-1}

M_e Mass of enzyme sample, g

z Axial position, m

Greek Symbols

α Heat transfer coefficient, $Wm^{-2}K^{-1}$

β Overall mass transfer coefficient, ms^{-1}

$\Delta\rho$ Solid liquid density difference, kgm^{-3}

ϵ Energy dissipation rate, s^{-1}

λ Heat conductivity, $Wm^{-1}K^{-1}$

μ Dynamic viscosity, $kgm^{-1}s^{-1}$

μ_T Turbulent viscosity, $kgm^{-1}s^{-1}$

ν Kinematic viscosity, m^2s^{-1}

ω Angular velocity, s^{-1}

ρ Liquid density, kgm^{-3}

ρ_p Density of solid particles, kgm^{-3}

σ Liquid surface tension, Nm^{-1}

τ_{ij} Laminar deformation tensor

Acronyms

DSW Deep Square Well

GA Glycoaldehyde

HPA Hydroxypyruvate Acid

$HPLC$ High-performance Liquid Chromatography

OTR Oxygen Transfer Rate

$PMMA$ Poly(Methyl Methacrylate)

SRW Standard Round Well

STR Stirred Tank Reactor

TFA Trifluoroacetic Acid

TK Transketolase

TPP Thiamine Diphosphate

Chapter 1

Introduction

1.1 Literature Review

1.1.1 The Need for Rapid Bioprocess Developement

The complexity of biological systems, from individual protein to whole cells, makes it exceedingly difficult to predict their behaviour under anything other than the most ideal conditions (Micheletti and Lye, 2006). This is due to the large number of variables and their degree of interaction that often affect the performance of individual bioprocess operations. Complexity is further increased when a linked sequence of bioprocess operations is considered. The need for pharmaceutical companies to investigate the effect of a large number of bioprocess variables and the pressure of cutting development time has led to a strong interest in small scale parallel experimentation. The industrial interest behind microscale bioprocessing is also driven by financial implications. The current average cost to develop a new drug and deliver it to the market is £0.5 billion

and the process takes nearly 10 years (DiMasi et al., 2003). Regulatory demands often require the manufacturer to establish the intended manufacturing process early during the material generation phase for initial clinical trials. One of the major obstacles at this point is the lack of clinical efficiency which can lead to unexpected failures at manufacturing scale. Any delay occurring during scale up can be costly and will directly affect the cost and the time required for a new drug release. Microscale bioprocessing represent a potential solution as it allows the collection of quantitative bioprocess information early on during the development of new drugs and a more reliable translation to manufacturing scale.

One approach has been the use of a smaller version of standard stirred bioreactors. There is also a second approach available that relies on the use of shaking to promote mixing, heat and mass transfer inside microwells (Micheletti and Lye, 2006). Some of the advantages of this approach are the ease of parallel experimentation, suitability for automation and the variety of available microwell geometries and the possibility of using different fill volumes (Lye et al., 2003; Marques et al., 2009).

1.1.2 Solid Suspension in Shaken Bioreactors

1.1.2.1 Microscale Unit Operations

In principle, microscale approach can be applied to the study of each unit operation in a whole bioprocess sequence (Lye et al., 2003). The resulting information could either directly mimic larger scales of operation performance or provide valuable insight into important scale-up issues. Techniques such as metabolic

engineering (Raab et al., 2006) and directed evolution (Hibbert et al., 2005) have made it possible to generate large number of potentially useful recombinant biocatalysts and as a result the majority of studies have focused on developing microbial fermentation processes for protein synthesis in microwell format. The necessity to grow and store microbial biocatalysts in microplate formats have been the catalyst for some of the most pioneering studies in this area. For example, work has been carried out on optimisation of oxygen transfer rates in deep-well microplates (Duetz et al., 2000).

Microbial fermentation studies have mostly centred on the quantification of E. coli growth kinetics (Kostov et al., 2001; Micheletti and Lye, 2006) and recombinant enzyme expression (Ferreira-Torres et al., 2005). Compared with other laboratory formats, microscale techniques have produced satisfactory results in terms of biomass growth and enzyme levels. Microtiter plates have been proven to be promising representative screening systems for multistep biocatalysis, particularly in aqueous phase systems (Marques et al., 2007). In order to enhance the performance of fermentation processes and attain high cell densities required by industry, customisation of microwell designs have also been considered. Different methods, including pH control in microwell environment, have been experimented with. This particular approach has led to enhanced biomass growth and erythromycin A biosynthesis in fermentations of Saccharopolyspora erythraea compared to other methods (Elmahdi et al., 2004).

By comparison there has been very little work on downstream processing operations in microwell formats. This is an important area requiring further study

in order to avoid stagnation in studies investigating the impact of fermentation conditions on the whole process performance. Studies have been carried out at the 10-100 mL scale (Reynolds et al., 2003), but the translation of these to microscale level has only just begun. Jackson et al. (2006) studied the interaction between fermentation and primary product recovery stages in microwell geometry. Another area of interest has been chromatography (Mazza et al., 2002; Rege et al., 2004). This is a particularly difficult operation to mimic in microwells due to the dynamics of product binding and the influence of mobile phase flow rate on mixing and mass transfer.

1.1.2.2 Fundamental Studies on Hydrodynamics of Shaken Systems

A) Microwell Plates

The majority of the fundamental studies on microwell systems have focused on gas-liquid mass transfer. Hermann et al. (2003) measured oxygen transfer rates in a single well of a standard round well plate using the sulphite-oxidation method for a wide range of shaking frequencies, shaking diameters and fill volumes. The results obtained showed an exponential increase of maximum oxygen transfer rate (OTR_{max}) at speeds higher than a critical value. It was also observed that well geometry can strongly affect OTR_{max} and in particular it was shown that wells with a square cross section had twice the transfer rate of a round well at constant operating conditions. The variation of the liquid height with shaking speed was measured at different shaking diameters and the experimental results showed good agreement with the Equation 1.1.

$$N_{crit} = \sqrt{\frac{\sigma d_w}{4\pi V_L \rho d_s}} \tag{1.1}$$

Equation 1.1 was obtained for a single fill volume in a 96-standard round well plate. Different flow hydrodynamics (Duetz and Witholt, 2001), which are observed in the 96-deep square well geometry, means that a different relationship between the critical speed and the operating conditions can be expected as this geometry exhibits better mixing capability due to turbulence caused by the instability of flow patterns.

Doig et al. (2005) have also reported gas-liquid transfer coefficient ($k_L a$) values for various round-well diameters. The measurements were based on both dynamic gassing out technique and on the growth kinetics of an obligate aerobe. A predictive correlation, as given in Equation 1.2, was proposed.

$$k_L a = c_1 \frac{D_{O_2}}{d_w} a_i Re^{0.68} Sc^{0.36} Fr^x Bo^y \tag{1.2}$$

Over the past few years effort has been made to provide a theoretical basis of assessing the mixing conditions in microwells by using computational fluid dynamics (CFD) techniques. Zhang et al. (2002) managed to obtain flow conditions in shaken microwells by solving the the relationship given in Equation 1.3.

$$\int_{\Delta t} \frac{\partial}{\partial t} \left[\int_{CV} (\rho\phi)\, dV \right] dt + \int_{\Delta t} \int_{A} \boldsymbol{n}.\,(\rho\phi\boldsymbol{u})\, dA dt = \int_{\Delta t} \int_{A} \boldsymbol{n}.\,(\Gamma_\phi \nabla\phi)\, dA dt + \int_{\Delta t} \int_{CV} S_\phi dV dt \tag{1.3}$$

The flow inside the microwell was assumed to be laminar. Simulation results showed that flow patterns, power input and energy dissipation rate in the shaken microwells were strongly affected by the size of the well and the volume of shaken liquid as well as the shaking frequency and amplitude. Simulations were also indicative of greater power consumption sensitivity to changes in shaking amplitude compared to frequency and that for otherwise similar conditions power consumption increased significantly as the volume of liquid in the well decreased.

Due to the complexity of the system, a small amount of work has been carried out providing a description of the fluid mechanics taking place in microwells and, in most cases, the focus has been on single phase systems. On the other hand, studies on multiphase systems in microwells are practically non-existent. Solid-liquid and liquid-liquid systems are often encountered in operations within the bioprocess industry. Suspended beads are frequently used in chromatography studies and multi-step biotransformations are carried out using organic-aqueous systems. Peter et al. (2006) tried to quantify hydrodynamical stresses in shake flasks by measuring maximum stable droplet size in non-coalescing liquid-liquid systems under a broad range of operating conditions. The maximum local energy dissipation rate was determined by comparing the maximum stable droplet diameters to those observed in a standard stirred tank reactor.

As the above review demonstrates, a number of useful parameters have been suggested that begin to characterise the engineering environment in shaken microwells. Shaking frequency seems to play a crucial role on oxygen transfer and as a result on the outcome of the fermentations with aerobic micro-organisms with

high oxygen demands. Although the importance of scale-up and its impact on microwell operations have been established, little data is available in the published literature on the subject. Also, studies concentrating on power consumption and mixing time are virtually non-existent. Given these observations it leaves us with little choice but to look into other shaken formats. A very interesting area is the work carried out to this date on characterising shake flasks. These studies can be helpful in giving guidelines for future research into microwell systems and their characteristics.

B) Shake Flasks

For the past few decades, conical flasks with working volumetric range of 50-500 mL have been widely used for cell culture process development. Although they have been in use for several years, only recently they have been characterised for power consumption. Büchs et al. (2000) used water to take measurements for different flask sizes, shaking frequencies and fill volumes and described the results using Equation 1.4 to within 30%.

$$P'_O = CRe^{-0.2} \tag{1.4}$$

Re was calculated by using d_f as the characteristic length and C was found to be equal to 1.94 using least-square non-linear fitting of the experimental data. Büchs et al. (2000) expanded the studies further by calculating the modified power number for a wide range of experimental conditions. Two different flow conditions were observed with respect to different power numbers which resulted from variation in Reynolds number: in-phase conditions in which the bulk of

the liquid movement was in phase with the shaking platform and out-of-phase conditions in which only a small amount of liquid followed the shaking platform. The latter case resulted in greatly reduced power consumption. Efforts were made to systematically describe the out-of-phase conditions and this resulted in a new non-dimensional number, called the Phase Number (Ph), which was derived from analogy with a partially filled, rotating horizontal drum. This is given in Equation 1.5.

$$Ph = \frac{d_s}{d_f}\left\{1 + 3\log_{10}\left[\frac{\rho\,(2\pi N_s)\,{d_f}^2}{4\mu} \times \left(1 - \sqrt{1 - \frac{4}{\pi}\left(\frac{{V_L}^{1/3}}{d_f}\right)^2}\right)^2\right]\right\} \quad (1.5)$$

According to the investigations, all the operating conditions at which $Ph >$ 1.26 are in-phase while out-of-phase conditions may exist when large flasks or high viscosity fluids are used.

1.1.3 Solid Suspension in Stirred Systems

Stirred tank reactors are the most important type of bioreactor used in industrial production processes (Asenjo and Merchuk, 1994). This is so mainly due to easy construction and high Power Number (van't Riet and Tramper, 1991). In these reactors, agitation is achieved by using different types of stirrers, which perform various functions such as providing adequate momentum, heat and mass transfer and mixing and homogenisation of suspensions (Asenjo and Merchuk, 1994). In order to optimise each of these tasks, the impellers would need to be of a different design, but, given that these tasks are carried out at the same

time, the final impeller design will always represent a compromise. The impellers which have been traditionally used in bioreactors are generally classified into axial and radial flow impellers (Asenjo and Merchuk, 1994). The most widely used impeller is a six-blade disk impeller, also known as a Rushton turbine, shown in Figure 1.1. A radial flow impeller, a suitably sized Rushton turbine is highly effective in dispersing gas, which is advantageous in gas-liquid operations, as long as shear is not an issue. The stirrer is usually positioned inside a reactor so that it sits a distance away from the bottom of the tank equal to its diameter. At lower distances, the interaction between the stirrer and the bottom will lead to a reduced power consumption while higher positions will result in complications in liquid circulation (van't Riet and Tramper, 1991).

1.1.3.1 Fundamental Studies on Hydrodynamics of Stirred Systems

The basic task of a reactor in a biotechnological production process is to guarantee the existence of an optimal environment in which the required biocatalysis activities can be carried out.

Oxygen mass transfer from the bulk of the gas phase to single organisms like bacteria and yeast cells is governed by the mass transfer resistance exhibited by the liquid phase (Asenjo and Merchuk, 1994). Various governing correlations suggested for stirred tank reactors are manifold and have been extensively reviewed by Reuss (1993). It has been shown that many of these correlations have been corrupted by erroneous measurements, while most of the measurements have been carried out at a very small scale. The general form of k_La can be mathematically written as given in Equation 1.6.

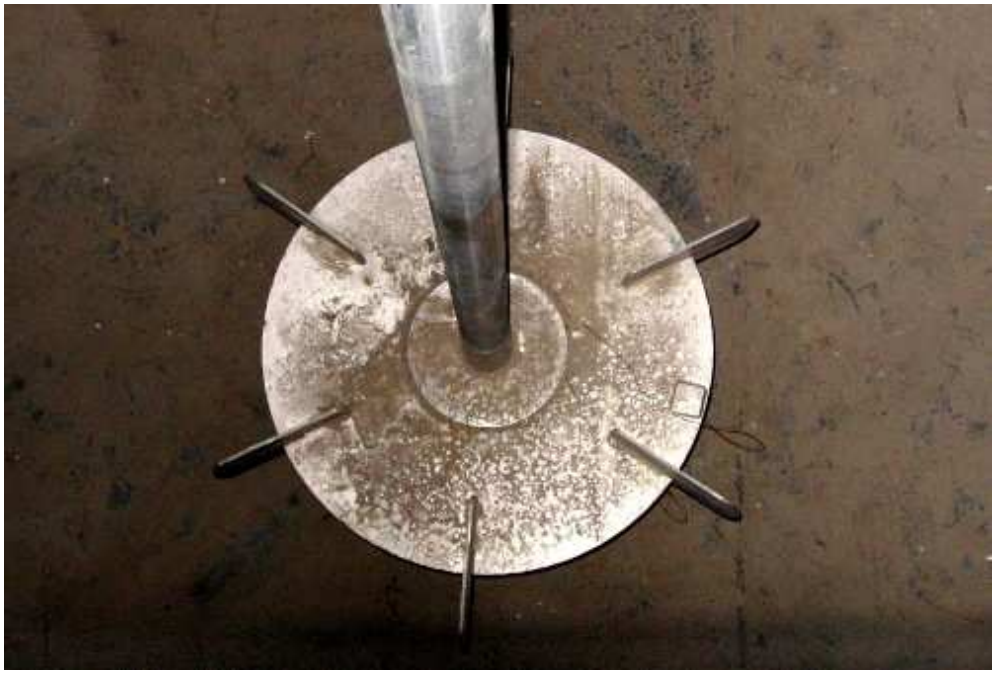

Figure 1.1: An example of a radial flow impeller; a six-bladed turbine, aka Rushton turbine.

$$k_L a = K \left(\frac{P}{V_L}\right)^{\alpha} {V_S}^{\beta}, \tag{1.6}$$

however, van't Riet (1979) has reported that the exponent show a fairly large variation ($0.4 < \alpha < 1$ and $0 < \beta < 0.7$). Reuss et al. (1986) have also suggested the following correlation by measuring the steady state $k_L a$ during fermentations of *Saccharomyces cerevisiae*.

$$\left(\frac{k_L a}{V_s}\right)\left(\frac{\nu^2}{g}\right)^{0.33} Sc^{0.3} = 5.5 \times 10^{-4} \left(\frac{P}{\rho g V_L V_S}\right), \tag{1.7}$$

where V_s is the superficial gas flow velocity, V_L is the liquid volume, P is the power input and ν is kinematic viscosity. Certain production processes, such as immobilised enzymes and cells and biofilms face added complications due to further transfer resistance due to diffusion limitations (Asenjo and Merchuk, 1994).

Increasing the oxygen supply rate by increasing the $k_L a$ value or by partial pressure of oxygen in the gas phase will result in an increase in the amount of heat generated due to increased metabolic activity. Various heat transfer data for unaerated stirred tanks have been reviewed by Henzler (1982) and correlated into Equation 1.8.

$$\frac{\alpha D_T}{\lambda_B} = 0.6 \left(\frac{N {d_i}^2}{\nu}\right)^{0.67} \left(\frac{C_{pb}\eta_b}{\lambda_b}\right)^{0.33}, \tag{1.8}$$

where, α is the heat transfer coefficient, λ_b is the heat conductivity, ν is kinematic viscosity, d_i is the impeller diameter, D_T is the tank diameter, N is the stirring frequency, C_p is the specific heat and η_b is the dynamic viscosity. It has

been shown that the influence of aeration is complex, might be related to flooding phenomena and depends on stirring frequency (Kipke, 1980; Steiff et al., 1980).

A key parameter for correlating the volumetric mass transfer coefficient, $k_L a$, is the power input which is usually expressed in a Power Number by Equation 1.9.

$$N_p = \frac{P}{N^3 {d_i}^5 \rho} \tag{1.9}$$

N_p can be correlated with the Reynolds Number and approaches a constant value under turbulent flow conditions for most types of impeller (Asenjo and Merchuk, 1994). Hughmark's equation, given below, has been recommended by van't Riet and Tramper (1991) for correlating the effects of gas dispersion in the impeller region and its interaction with the fluid dynamics inside the tank.

$$\frac{P_G}{P_{UG}} = 0.1 \left(\frac{\dot{V}_G}{N V_L} \right)^{-0.25} \left(\frac{N^2 {d_i}^4}{g H_L {V_L}^{0.67}} \right)^{-0.20} \tag{1.10}$$

Suspension of solid particles in liquids in mechanically agitated tanks features in many operations in process industries including food, pharmaceutical, minerals, chemical and biochemical. In the chemical industry alone, 80% of products involve solid-liquid processing (Shamlou, 1993). Flow regime in the bulk of the vessel is normally determined by the impeller Reynolds Number. With low concentration of solids, low liquid viscosity and with particles having free-settling rates from around 2.5 mms^{-1} to about 100 mms^{-1} , the presence of particles may be assumed to have little effect on the flow properties of the mixture in the vessel, but the settling tendency of the particles has a dominating influence on

the behaviour of the suspension (Shamlou, 1993).

Homogeneous suspension is only possible if liquid velocity is high and flow is fully turbulent. This is in general a very energy intensive requirement. If liquid motion is not sufficiently fast, particle concentration gradients will develop mainly in the axial direction as particles settle and accumulate at the bottom of the vessel. This is called heterogeneous suspension and most industrial suspensions are designed to work in this regime. As impeller speed, and therefore liquid velocity, reduces more and more particles will settle until, eventually, a permanent bed of particles is formed at the base of the vessel. This condition is generally known as saltation and the corresponding impeller speed at which it occurs gives a measure of minimum liquid velocity needed to keep the particles just suspended. This velocity is critical for optimum operating conditions (Shamlou, 1993).

There are many empirical correlations for calculating the just suspension speed, N_{js} (Nienow, 1968; Subbarao and Taneja, 1979). The pioneering work, however, was carried out by Zwietering (1958), which covered experimentally a wide range of impeller types and sizes, off bottom clearances, vessel sizes and physical properties and provides N_{js} values broadly similar to a large number of other studies. Zwietering's correlation is given in Equation 1.11.

$$N_{js} = S\nu^{0.1}{d_p}^{0.2}\left(g\frac{\Delta\rho}{\rho}\right)^{0.45}B^{0.13}D^{-0.8}, \tag{1.11}$$

where S is a dimensionless group given as

$$S = \frac{N D^{0.85}}{\nu^{0.1} {d_p}^{0.2} \left(g\frac{\Delta\rho}{\rho}\right)^{0.45} B^{0.13}} \tag{1.12}$$

and ν is fluid kinematic viscosity, d_p is particle diameter, g is acceleration due to gravity, $\Delta\rho$ is the solid and liquid density difference, ρ is liquid density, B is solid to liquid mass ratio multiplied by 100 and D is impeller diameter. Although developed for stirred tank geometries, it is likely that the key factors influencing particle suspension in stirred bioreactors, such as solid volume fraction, particle density and particle diameter, will also influence particle suspension in shaken microwells.

1.1.3.2 Computational Simulation of Flow Properties in Stirred Systems

As mentioned above, the design of stirred bioreactors includes the specification of the geometrical configuration and the optimisation of the operating conditions in order to meet the required operation. The traditional method for meeting this requirement has been the use of empirical information presented in various correlations with the inevitable hiding of localised data. Detailed description of the turbulent flow field, to be used in conjunction with other transport equations is the only way to achieve further improvements in stirred tank and process design (Schmalzriedt and Ruess, 1999; Togatorop et al., 1994). The improving nature of commercial computational fluid dynamics software and increasing computer power are allowing for a better simulation of the three-dimensional and turbulent flow structures in stirred tanks.

The transport equations describing the instantaneous behaviour of turbulent liquid are three Navier-Stokes equations (transport of momentum corresponding to the three spatial coordinates r, z, ϕ in a cylindrical polar coordinate system) and a continuity equation. Jenne and Reuss (1999) describe the two in Equations 1.13 and 1.14.

$$\frac{\partial\left(\rho u_i\right)}{\partial t}+\frac{\partial\left(\rho u_j u_i\right)}{\partial x_j}=-\frac{\partial}{\partial x_j}\left(\tau_{ij}\rho u_i' u_j'\right)-\frac{\partial p}{\partial x_i}+\rho g_i \tag{1.13}$$

$$\frac{\partial p}{\partial t}+\frac{\partial}{\partial x_i}\left(\rho u_i\right)=0 \tag{1.14}$$

Computation of the turbulent flow in a stirred tank reactor is often based on the so-called $k-\epsilon$ model (Asenjo and Merchuk, 1994), where k is the turbulent kinetic energy and ϵ is its dissipation rate. Jenne and Reuss (1999) have compared different turbulence models and found that an optimised Chen-Kim variant would allow for an accurate simulation of the mean flow and turbulence quantities in the out flow of the impeller and in the bulk region.

Six different two-equation turbulence models were used by Jones et al. (2001) to investigate the flow inside an unbaffled stirred tank and the results were also compared with experimental laser doppler velocimetry (LDV) data. It was discovered that the radial velocity component in the impeller discharge region is overpredicted by each of the models, the tangential velocity component in the impeller discharge region is predicted well by the models, but is underpredicted near the shaft and the $k-\epsilon$ model is the only model which produces reasonable kinetic energy predictions in the impeller discharge region. Hartmanna et al. (2004) have

shown that large eddy simulations (LES), in comparison with Reynolds-avaraged Navier-Stokes (RANS), is more accurate for the purpose of calculating the turbulent kinetic energy, while both methods performed satisfactorily in representing the flow field.

Kasat et al. (2008), have studied the interaction between solid suspension quality and liquid phase mixing process in a stirred tank reactor by using a standard $k-\epsilon$ model. They found that the mixing time increases with an increase in the impeller rotational speed, then drops gradually until the just off-bottom suspension condition is reached. The mixing time would then remain constant until further gradual decline as the system approached full suspension. LES and the Euler-Euler computational fluid dynamics models have also been compared with regards to their ability to predict solids dynamics in a solid-liquid stirred tank reactor (Guha et al., 2008). It was shown that both models fail to accurately solve the flow field in regions close to the impeller.

1.1.4 Scale-up of Biocatalyst Processes

Industrialisation of any bioprocess will invariably require some form of scale-up study. Bioprocesses have been traditionally developed at at least three different scales (Ju and Chase, 1992):

1. Laboratory scale for conducting the initial studies
2. Pilot plant for establishing the optimum operating conditions
3. Plant scale for monetisation of the process

In recent years though, given the increasing number of bioprocess candidates which require thorough evaluation, an additional step has been introduced before the first step mentioned above which is carried in small scale bioreactors such as shake flasks, mirowell plates and miniature bioreactors.

Scale-up studies aim to establish the conditions at which a particular bioprocess at a large scale behaves as performed and optimised at small scale (Diaz and Acevedo, 1999; Oldshue, 1985). The high cost of evaluating a process at large scale is an additional reason to assess its performance at small scale and to establish whether it will work or not (Doran, 2000). Although the basic concept behind scale-up is the theory of similarity, and the large volume of literature which deals with it, there is not a single, common strategy available. According to Schmidt (2005), for any product, process or facility, a new scale-up procedure should be designed.

Bioprocesses, in general, can be studied based on a combination of process factors such as the number of precultures and sterilisation conditions, chemical factors such as medium concentration and composition and physical factors such as heat and mass transfer, mixing, shear and power consumption. The most important environmental factors which, according to Stanbury et al. (2003), can be affected by scale-up include:

- Nutrient availability
- pH
- Temperature

- Dissolved oxygen concentration
- Hydrodynamic shear
- Dissolved carbon dioxide concentration
- Foam production

The above list, which is specifically for cell culture, suggests that the main considerations in scale-up would be aeration and mixing (Stanbury et al., 2003).

1.1.4.1 Scale-up Concepts

Originally, the three main concepts used in scale-up were geometric similarity, kinematic similarity and dynamic similarity (Johnston and Thring, 1957). For various reasons, they are now regarded as inadequate and Oosterhuis and Kossen (1985) have suggested four different concepts:

- **Semi-fundamental method:** scale-up is based on simplified models in an attempt to avoid using complex momentum balance equations. The majority of models refer to bulk flow and omit any information about flow near important regions such as cooling coils, stirrer blades and tank walls. These methods are rather unreliable as they are based on observations in small scale equipment and the scale-up is based on extrapolation.
- **Fundamental method:** this is based on solving all the micro-balances for momentum transfer, heat transfer and mass transfer in a given system. This makes it a complex method as transport equations have to be solved in three-dimensional space using complicated boundary conditions. Also,

momentum balances are usually set up for homogeneous fluids and therefore not very realistic. But the main problem is the impossibility of solving the micro-momentum balance.

- **Rules of thumb:** these include the most common scale-up procedures such as constant power per volume ratio, constant k_La, constant impeller tip speed and constant oxygen tension. These are further expanded in Section 1.1.4.2.

- **Dimensional analysis:** this is a widespread method, commonly used in scale-up of the chemical engineering problems and is based on maintaining constant values of dimensionless groups of parameters during scale-up. Given that a dimensionless group is either a ratio or a time constant for the different mechanisms involved, in theory, by keeping all the dimensionless groups constant, the relative importance of each mechanism can be kept constant. In practice though, not all dimensionless groups can be kept constant, which in some cases can result in unrealistic predictions.

1.1.4.2 Most Commonly Applied Criteria for Scale-up

In absence of a standard method for bioprocess scale-up and because each microorganism and individual process demands its own scale-up methodology, the process characteristics which have been commonly suggested to be maintained constant during scale-up (Hosobuchi and Yoshikawa, 1999; Ju and Chase, 1992; Oosterhuis and Kossen, 1985; Stanbury et al., 2003) have been listed in Table 1.1.

Impeller Reynolds Number can be kept constant during scale-up. The

Table 1.1: Parameters and coefficients important in mixing, oxygen transfer and aeration which are suitable as scale-up variables. They can be kept constant alone or in combination with each other or other relevant variables (Schmidt, 2005)

Parameter/Coefficient	Mathematical formulation
Impeller Reynolds Number	$Re_i = (\rho N d_i)/\mu_v$
Power input per unit volume (W)	$P/V = N_p \rho N^3 {d_i}^5$
Mixing time (s)	$T_m = V/Q$
Volumetric mass transfer coefficient (s^{-1})	$k_L a = C(P/V)^\alpha (V_s)^\beta$
Superficial gas velocity (ms^{-1})	$V_s = Q/A$
Oxygen transfer rate $(KgO_2 m^{-3} h^{-1})$	$OTR = k_L a(C^* - C_L)$
Volumetric gas flow rate per unit volume of liquid	Q/V or vvm
Impeller tip speed (ms^{-1})	$U_t = 2\pi N d_i$

issue with this method is that it does not take into account the influence that aeration has on the process (Ju and Chase, 1992). Reynolds number can of course be replaced with other dimensionless groups but this has resulted in limited success for different reasons such as unrealistic operating parameters (Junker, 2004).

Constant power input per unit volume is a popular scale-up method with a typical power per unit volume ratio of between 1 and 2 kWm^{-3} (Abia et al., 1973). This method has been successfully applied to many antibiotic fermentations (Ju and Chase, 1992; Schmidt, 2005) as the primary scale-up factor. In an aerated bioprocess, formation of cavity bubbles behind the impeller blades (Sensel et al., 1993) reduces the required power input by 60-65% compared to ungassed conditions (Wang et al., 1979). The main shortcoming of this method is

the tendency to overestimate the required motor size, meaning scale-up at larger scales are impractical due to motor size limitations (Cui et al., 1996; Hughmark, 1980; Luong and Volesky, 1979; Michel and Miller, 1962; Mockel et al., 1983).

Mixing time, defined by Abia et al. (1973) as "the period of time which is needed for a liquid droplet passing into an agitated vessel filled with a fluid with the same physical properties as the droplet to be completely mixed with the bulk of the fluid", can also be employed as a scale-up parameter. The main issue with this method is that as scale increases, the contents of a bioreactor become less homogeneous, meaning changes in oxygen and nutrient concentration, as well as inconsistent pH and temperature which have the potential to affect process productivity (Bonvillani et al., 2006; Larsson et al., 1996).

Volumetric mass transfer coefficient is, according to Schmidt (2005), the most popular scale-up method applied to aerobic fermentations, comprising approximately 30% of industrial processes (Mavituna, 1996). Oxygen acts as a rate-limiting factor in growth of cell cultures as scale increases (Shin et al., 1996), hence obtaining constant k_La in process scale-up is paramount to achieving the oxygen levels demanded by a given cell culture. The k_La values can be kept constant at different scales by making changes to stirring frequency and aeration rates (Stanbury et al., 2003).

1.1.5 Biocatalyst Immobilisation

Enzymes are protein molecules which serve to accelerate the chemical reactions of living cells by up to several orders of magnitude. Without enzymes, most biochemical reactions would be too slow to even carry out life processes. Enzymes display great specificity and are not permanently modified by their participation in reactions. This particular property makes them highly cost effective because they can be used more than once. One major obstacle to this is the difficulty to separate the enzymes from the reactants and/or products when they are all mixed together in a solution. This can be overcome by attaching the enzyme to a support surface in some way and recovering them once the product has been removed. The above process is called enzyme immobilisation and usually consists of attaching the enzyme to a solid support over which a substrate is passed and converted to product. The length of this extended re-use depends on the degree of adequacy of operational stability.

Bioconversions that rely on the use of immobilised enzymes are frequently found in the chemical and pharmaceutical industries (Carpio et al., 2000; Krajewska, 2004; Liese et al., 2006) due to improved enzyme stability and ease of biocatalyst recovery (Mateo et al., 2007).

1.1.5.1 Enzyme Immobilisation

Immobilisation techniques were first developed in the 1960s to allow for reuse of expensive biological catalysts, including enzymes. Even though large scale methods for enzyme isolation and purification became available at the time, the cost

of these water-soluble enzymes was often to high to justify their economic use as industrial catalysts and remains so to this day. Although cells are already insoluble particles, their mechanical properties can be improved by immobilising them on the surface of or inside more robust particles.

Immobilisation can be carried out through different methods. These are listed in Table 1.2 and will be covered more extensively in Section 1.1.6.

Table 1.2: Methods and mechanisms used in biocatalyst immobilisation.

Bound		Entrapped	
Binding to carriers	Cross-linking	Matrix entrapped	Membrane enclosure

1.1.5.2 Advantages and Disadvantages of Immobilisation

Like any other process, enzyme immobilisation has a series of potential advantages and disadvantages (Brocklebank et al., 1999; Katchalski-Katzir, 1993). These are listed in Table 1.3

1.1.5.3 Effects of Immobilisation on Biocatalyst Kinetics

Immobilisation of a biocatalyst will alter the apparent kinetic properties of the enzyme (Brocklebank et al., 1999; Mateo et al., 2007; Vishvanath et al., 1995). These can be attributed to changes in enzyme conformation, steric hindrance of enzyme catalysis, diffusional limitations or influences on the micro-environment.

Table 1.3: Advantages and disadvantages of biocatalyst immobilisation.

Advantages	Disadvantages
Easier reactor operation and control	Loss in activity through immobilisation
Easier product recovery and purification	Reduced activity per unit volume
Wider choice of reactors	Diffusional limitation of reaction rate
Protection of catalyst from interfacial damage	Additional cost
Improved operational stability	

The latter can be caused by either hydrophobic or electrostatic interactions. Such effects result in a change in the apparent k_m values or pH-activity profiles of the immobilised enzyme. While using immobilised enzymes it is important to consider limitations on substrate and product diffusion and catalyst distribution.

1.1.6 Methods of Immobilisation

The most important aspect of immobilising enzymes on solid particles is the minimisation of potential damages that can cause reduction in enzyme activity. The nature of these damages are usually related to changes in chemical structure or reactive groups in the binding site of the enzyme. It is essential to avoid reaction with the active amino acids of the enzyme. Alternatively, an active site can be protected during attachment as long as the protective groups can be removed later on without loss of enzyme activity. In some cases, this protective function can be fulfilled by a substrate or a competitive inhibitor of the enzyme.

The responsibility for retaining the structure in the enzyme rests with the surface on which the enzyme is immobilised. This is achieved through hydrogen binding (Hanefeld et al., 2008) or the formation of electron transition complexes. The effect is that the enzymes will be thermally more stable due to less vibration. The micro-environment of the surface and enzyme has a charged nature (Hanefeld et al., 2008) that can cause a shift in the optimum pH of the enzyme of up to 2 pH units. This can happen in parallel with a general broadening of the pH range in which the enzyme can work, allowing enzymes with different pH regions to work together. As mentioned in Section 1.1.5.1, there are different methods of immobilisation as seen in Figure 1.2; bound and entrapped. Bound immobilisation can be further divided into binding to carriers and cross-linking with entrapped immobilisation breaking down into matrix entrapped and membrane enclosure.

1.1.6.1 Immobilisation by Binding

A) Carrier Binding

The carrier binding method is the oldest immobilisation technique for enzymes. In this method, the amount of enzyme bound to the carrier and the level of activity after immobilisation depend on the nature of the carrier. The selection of the carrier depends on the nature of the enzyme itself, as well as the particle size, surface area, molar ration of hydrophilic to hydrophobic groups and chemical composition (Hanefeld et al., 2008).

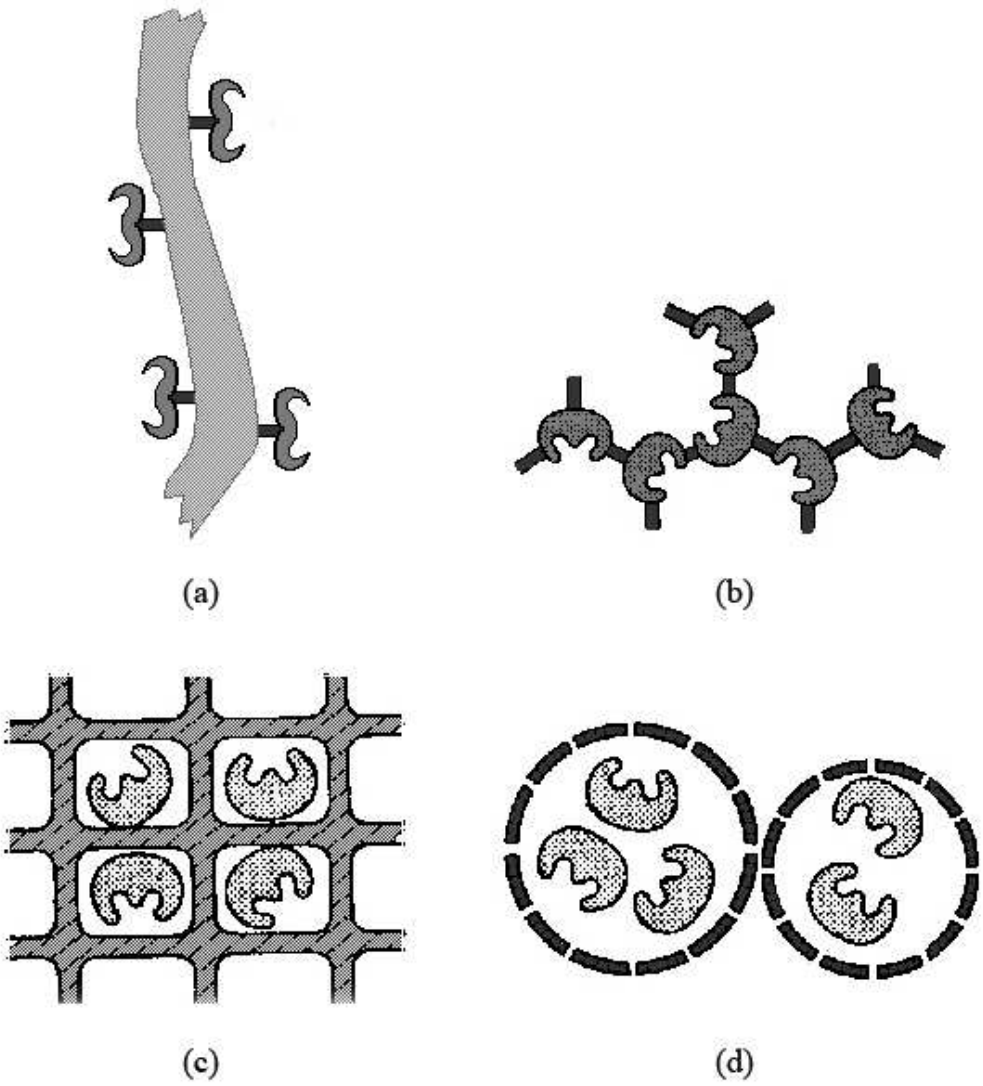

Figure 1.2: Different methods of immobilisation; (a) Carrier bound, (b) Cross-linked, (c) Matrix entrapped and (d) Membrane entrapped.

Generally speaking, the level of the activity of the immobilised enzyme depends on the ratio of the hydrophilic groups to hydrophobic groups and the concentration of the bound enzymes. Some of the most commonly used carriers for enzyme immobilization are polysaccharide derivatives such as cellulose, dextran, agarose, and polyacrylamide gel. According to the binding mode of the enzyme, the carrier binding method can be further divided into three more categories.

Physical adsorption mode is based on the physical adsorption of the protein on the surface of water insoluble carriers (Kubitzki et al., 2008; Toogood et al., 2002). This means the method causes little or no conformational change of the enzyme or destruction of its active centre. This method can be cheap and simple provided a suitable carrier is found. However, it has the disadvantage that the adsorbed enzyme may leak from the carrier during use due to a weak binding force between the enzyme and the carrier.

Ionic binding mode relies on the ionic binding of the enzyme protein to water-insoluble carriers containing ion-exchange residues. The binding of an enzyme to the carrier is easily carried out, hence, the ionic binding method causes little changes in the conformation and the active site of the enzyme (Topoglidis et al., 2000). Therefore, this method yields immobilized enzymes with high activity in most cases. Leakage of enzymes from the carrier may occur in substrate solutions of high ionic strength or upon variation of pH. This is because the binding forces between enzyme proteins and carriers are relatively weak.

Covalent binding mode is the most intensely studied of the immobilisation

technique (Fernandez-Lafuente et al., 1998; Wang and Carlisle, 2006). This method is based on the binding of enzymes and water insoluble carriers by covalent bonds (Brocklebank et al., 1996; Kubitzki et al., 2008). When trying to select the type of reaction by which a given protein should be immobilized, the choice is limited by two characteristics:

- The binding reaction must be performed under conditions that do not cause loss of enzymatic activity
- The active site of the enzyme must be unaffected by the reagents used

B) Cross-linking

Immobilisation of the enzymes has been achieved by intermolecular cross linking of the protein to either other protein molecules or to functional groups on an insoluble support matrix (Toogood et al., 2002). Generally, cross-linking is best used in conjunction with one of the other methods. It is used mostly as a means of stabilizing adsorbed enzymes and also for preventing leakage from polyacry lamide gels.

The most common reagent used for cross-linking is glutaraldehyde (Mateo et al., 2007; Migneault et al., 2004). Cross-linking reactions are carried out under relatively severe conditions. These harsh conditions can change the conformation of active centre of the enzyme; and so may lead to significant loss of activity.

1.1.6.2 Immobilisation by Entrapment

The entrapment method of immobilisation is based on placement of an enzyme within the lattice of polymer matrix or membrane (Toogood et al., 2002). It is done in such a manner as to retain the enzyme while allowing penetration of substrate. The major difference between this method and immobilisation through binding is that the enzyme itself is not attached to the lattice of the polymer matrix or membrane and therefore has a wide applicability. The conditions used in the chemical polymerisation reaction are relatively severe and result in the loss of enzyme activity. This means immobilisation conditions should be carefully selected for different enzymes.

A) Matrix Entrapped

This type of entrapment involves entrapping enzymes within the interstitial spaces of a cross-linked water-insoluble polymer. Some synthetic polymers such as polyarylamide, polyvinylalcohol and natural polymer (starch) have been used to immobilize enzymes using this technique.

B) Membrane Entrapped

The second method for entrapping involves enclosing the enzymes within semi permeable polymer membranes. The preparation of enzyme micro capsules requires extremely well-controlled conditions and the procedures for micro-encapsulation of enzymes can be classified as

- Interfacial polymerisation method

- Liquid drying
- Phase separation

1.1.7 Transketolase

Transketolase, shown in Figure 1.3, is a dimetric protein with a molecular weight of around 130-170 kDa. In vivo the enzyme is involved in the pentose phosphate pathway (Lindqvist et al., 1992). It has been successfully isolated from yeast, spinach, pig and on a large scale from *E.coli*. The enzyme catalyses the reversible stereospecific transfer of a two carbon ketol group to an aldol acceptor (Lindqvist et al., 1992). The enzyme catalyses requires two cofactors; thiamine pyrophosphate (TPP) and a divalent metal ion for full activity. The TPP binds to the inactive enzyme which is called the apo-enzyme and has two TPP binding sites. The active enzyme containing TPP is known as the holo-enzyme.

1.1.7.1 Structure and Mechanism

As mentioned, transketolase is a dimetric protein, both subunits are identical and contain a binding site for TPP and for the substrate. The binding site is made up of amino acids from both subunits (Lindqvist et al., 1992), meaning that transketolase monomers cannot be active. In fact most of the intra-domain interactions in the yeast enzyme are present inside or close to the active site. TPP binds to the apo-enzyme at a tryptophan side chain in the active centre which results in the ionisation of the C_2 carbon (Cavalieri et al., 1975) on TPP making it a potent nucleophile. The electron is donated to the ketol donor making preparing it to transfer the hydroxy ketone group to the accepting aldehyde. The chirality is

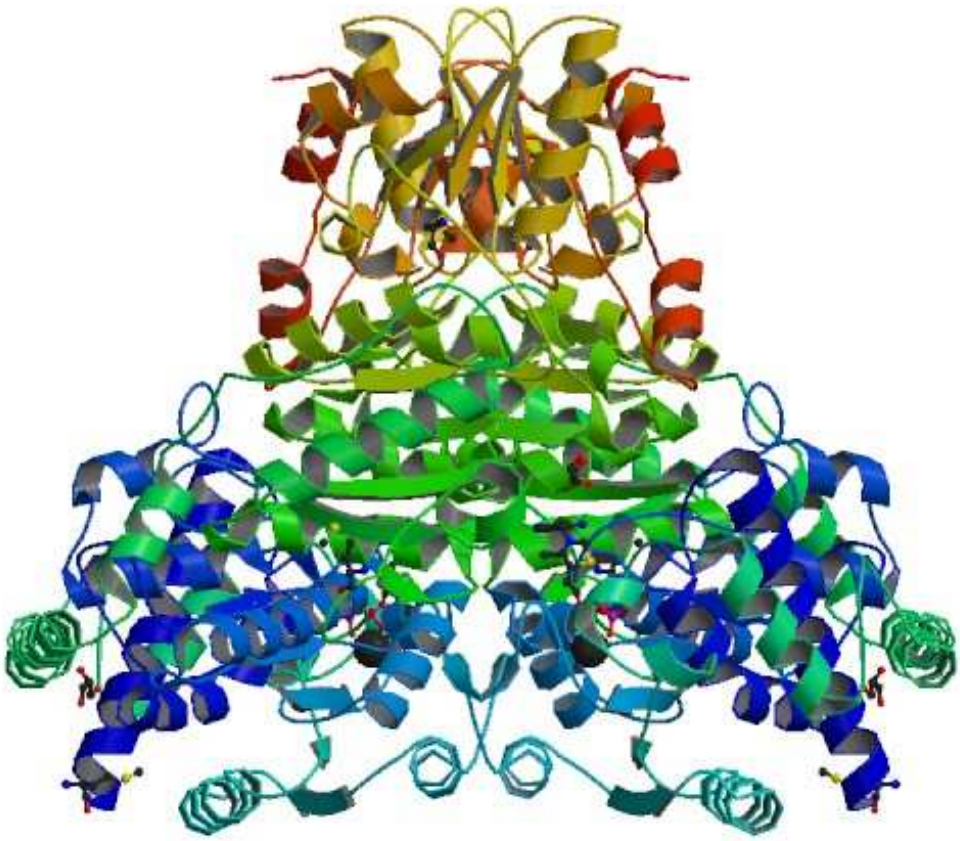

Figure 1.3: Crystal structure of transketolase in complex thiamine diphosphate and calcium ion: N-terminal domain is shown in blue, middle domain in green and C-terminal domain in orange. Calcium ions are shown as dark circles. (Lindqvist et al., 1992).

introduced at the accepting aldehyde moity, which must contain a hydroxyl group in the S position. The thiamine pyrophosphate is consequently heavily involved in catalysis an is subsequently essential for the enzyme to display any activity. The active centre of the enzyme is not large enough to accommodate both substrates simultaneously. As a result it is likely that the reaction mechanism follows a ping pong bi bi type mechanism. This particular mechanism indicates that the first substrate enters the active site and complexes with the enzyme forming the first product. Only after this complex has been formed can the second substrate enter the active site to successfully form a second enzyme-substrate complex thereafter releasing the product and the enzyme. This would suggest that the reaction mechanism is as shown in Figure 1.4.

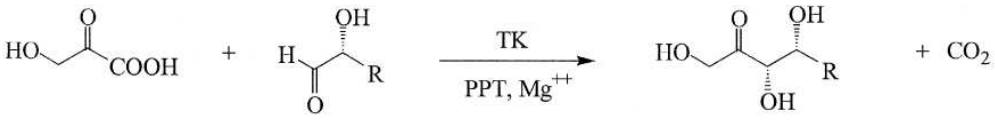

Figure 1.4: Transketolase-catalysied transfer of the ketol group from hydroxypyruvic acid (left) to glycolaldehyde, liberating L-erythrulose and carbon dioxide (Brocklebank et al., 1996).

1.1.7.2 Model Reaction

The general transketolase reaction is a reversible scheme and as a consequence complete conversion of the substrate to product cannot be achieved. There are certain implications associated with this that would be important if the enzyme was to be used as an industrial biocatalyst. For example, the product stream will also contain substrate which means down stream processing will be more

complex. The selection of hydroxypyruvic acid (HPA) as a ketol donor will release carbon dioxide as the co-product of the reaction Brocklebank et al. (1996). The carbon dioxide can take no further part in the reaction and as a result the reaction becomes irreversible. It is likely that most industrial reactions utilising transketolase will use HPA as the ketol donor to overcome the problem associated with equilibrium, and most synthesis routes using transketolase described in the literature involve HPA as the ketol donor. The production of carbon dioxide will also mean that there is no soluble co-product which must be removed from the product, thus, reducing the cost of the down stream processing.

Several aldehyde acceptor molecules have been tested with the transketolase and HPA system. The most reactive aldehyde has been shown to be glycolaldehyde (GA). The reaction between HPA and GA is shown in Figure 1.4. The reaction, which produces L-erythrulose and carbon dioxide, proceeds with a loss of one proton.

1.1.7.3 Immobilisation

The ability to produce *E. coli* transketolase in large quantities at pilot scale has provided the industry with sufficiently low costs to contemplate its use in commercial biotransformations. The fact that the metal ion cofactors and the TPP are not directly consumed in the biotransformation means that cofactor recycling is not necessary. Many of the most useful aldehydes are insoluble in water and may not enter the intact cell unless its membrane has been made more permeable. These consideration has led to the use of isolated enzyme as the biocatalyst (Brocklebank et al., 1996).

As mentioned in Section 1.1.6, immobilisation can be achieved in several methods. Due to regulatory demands that prohibits the presence of biological compounds in the product stream, covalent binding is often the preferred method of immobilisation. This type of bound produces a strong link between the enzyme and its supporting matrix which prevents the protein from detaching itself from the surface of the support.

In some cases the support may need to be activated by the addition of electrophilic groups. For example, in case of Eupergit-C®, these are oxirne groups which make the support more reactive towards the nucleophile groups available on the enzyme. The available nucleophilic groups on the enzyme can be terminal amine, other amines and hydroxyl or thiol groups (Brocklebank et al., 1996). High pH values are usually helpful in promoting reaction. It is also important to take into account the effect of the pH value of the binding buffer solution on the stablity of the enzyme and the resolution of the TPP and Mg^{2+} cofactors from the holoenzyme (Woodley et al., 1995). Therefore it is essential to use a binding pH that causes minimal denaturation of the enzyme. Epoxide groups are strong electrophiles and will readily react with amine groups at pH values approaching neutrality.

1.1.8 Proteases

Proteases are a family of enzymes that carry out proteolysis by hydrolysing the peptide binds that connect the amino acids together in the polypeptide chain

which forms a protein (Barrett et al., 1998). They can be classified according to their activities and functional groups. According to Fersht (1998), these classes are:

- Serine proteases
- Cysteine proteases
- Zinc proteases
- Carboxyl proteases

The serine proteases are endopeptidases with a reactive serine residue and an optimal pH condition around neutrality. Carboxyl proteases are endopeptidases carrying catalytically important carboxylates and best operate at low pH conditions. Cysteine proteases have cysteine residues instead of serine, while zinc proteases are metaloenzymes which operate optimally at neutral pH. Many of these proteases are small monomeric enzymes of M_r 15,000 to 35,000 and are very well understood due to ease of kinetic and structural studies (Fersht, 1998).

Proteases are found in large numbers in digestive systems and are involved in a wide range of important biological activities. Some viruses encode proteases that act in their maturation. Adenoviruses encode a cysteine protease; picornaviruses encode a serine protease; and retroviruses, such as HIV, encode an aspartyl protease (Babé and Craik, 1997). Proteases such as Protex 51FP, Protex 6L and Protex 7L have proven to be very efficient at extracting oil from soybean flakes, reaching 90% extraction rates (Wu et al., 2009).

1.1.8.1 Serine Proteases

The mammalian serine proteases have a common tertiary structure as well as a common function and their activities peak at around pH 7.8 and fall off at around pH 6.8. To begin with, the enzyme and substrate form a noncovalent enzyme-substrate complex which is held together by physical attractive forces. Then the first tetrahedral intermediate is formed by hydroxyl Ser-195 working on the substrate. The intermediate then collapses to give the acylenzyme and release the amine or alcohol (Fersht, 1998).

1.1.8.2 Cysteine Proteases

The plant enzymes papain, ficin, bromelain and actinidin are from the same structurally homologous family. In addition to these, there are five superfamilies of enzymes which have active-site cysteine. They include calpain, clostripain, picornavirus proteinase, streptococcal proteinase and interleukin-1--converting enzyme (Brocklehurst et al., 1998). It has been suggested by Fersht (1971) that the reactive form is $[RS^- \cdot ImH^+]$, where **Im** denotes the imidazole of the histidine and **RSH** denotes the cysteine.

1.1.8.3 Immobilisation

Proteases have been successfully immobilised on different carriers. Papain and chymotrypsin were immobilised onto the surface of copoly (ethylene / acrylic acid) fibre by Emi and Murase (1990). The activity of covalently immobilised proteases was found to be higher towards small ester substrates but lower towards casein which is a substrate with a higher molecular weight. The specific activity

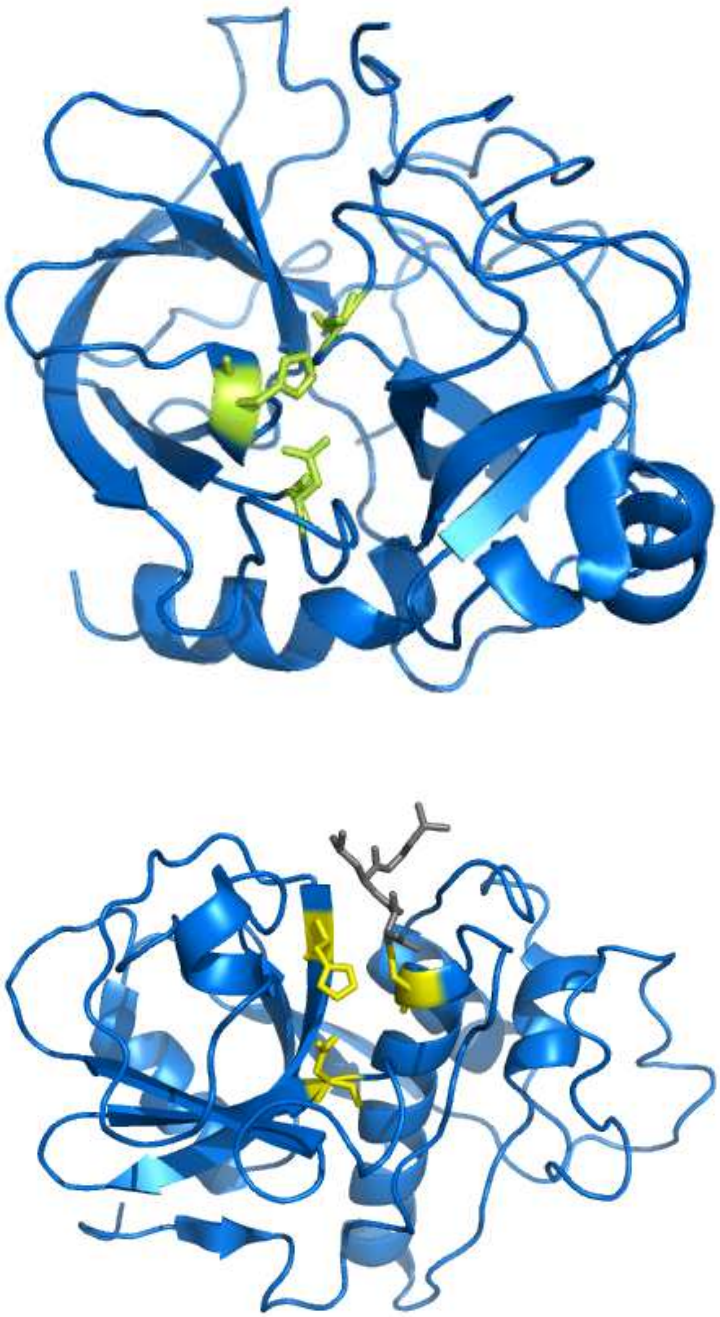

Figure 1.5: Crystal structure of two different proteases. Bovine chymotrypsin, a serine protease, with catalytic residues shown as yellow sticks at the top and papain, a cysteine protease, in complex with its covalent inhibitor E-64 at the bottom (Yamamoto et al., 1991).

was almost constant, while the thermal stability was higher than that of the ionic interaction or native protease. The durability of the enzymes were also increased. Ficin and bromelain have also been immobilised onto the surface of porous chitosan beads through covalent binding (Hayashi and Ikada, 1991). They behaved in similar fashion towards substrates with low and high molecular weights. The immobilised proteases exhibited and apparent rise in k_m values while registering lower V_m values compared to free enzymes. The pH, thermal and storage stability of the immobilised proteases had also increased.

1.2 Aim and Objectives

As described in Sections 1.1.3.1 most of the work to date on solid-liquid suspensions has focused on stirred bioreactor geometries at laboratory scales and above. Given the current trends to miniaturisation in early stage bioprocess development (DiMasi et al., 2003; Marques et al., 2009; Micheletti and Lye, 2006) there are significant gaps in our knowledge regarding processes involving solid-liquid suspension in particular in shaken systems (Section 1.1.2.2) and miniature ($< 0.5\ L$) stirred tank bioreactors (Lye et al., 2003; Micheletti et al., 2006). Given the increasing application of such systems in both the chemical and biochemical industries, it would be extremely beneficial to carry out a fundamental study of solid-liquid suspension in these small scale devices. Therefore, the aim of the thesis is to establish a fundamental engineering understanding of solid-liquid suspension behaviour at small scales in order to underpin approaches toward the high throughput evaluation, design and scale-up of bioconversion processes. The specific objectives necessary for reaching this aim are given below.

- Initial work will focus on measurement and modelling of solid-liquid suspension in shaken microscale bioreactors. High speed video and image analysis techniques will be used to observe and quantify particle suspension as a function of particle properties and shaking conditions. Attempts will be made to develop predictive correlations describing particle suspension and to show the influence the quality of the suspension has on immobilised enzyme kinetics. This work is presented in Chapter 3.

- Subsequent studies will address the application of Zweitering's correlation (Equation 1.11) to miniature and laboratory scale stirred tank bioreactors. Again, high speed video and image analysis will be used to measure and quantify particle suspension. This will be complemented by computational modelling of fluid flow in these bioreactors in order to explain the observed particle suspension behaviour and the influence on measured enzyme kinetics. This work is presented in Chapter 4.

- Finally comparisons of enzyme kinetic measurements across the two stirred bioreactor geometries and scales will be made in order to define appropriate criteria for scale translation. This work is presented in Chapter 5.

Chapter 6 provides an overall summary of the research findings and their likely impact on industrial bioprocesss development. Considerations for further work are also described.

Chapter 2

Materials and Methods

2.1 Chemicals and Suppliers

Reverse Osmosis (RO) water, prepared from a RiOs 16 Reveres Osmosis System (Millipore, Watford, UK) was used in all experimental work. All other chemicals used were of analytical grade and were obtained from Sigma-Aldrich (Dorset, UK). All the commercial adsorbents evaluated in this project were also purchased from Sigma-Aldrich, apart from IB-150 which was originally donated by ChiralVision (Lieden, Netherlands) and subsequently purchased from them in higher volumes. Immobilised Protex $6L^2$ was also purchased from ChiralVision.

2.2 Particle Preparation

XAD-7 and XAD-16 particles were wetted, as per the manufacturer's instructions, by transferring them to a 500 ml Erlenmeyer flask and by adding a sufficient amount of ethanol in order to cover the adsorbent bed. The flask was gently

stirred and left to stand for 30 *min*. The ethanol was then removed by decanting and the adsorbent covered by a sufficient amount of RO water, stirred and left to stand for a further 30 *min*. The adsorbent was then filtered and washed using several bed volumes of RO water. Finally, the adsorbent slurry was diluted in RO water and stored at 4 °C in an Erlenmeyer flask until use. IB-150 particles were wetted by transferring them to a 500 *ml* Erlenmeyer flask and by adding a sufficient amount of RO water in order to cover the particle bed. The solution was then stored at 4 °C in an Erlenmeyer flask until use. Particles were stored in this way for a maximum of 4 weeks before use.

2.3 Particle Characterisation

A Malvern Mastersizer 2000 (Malvern, UK) was used to measure the particle size distribution for each adsorbent. Samples prepared as described in Section 2.2 were used and three independent measurements were taken in order to determine the particle size distribution. The measurement principle of the Mastersizer is based on static light scattering (Horvath, 2009). To measure the density of each particle type, sample slurries were filtered from the RO water storage solutions through circular (47 mm ϕ) Whatman® GF/A filters (Banbury, UK) with a particle retention size of 1.6 μm. Each sample of adsorbent was then weighed and its volume measured by displacement using a measuring cylinder filled with a known volume of water. All particle size and density measurements were made in triplicate.

2.4 Bioreactor Geometries

2.4.1 Microwell Geometries

Three different mimics of single wells from commonly used microwell plate geometries were fabricated and used in this project for the purpose of suspension studies; one 24-standard round well (24-SRW) with a flat base, one 24-deep square well (24-DSW) with a pyramidal base and a 96-deep square well (96-DSW) with a pyramidal base. Each mimic was fabricated from poly(methyl methacrylate) (PMMA) for which the dimensions are given in Figure 2.1. All kinetic measurements were carried out in 24-DSW plates. Shaking was conducted using a Kühner Lab-Shaker LS-X (Basel, Switzerland) capable of variable shaking diameters ($1 - 50mm$) and shaking frequencies (maximum of 13.33 s^{-1}).

2.4.2 Stirred Bioreactor Geometries

The two stirred tank bioreactors used in this study were of two different scales. See Figure 2.2 for an schematic view of both bioreactors. One was a laboratory scale bioreactor with a nominal volume of 5.0 L and fabricated from glass. It's height was approximately twice its diameter, d_v. It was used in conjuncture with four equally spaced vertical baffles of width $d_v/10$ and thickness $\approx d_v/160$. A six-bladed Rushton turbine of diameter d_i, equal to $d_v/3$ was used, fixed at a clearance from the vessel bottom equal to $d_v/3$. The other was a miniature bioreactor with a nominal volume of 0.170 L and fabricated from glass. It's height was equal to its diameter, d_v. It was fitted with four equally spaced vertical baffles of

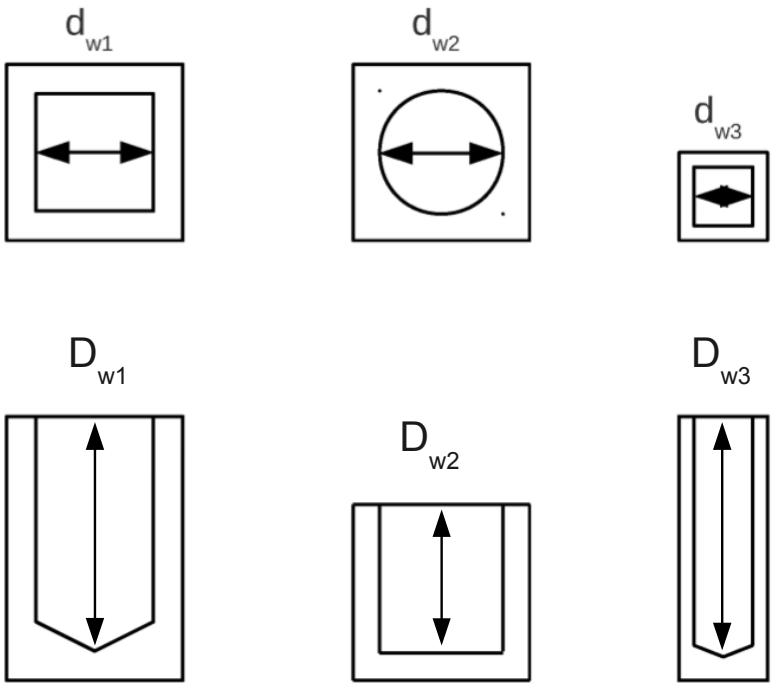

Figure 2.1: Schematic representation of the three microwell geometries used in this study; on the left 24-DRW for which $d_{w1} = 0.016\ m$ and $D_{w1} = 0.04\ m$, in the middle 24-SRW for which $d_{w2} = 0.017\ m$ and $D_{w2} = 0.016\ m$ and on the right 96-DSW for which $d_{w3} = 0.008\ m$ and $D_{w3} = 0.04\ m$.

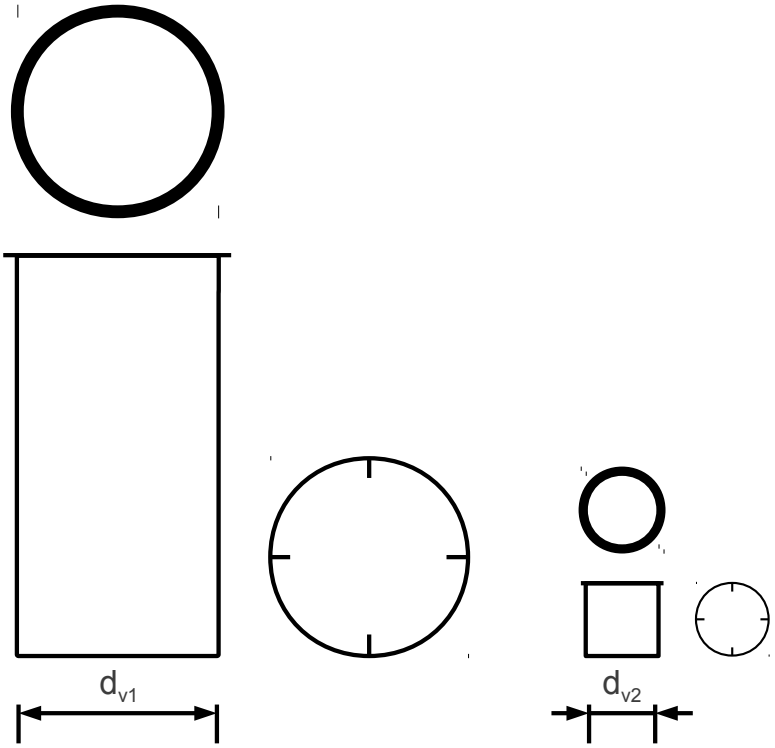

Figure 2.2: Schematic representation of the two stirred tank geometries and their respective baffles used in this study; on the left laboratory scale bioreactor for which $d_{v1} = 0.164\ m$ and on the right miniature scale bioreactor for which $d_{v2} = 0.06\ m$.

width $d_v/10$ and thickness $\approx d_v/60$. A six-bladed Rushton turbine of diameter d_i, equal to $d_v/3$ was used, fixed at a clearance from the vessel bottom equal to $d_v/3$.

In both cases, the working volume was fixed so that the liquid height inside the reactor would be equal to its diameter. This meant a working volume of 0.170 L and 3.5 L for the miniature and laboratory scale bioreactors respectively. Stirring was conducted using an overhead EUROSTAR digital electric motor (IKA®, Staufen, Germany).

2.5 Characterisation of Stirred Bioreactor Power Input

The Power Numbers of the different turbines used in this study were measured using two differently sized air bearing dynamometer (University College London, UK); the setup is similar to that described by Nienow and Miles (1969). In each case, the air bearings consisted of two main elements: one static (lower section) and the other a floating top plate (upper section), air was introduced into the static section, enabling free and essentially frictionless movement of the top plate. The resulting torque generated by the rotating stirrer in the liquid caused the vessel to freely rotate with the top plate in the same direction as the impeller. A rigid arm that was fixed to the top plate of the air bearing enabled the torque to be measured as a force transmitted to a pre-calibrated force sensor (FS Series, Honeywell, USA). From these measurements the power draw can be calculated

from Equation 2.1

$$P = FR\omega, \tag{2.1}$$

where P is the power, F is the applied force, R is the length of the arm pressing against the force sensor and ω is the angular velocity given by:

$$\omega = 2\pi N_s, \tag{2.2}$$

where N_s is the stirring frequency.

2.5.1 Miniature Scale Reactor

The glass vessel from the small bioreactor containing four equidistant baffles and filled with 0.170 L of RO water was mounted onto the top plate of the small air bearing dynamometer (96 mm ϕ). The turbine was then located vertically in the vessel and, in order to facilitate power measurement, this was driven with an overhead electric motor and positioned so that the distance from the bottom of the vessel was 20 mm. Turbine dimensions can be found in Figure 2.3. All instances of power measurement were carried out in triplicate with a maximum variance of 3.8%.

2.5.2 Laboratory Scale Reactor

The glass vessel from the large bioreactor containing four equidistant baffles and filled with 3.5 L of RO water was mounted onto the top plate of the large air bearing dynamometer (250 mm ϕ). The turbine was then located vertically in the

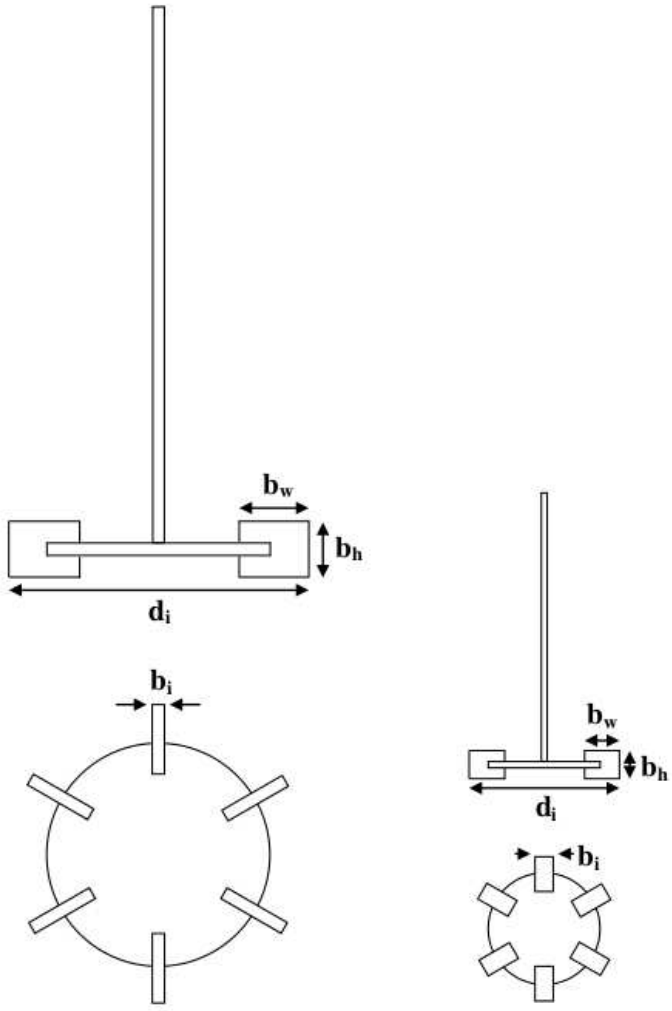

Figure 2.3: Schematic representation of the two Rushton turbines used in this study; on the left is the turbine used in conjuncture with the laboratory scale vessel for which $d_i = 0.0547\ m$, $b_i = 0.0012\ m$, $b_h = 0.008\ m$ and $b_w = 0.012\ m$. On the right is the turbine used in conjuncture with the miniature scale vessel for which $d_i = 0.02\ m$, $b_i = 0.002\ m$, $b_h = 0.004\ m$ and $b_w = 0.005\ m$.

vessel and, in order to facilitate power measurement, was driven with an overhead electric motor and positioned so that the distance from the bottom of the vessel was 54.7 mm. Turbine dimensions can be found in Figure 2.3. All instances of power measurement were carried out in triplicate with a maximum variance of 4.5%.

2.6 Visualisation of Particle Suspension

2.6.1 Shaken Systems

High speed video capture was achieved using a Vision Research Phantom V5.1 camera (Wayne, NJ, USA) courtesy of the EPSRC Equipment Loan Pool. The camera was attached to the shaking platform in order to provide a fixed frame of reference, as shown in Figure 2.4. Image data used for quantitative analysis of particle suspension and dispersion was recorded for different combinations of particle density (ρ_p), well geometry (d_w), liquid fill volume (V_f), solid volume fraction (S_f), shaking diameter (d_s) and shaking frequency (N_s). Recording was carried out, at 60 fps, from the moment the shaking platform was switched on until a steady-state particle suspension was achieved. The resulting individual frames were then read into an image analysis code, as described in Section 2.7.1.

2.6.2 Stirred Systems

Hi speed video capture was achieved using a Canon 7D camera (Ōta, Tokyo, Japan). The camera was placed under the vessel in order to record, at 60 fps, an image looking at the bottom of the tank, as shown in Figure 2.5. Image data used

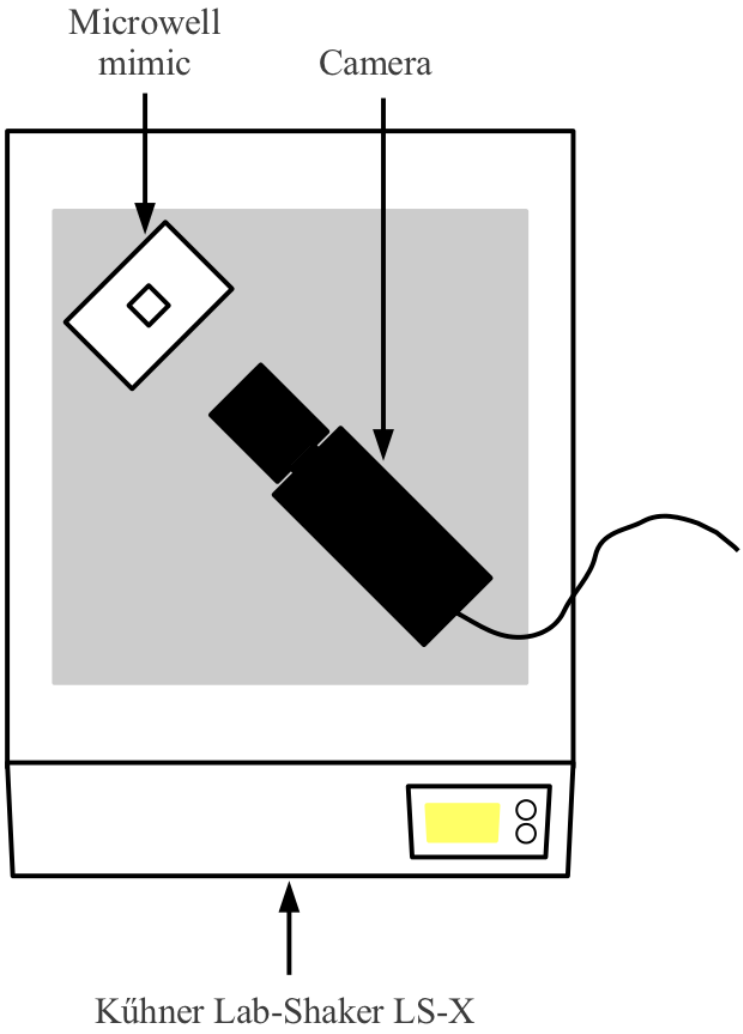

Figure 2.4: Experimental configuration used in visualisation of particle suspension in shaken systems.

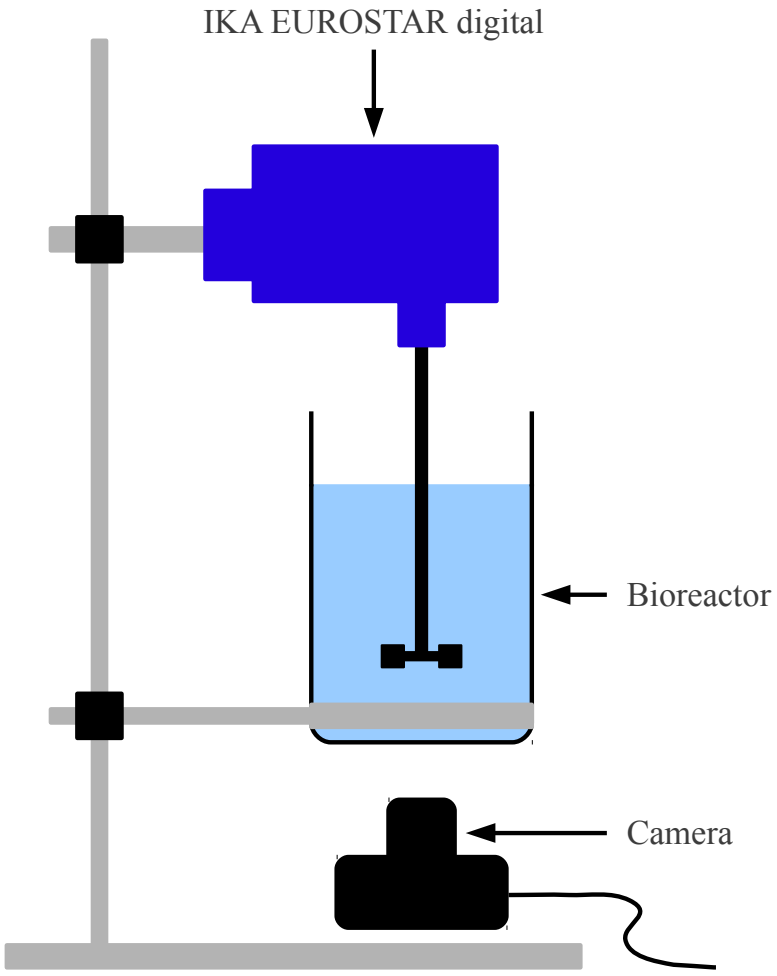

Figure 2.5: Experimental configuration used in visualisation of particle suspension in stirred systems.

for quantitative analysis of particle suspension and dispersion was recorded for different combinations of particle density (ρ_p), tank geometry (d_v), solid volume fraction (S_f), turbine diameter (d_i) and stirring frequency (N_s). Recording was carried out in two stages. The first stage was from the moment the stirrer was switched on until 20 s was passed. The recording was then stopped and switched back on again after 3 min had elapsed and continued for a further 25 s. Initial experiments showed that equilibrium particle suspension had been achieved by this time. The individual frames were then read into an image analysis code, as described in Section 2.7.2.

2.7 Quantification of Particle Suspension

2.7.1 Shaken Systems

A MATLAB (MathWorks, Cambridge, UK) routine was written to automatically identify circular particles in the high speed video images acquired as described in Section 2.6.1. The routine also counts the number of such objects in each individual frame. The process starts by opening an image file, mapping all its pixels on a Cartesian coordinate system and storing its intensity information, pixel by pixel, in a matrix. The information matrix is then cropped to the edge of the inner walls of the microwell mimic in order to reduce the time it takes to process a single frame. The matrix is then filtered by subtracting a noise mask, built from a noise model, based on the noise pattern of the original image. The next step is the construction of a circumference mask in order to identify potential particles. This is done by drawing a circle in a matrix with a diameter close to

the mean diameter of the target particles, given in Table 3.1. This mask is then used to filter the original image matrix using convolution techniques. The matrix is then converted to black and white by using its own average as the grey point followed by removal of any feature that is smaller than 50 pixels, i.e. considering them as noise. Each distinguishable object is then labelled and its corresponding pixels found. These pixels are then filtered through in order to find the maximum intensity within each group. These intensity values are then used to further narrow the range of potential particles as their average intensity will be higher than the rest of the objects due to convolution with the circumference mask. Finally, the matrix is filtered through and objects whose silhouette closely mirrors that of a circle are separated from the rest and their numbers are counted. The above procedure is carried out for all images (usually >1400 frames) captured during a given experiment.

2.7.2 Stirred Systems

A MATLAB routine was written to automatically process the high speed video images acquired as described in Section 2.6.2. The process starts by opening the first image in a sequence, mapping all its pixels on a Cartesian coordinate system and storing its intensity information, pixel by pixel, in a matrix. The information matrix is then cropped to the edge of the tank in order to reduce the time it takes to process a single frame. This information is then used to calculate a global gray threshold value, between 0 and 1, necessary to carry out further analysis. Consecutive images, set to a predefined time-step, are opened,

their pixels are mapped on a Cartesian coordinate system and their intensity information stored pixel by pixel. Then, from each image, eight identical crops are made and converted to grayscale using the previously calculated gray threshold. All the identical crops from either of the two images are then compared for any difference in their intensity values and the difference is articulated using a number between 0 and 1. This procedure is carried for all images (usually >900 frames) captured during this sequence for all the experiments. Although these areas remained the same for each individual experiment, they varied across different experiments as to make the quantification more accurate. This was necessary due to variation of the areas on which particles would concentrate on the bottom of the tank in different experiments.

2.8 Computational Modelling of Stirred Tank Bioreactor Hydrodynamics

All simulations were carried out using COMSOL Multiphysics® (COMSOL Group, Stockholm, Sweden), which provides the facilities for all the steps in the modelling process - definition of geometry, meshing, specification of physics, solving and visualising the results. Availability of predefined physics interfaces allow quick modelling of many different problems. Two different simulations were carried out at each scale to look at the effects of stirring frequency on velocity field near the bottom of the tank. One experiment was conducted at both scale for low impeller speeds and solved with a laminar flow model. The Navier-Stokes equations solved for this laminar flow model are given in Equations 2.3 and 2.4

for continuity and momentum respectively. The continuity equation is given in compressible form.

$$\frac{\partial \rho}{\partial t} + \nabla \cdot (\rho \mathbf{u}) = 0 \tag{2.3}$$

$$\rho \frac{\partial \mathbf{u}}{\partial t} + \rho \mathbf{u} \cdot \nabla \mathbf{u} = -\nabla p + \nabla \cdot \left(\mu(\nabla \mathbf{u} + (\nabla \mathbf{u})^T) - \frac{2}{3}\mu(\nabla \cdot \mathbf{u})\mathbf{I} \right) + \mathbf{F} \tag{2.4}$$

For simulating high impeller speed in the miniature scale reactor a laminar method was used with equation similar to the ones given above. Flow induced at high impeller frequency was simulated in the laboratory scale reactor by using a Reynolds-averaged Navier-Stokes (RANS) model. In this model, the continuity and momentum equations take the form given by Equations 2.5 and 2.6.

$$\rho \nabla \cdot \mathbf{u} = 0 \tag{2.5}$$

$$\rho \frac{\partial \mathbf{u}}{\partial t} + \rho(\mathbf{u} \cdot \nabla)\mathbf{u} = \nabla \cdot \left[-p\mathbf{I} + \mu(\nabla \mathbf{u} + (\nabla \mathbf{u})^T) \right] + \mathbf{F} \tag{2.6}$$

The turbulence model used was the standard $k - \epsilon$ model. This model introduces two additional transport equations and two independent variables: the turbulent kinetic energy, k, and the dissipation rate of turbulent energy, ϵ. Turbulent viscosity was modelled by Equation 2.7.

$$\mu_T = \rho C_\mu \frac{k^2}{\epsilon}, \tag{2.7}$$

where C_μ is a model constant.

The transport equations for k and ϵ are given by Equations 2.8 and 2.9 respectively.

$$\rho\frac{\partial k}{\partial t} + \rho\mathbf{u}\cdot\nabla k = \nabla\cdot\left(\left(\mu + \frac{\mu_T}{\sigma_k}\right)\nabla k\right) + P_k - \rho\epsilon \tag{2.8}$$

$$\rho\frac{\partial \epsilon}{\partial t} + \rho\mathbf{u}\cdot\nabla \epsilon = \nabla\cdot\left(\left(\mu + \frac{\mu_T}{\sigma_\epsilon}\right)\nabla \epsilon\right) + C_{\epsilon 1}\frac{\epsilon}{k}P_k - C_{\epsilon 2}\rho\frac{\epsilon^2}{k} \tag{2.9}$$

where $C_\mu = 0.09$, $C_{\epsilon 1} = 1.44$, $C_{\epsilon 2} = 1.92$, $\sigma_k = 1.0$ and $\sigma_\epsilon = 1.3$.

In order to solve these flow models, a three-dimensional model of the each reactor geometry, complete with impeller and baffles, was drawn to scale using COMSOL's internal geometry module. This domain was then discretised using tetrahedral mesh elements with two different mesh sizes; a finer mesh size was used to discretise the area surrounding the impeller and baffles and a coarser mesh size was used to discretise the rest of the domain. An example of a meshed domain, corresponding to the laboratory scale reactor, is given in Figure 2.6. The meshing algorithm was refined for fluid dynamics. For further information on mesh properties see Table 2.1.

In case of the miniature scale reactor, the simulation for high impeller speed was carried out at 21.67 s^{-1}, while the low impeller speed simulation was conducted at 5 s^{-1}. These figures were respectively 6.67 s^{-1} and 0.83 s^{-1} for the laboratory scale reactor.

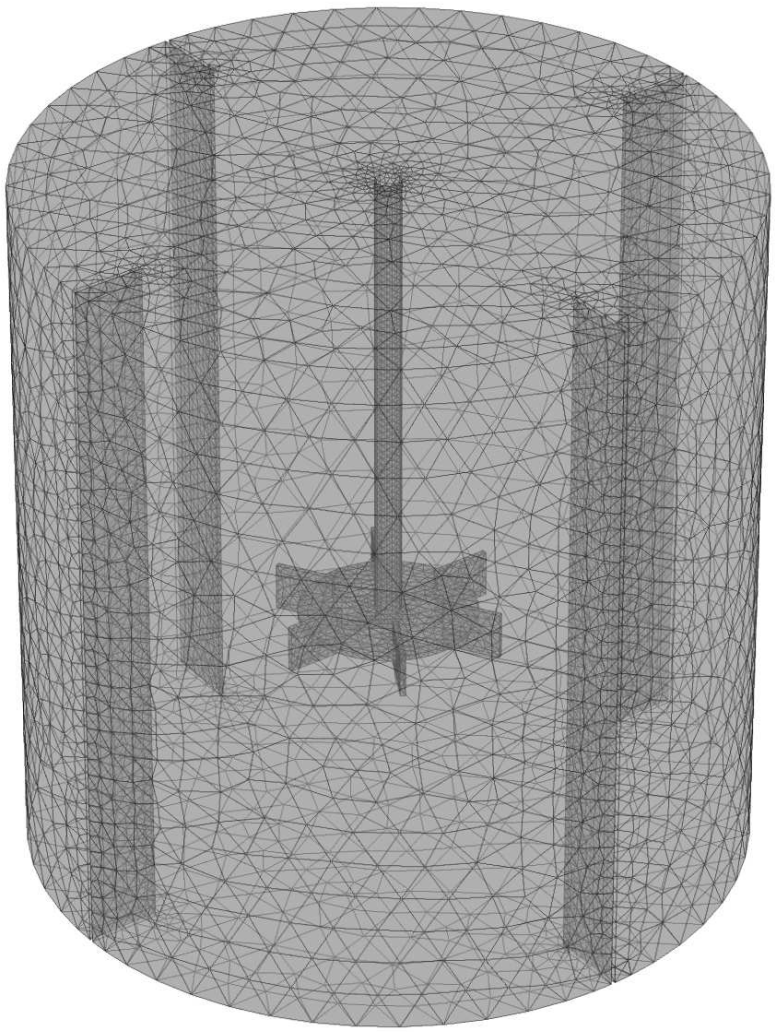

Figure 2.6: The mesh used to simulate the flow inside the laboratory scale reactor, showing higher mesh density around the impeller and baffles. Mesh generated using COMSOL's internal meshing module.

Table 2.1: Properties of the different types of mesh used in various simulations. Mesh generated using COMSOL's internal meshing module.

	Maximum element size m	**Minimum element size** m	**Maximum element growth rate**	**Resolution of curvature**	**Resolution of narrow regions**
Small (M_1)	0.01	0.00024	1.4	0.4	0.7
Small (M_2)	0.004	0.00189	1.5	0.6	0.5
Large (M_1)	0.01	0.00164	1.45	0.5	0.6
Large (M_2)	0.004	0.00295	1.5	0.6	0.5

2.9 Measurement of Enzyme Kinetics

2.9.1 Transketolase Bioconversion

2.9.1.1 Transketolase Production and Purification

His_6-tagged wild-type *E. coli* transketolase (TK) was produced by over-expression from *E. coli* XL10-Gold containing the engineered plasmid pQR791 (kindly supplied by Prof. John Ward, Institute of Structural and Molecular Biology, UCL).

All fermentations were performed using a Luria Bertani (LB) media. LB media was prepared by dissolving 10 gL^{-1} NaCl, 10 gL^{-1} tryptone and 5 gL^{-1} yeast extract in deionised water and the pH set to 7 with 1 M NaOH. The LB media was then sterilised by autoclaving. LB agar was prepared by mixing 15 gL^{-1} of agar in LB medium and autoclaving the agar preparation. This autoclaved agar preparation was then allowed to cool down to $\approx 55\,^{\circ}C$ and mixed with ampicillin

at a final concentration of 150 $\mu g m L^{-1}$. Each standard petri dish was filled with $\approx 20\ mL$ of LB agar and allowed to set.

A culture from a frozen glycerol stock was streaked on a petri dish of LB agar and the dish incubated overnight at 37 °C. A single *E. coli* colony was picked from the plate and transferred to a 250 mL shake flask containing 20 mL of LB medium. The flask was incubated for $\approx 16\ h$ while shaking at 250 rpm using a SI 50 Orbital Shaker (Stuart Scientific, Redhill, UK). Finally, 20 mL of this culture was transferred to a 1 L shake flask containing 180 mL of LB medium.

Following overnight incubation at 37 °C and orbital shaking of 250 rpm, the broth was centrifuged for 10 min at 4000 rpm and the supernatant decanted. To purify the intracellulary synthesised TK, the pellet was re-suspended in binding buffer of 500 mM NaCl, 20 mM Tris-HCL and 5 mM Imidazole at pH 7. Following sonication of the pellet to disrupt the cells, the lysate was centrifuged at 5000 rpm at 4 °C to remove cell debries. The TK-containing supernatant was recovered and added to an appropriate amount of His-Select® Nickel Affinity Gel (Sigma-Aldrich, Dorset, UK) and gently mixed on an orbital shaker at 175 rpm for 15 min. The mixture was then centrifuged at 5000 rpm for 5 min and the supernatant removed. 10 volumes of equilibration buffer containing 50 mM Na_3PO_4, 300 mM NaCl and 10 mM Imidazole at pH 7.5 was added to the affinity gel, mixed at 175 rpm for 4 min on an orbital shaker and centrifuged at 5000 rpm for 5 min. Elution of the bound TK was performed by adding 2 volumes of elution buffer containing 1 M Imidazole, 500 mM NaCl and 20 mM Tris-HCL to the affinity gel. Finally the supernatant was dialysed for 24 hours against 250

mM Tris-HCL at pH 7.5 and 4 °C.

2.9.1.2 Transketolase Immobilisation and Bioconversion

Enzyme immobilisation was carried out by first mixing 0.225 ml of TK solution, obtained as described in Section 2.9.1.1, with 1.35 ml of cofactor solution containing 2.4 mM thiamine diphosphate (TPP) and 9 mM $MgCl_2$ at pH 7. This solution was then left to incubate for 20 min. 0.075 g of IB-150 particles were then added to this solution and the mixture was shaken at room temperature over night. Finally the beads were washed with the same buffer used in subsequent bioconversion studies. All immobilised TK preparations were carried out using freshly purified TK and used within two days.

All immobilised enzyme bioconversions were carried out in 24-DSW plates using a range of shaking frequencies and diameters used in the particle suspension studies (Section 2.6.1). The equivalent of 0.075 g of IB-150 beads was added to 3.425 ml of substrate solution ($S_f = 2.5\%$) containing 50 mM β-hydroxypyruvate acid (HPA) and 25 mM glycolaldehyde (GA), pH 7, to start the reaction. Reactions were sampled at equal intervals of 30, 60 and 120 min. All reactions were quenched by addition of 0.180 ml of 0.1% v/v trifluoroacetic acid (TFA) at appropriate time points and prior to HPLC analysis (Section 2.10.1).

2.9.2 Protex 6L^2 Bioconversion

Protex 6L^2 was purchased immobilised on IB-150 adsorbents from ChiralVision and no further work was needed to prepare them for use in reactions. The im-

mobilised enzyme bioconversions were carried out in stirred tank reactors using a range of stirring frequencies and two different tank and turbine sizes described in Section 2.4.2. All reactions were quantified as described in Section 2.10.2. All reactions carried out in this section yield an acidic product, thus decreasing the pH value of the reaction media as time goes on.

Initial reactions, aimed at establishing the effects of particle suspension on enzyme reaction kinetics were carried out in the miniature scale reactor. These were conducted by adding the equivalent of 0.66 g of dry IB-150 adsorbents carrying Protex 6L^2 and the equivalent of 0.66 g of dry IB-150 adsorbents with no enzyme attached to 165.75 ml of substrate solution ($S_f = 2.5\%$) containing 41.44 ml of 100 mM KH_2PO_4, 74.58 ml RO water and 49.725 ml of 98% (−)-Ethyl L-lactate, pH 6.8. A further set of experiments, aimed at studying the effects of scale-up on enzyme reaction kinetics, was conducted in the miniature tank by adding the equivalent of 0.264 g of dry IB-150 adsorbents carrying Protex 6L^2 and 1.056 g of dry IB-150 adsorbents with no enzymes attached to a substrate solution prepared as described above.

A further set of reactions was carried out to establish the effects of particle suspension on enzyme reaction kinetics in the laboratory scale tank. These were conducted by mixing the equivalent of 13.63 g of dry IB-150 adsorbents carrying Ptotex 6L^2 and 13.63 g of dry IB-150 adsorbents with no enzymes attached. This mixture was then added to 3412.5 ml of substrate solution ($S_f = 2.5\%$) containing 853.13 ml of 100 mM KH_2PO_4, 1535.63 ml RO water and 1023.75 ml of 98% (−)-Ethyl L-lactate, pH 6.8. A final set of experiments, aimed at studying the

effects of scale-up on enzyme reaction kinetics, was conducted in the laboratory bioreactor by adding the equivalent of 5.452 g of dry IB-150 adsorbents carrying Protex 6L[2] and 21.808 g of dry IB-150 adsorbents with no enzymes attached to a substrate solution prepared as described above.

2.10 Quantification of Immobilised Enzyme Kinetics

2.10.1 HPLC System

A Dionex (Camberley, UK) Microbore HPLC system controlled by Peaknet 5.1 software was employed for all HPLC analysis. The system comprised of a GP40 gradient pump, an LC30 column oven, a PC10 pneumatic controller and a AD20 UV detector module. A multiwell plate autosampler (Spark, Emmen, NL) was integrated into the Dionex system.

A 15 min isocratic assay was adapted from an existing HPLC assay for the TK reaction components (Mitra and Woodley, 1996). HPLC analysis of GA, β-HPA and L-erythrulose was carried out using an Aminex 87H column (Bio-rad, Hemel Hempstead, UK) at 60 °C, mobile phase 0.1% v/v TFA, flow rate 0.6 $mlmin^{-1}$. The detection was via a UV detector at 210 nm. Samples were quenched and diluted with 0.1% v/v TFA. Retention time was 8.40 min for β-HPA and 11.40 min for L-erythrulose. The progress of the reaction was followed by the appearance of L-erythrulose product, the peak area of which was used in

all the subsequent analyses. In order to obtain L-erythrulose concentrations from these peak areas, a calibration curve was produced by running an HPLC analysis on known concentrations of L-erythrulose under similar conditions as described here. This calibration curve is given in Appendix C.

2.10.2 pH-stat System

The pH value of Protex $6L^2$ reactions were monitored and kept at a constant value of 6.8 using a 902 Titrando (Metrohm, Runcorn, UK) equipped with a 20 *ml* dosing unit and controlled remotely through the *tiamo*^{TM} software (Metrohm, Runcorn, UK). 0.5 *M* NaOH was used as the titrant reagent in all cases. The pH of the reaction was monitored from the start of mixing and the consumption of NaOH recorded for a period of 5 *min*. Titration flow was set to the maximum permissible rate. The specific activity of the enzyme was then calculated by Equation 2.10.

$$S_a = \frac{T_c \times T_m \times 1000}{M_e}, \tag{2.10}$$

where, S_a is the specific enzyme activity, T_c is the rate of titrant consumption, T_m is the concentration of titrant and M_e is the mass of enzyme carriers which was used to run the reaction.

Chapter 3

Solids Suspension in Shaken Miniature Bioreactors

3.1 Introduction and Aims

As described in Section 1.1.1, the need for rapid, parallel and automated bioprocess development has led to an increased interest in miniature and micro-litre scale bioreactor technologies. One prerequisite of this approach is to be able to understand such devices from an engineering perspective in order to ensure reliable qualification of bioprocess parameters and their relation to larger scale bioreactors. Although some work has been carried out in this regard, such as measurement of oxygen transfer rates (OTR) in single-phase systems (Hermann et al., 2003) or measurement of gas-liquid mass transfer coefficients (k_La) in various round-well geometries (Doig et al., 2005), there still remain many unexplored characteristics, particularly for multi-phase systems (Section 1.1.2.2).

The aim of this chapter is to develop predictive correlations describing particle suspension in shaken bioreactors and to show how the quality of suspension influences

the quantification of immobilised enzyme kinetics. The specific objectives include:

- Visual observation and recording of the suspension process at various combinations of operating conditions such as well geometry, shaking diameter and frequency and particle density by employing high speed imaging equipment.
- Automated quantification of this visual data by creation of an image analysis routine in order to quantify the percentage of particles in suspension.
- Correlation of the results into a mathematical formulation in order to make the prediction of shaking frequency required to achieve full suspension for a given set of operating conditions possible.
- Quantification of the influence of suspension quality on the kinetics of an immobilised enzyme bioconversion.

Transketolase will be used in immobilised enzyme kinetics determination. The selection was made due to its application in various biocatalysis processes such as carbon-carbon bond synthesis (André et al., 1998; Brocklebank et al., 1999; Woodley et al., 1995; Zimmermann et al., 1999).

3.2 Selection of Particles and Operating Conditions

A broad range of particles used in various bioprocess applications (Kallenberg et al., 2005; Kourilov and Steinitz, 2002) were initially considered with regard to their physical characteristics such as size, shape and density. Table 3.1 shows the final list of particles selected for this study which are representative of those surveyed. The chosen particles provide a suitable range of sizes and densities either close to, greater

than or less than that of water. The only type of particle not represented here are the dense composite particles ($\rho > 1.33 gml^{-1}$) developed specifically for expanded bed adsorption applications (Lan et al., 1999; Tong and Sun, 2002). The solids volume fraction, S_f, was varied between 0.1% and 2.5%. The largest value of 2.5% corresponded to typically used immobilised biocatalyst concentrations in stirred bioreactor applications.

Table 3.1: Physico-chemical characteristics of the particles used in this study. Physical properties taken from the manufacturer's literature or measured as described in Section 2.3.

Particle	**Chemical nature**	**Nominal particle diameter** *mm*	**Measured particle diameter** *mm*	**Nominal wet density** gml^{-1}	**Measured wet density** gml^{-1}
XAD-7	acrylic ester	0.251-0.853	0.360-1.090	n/a	1.33
XAD-16	polyaromatic	0.251-0.853	0.250-1.050	1.02	1.092
IB 150	acrylic polymer	0.150-0.300	0.138-0.316	n/a	0.81

n/a: not available

Microwell geometries were selected based on the popularity of the available formats for bioprocess studies (Micheletti et al., 2006; Singh et al., 2003). These tend to rely on larger well sizes than used for high throughput drug discovery, i.e. 384 and 1536 well plates, because of the need for sampling and bioprocess kinetics determination (Lye et al., 2003). Shaking diameters were chosen in order to provide a wide range of operating conditions and also match the shaking diameters of most commercial laboratory shaking platforms. These, almost universally provide an orbital shaking motion which was studied here.

Once the initial parameter ranges had been finalised, single liquid phase experiments were performed in order to establish the maximum fill volume for each microwell geometry as a function of shaking frequency and diameter. Water was used in all experiments given that this has similar physical properties (density, viscosity, etc.) to the liquid media used in typical fermentation and bioconversion processes (Chen et al., 2009; Minier and Goma, 1982). The maximum fill volumes were determined using high speed video and represent the maximum liquid volume in each well geometry at which no breakage and/or splashing of the liquid surface occurs at a given shaking frequency and diameter.

3.3 Visualisation and Quantification of Particle Suspension Kinetics

In order to accurately quantify particle suspension a MATLAB routine (see Appendix A for full details) was initially developed to automatically analyse the experimental video images. The principles of image analysis and quantification approach are described in Sections 2.6.1 and 2.7.1. Representative images from the high speed video camera and the outputs from the MATLAB analysis are shown in Figure 3.1. The particles used were XAD-16 suspended at a shaking frequency of 5.92 s^{-1} and 0.003 m orbital shaking diameter in a 24-DSW mimic. The total well fill volume (solid + liquid, V_f) was 4.5 ml with a solids volume fraction of 0.1% v/v. The top row of images, Figure 3.1(a), show the development of fluid flow and particle suspension from the onset of shaking to $t \simeq 35$ s. Once shaking is started the surface of the liquid phase begins to deform ($t \simeq 18$ s) and the free surface is then seen to follow an orbital motion around the well, in-phase with the imposed orbital shaking. All particles are initially at the base of the

well ($\rho = 1.092\ gml^{-1}$), but are obscured from view in the first image due to the pyramidal base of the 24-DSW mimic. By $t \simeq 18\ s$ the particles are lifted off the base and are seen dispersed throughout the liquid phase both axially and radially. By the final frame ($t \simeq 33\ s$) a pseudo equilibrium state is reached where all particles are suspended.

The bottom row of images, Figure 3.1(b), shows the corresponding MATLAB analysis of each frame. The computational routine initially identifies the liquid surface but discards it during subsequent analysis since its aspect ratio does not fit the pre-defined criteria for circular particles (Section 2.7.1). It then identifies and counts all the particles seen visually in the images above. Careful analysis of the video images and the MATLAB outputs indicates that all particles, both those closer to the microwell wall as well as those within the bulk fluid are identified and counted at this solids volume fraction.

The rapid suspension of particles in shaken microwells is desirable so that the diffuse layer around them is rapidly reduced to such an extent as to reduce its limiting factor when such a system is used for quantification of immobilised enzyme kinetics for bioprocess design purposes (Chen et al., 2009). It is also important to identify conditions in which particles are fully suspended such that particle motion helps minimise any substrate mass transfer limitations. Further experiments were thus carried out to establish the kinetics of particle suspension over a wider range of shaking frequencies. Figure 3.2 summarises representative results for XAD-16 particle suspension in a 24-SRW mimic shaken at a diameter of 0.006 m with a total fill volume of 2 ml at 0.5% solid volume fraction. The shaking frequency was varied from a low value at which no particle suspension was achieved until the point at which breakage of the liquid surface was observed. The data points in Figure 3.2 correspond to MATLAB quantification of

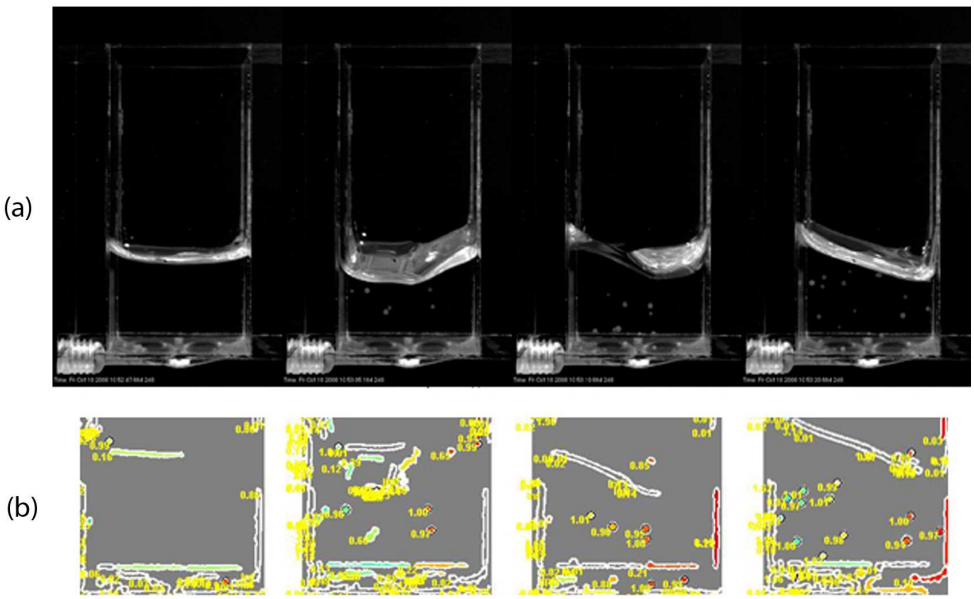

Figure 3.1: Sample video frames showing (a) the kinetics of particle suspension and motion of the liquid surface and (b) the corresponding MATLAB identification of particle suspension within the bulk fluid. Frames were taken at 0.25 s, 17.75 s, 23.25 s and 33.25 s after the start of shaking. Experiments performed as described in Section 2.6.1. Operating conditions: XAD-16, 24-DSW, $V_f = 4.5$ ml, $S_f = 0.1\%$ v/v and $d_s = 0.003$ m. Particle characteristics as described in Table 3.1.

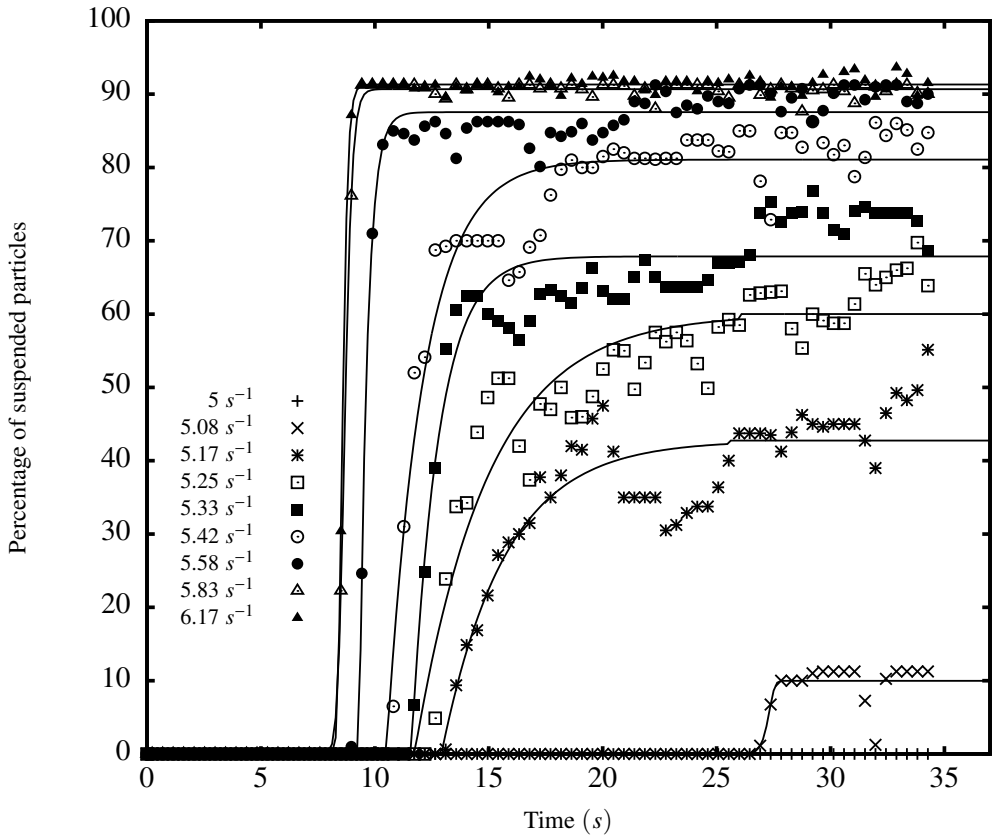

Figure 3.2: Kinetics of XAD-16 particle suspension as a function of shaking frequency. Number of particles quantified as described in Section 3.3 and solid lines fitted using Equation 3.1. Experimental conditions as described in Section 2.6.1. Operating conditions: XAD-16, 24-SRW, $V_f = 2.0\ ml$, $S_f = 0.5\%$ v/v and $d_s = 0.006\ m$. Particle characteristics as described in Table 3.1.

individual high speed video images. The solid lines were plotted using the sigmoidal relationship given by Equation 3.1:

$$y = y_o + \frac{a}{1 + e^{-\left(\frac{x - x_o}{b}\right)^c}} \tag{3.1}$$

where a, b and c are constants. Equation 3.1 was solved iteratively using SigmaPlot (Systat Software, Inc., CA, USA) by fitting it to the experimental data.

Figure 3.2 indicates that at low shaking frequencies no XAD-16 particle suspension is achieved. As the shaking frequency is increased, both the rate and the number of particles counted as being in suspension are seen to rise. For each shaking frequency a pseudo-steady state level of suspension is attained. At shaking frequencies above 5.83 s^{-1}, >90% of particles are suspended in less than 10 s. Visual observation also confirmed that in cases where >90% of particles were suspended, acceptable distribution of particles both axially and radially throughout the well was also achieved. These results demonstrate that for a given combination of particle characteristics and shaking conditions a minimum shaking frequency is required to ensure adequate suspension and dispersion of particles through the fluid in a microwell.

3.4 Steady State Particle Suspension and Dispersion

Having established in Section 3.3 a method for automatically quantifying particle suspension from the high speed video data, this was used to examine how the observed pseudo steady-state particle suspension (and dispersion) varied over a range of operating conditions. Based on analogy with stirred tank bioreactors and Zwietering's

correlation given in Equation 1.11, the following factors are likely to be the most important: particle density, well geometry, total fill volume and solid volume fraction. According to previous studies to quantify OTR and k_La in microwells, shaking frequency and shaking diameter are also likely to be critically important factors (Doig et al., 2005; Hermann et al., 2003).

Figure 3.3 summarises the effect of shaking frequency and diameter on the pseudo-steady state level of XAD-16 particle suspension quantified in each experiment. The solid lines were fitted as described earlier to the sigmoidal function expressed by Equation 3.2.

$$y = y_o + \frac{a}{1 + e^{-\left(\frac{x - x_o}{b}\right)}}, \tag{3.2}$$

where a and b are constants. These results indicate that at larger shaking diameters lower shaking frequencies are required to achieve >90% XAD-16 particle suspension. Again, for each orbital shaking diameter there is a minimum shaking frequency necessary to ensure the level of particle suspension likely to be necessary for accurate immobilised enzyme kinetics determination. These results follow very similar trends to those reported between OTR_{max} and shaking frequency and diameter in 96-well microwell plates (Hermann et al., 2003).

Figure 3.4 quantifies the influence of particle density on the percentage of suspended particles as a function of shaking frequency. The solid lines were fitted as described above using Equation 3.2. At the highest shaking frequencies the densest particle, XAD-7, attains a maximum of 80% suspension. Inspection of the video images suggests a proportion of the particles remain at the base of the well and are never suspended. In contrast, at equivalent or lower shaking frequencies, the two other par-

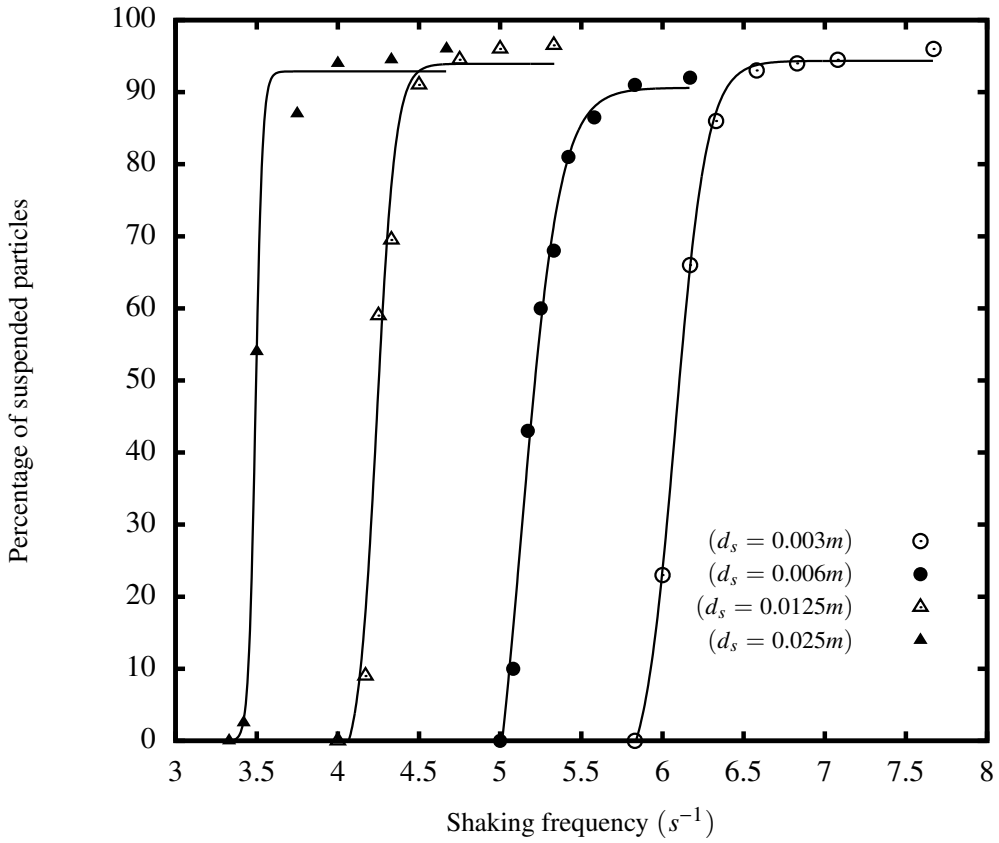

Figure 3.3: Steady state suspension of XAD-16 particles as a function of shaking diameter, d_s, and frequency. Solid lines fitted using Equation 3.2. Experimental conditions as described in Section 2.6.1. Operating conditions: XAD-16, 24-SRW, $V_f = 2.0\ ml$, $S_f = 0.5\%$ v/v. Particle characteristics as described in Table 3.1.

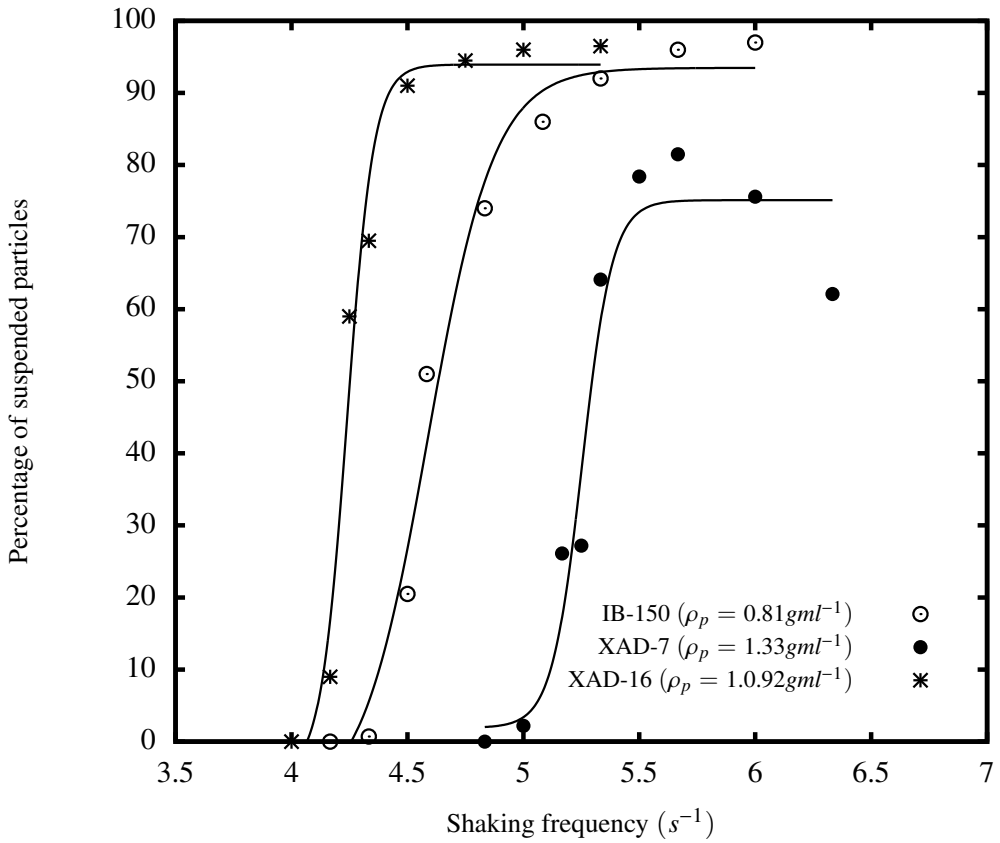

Figure 3.4: Steady state suspension of XAD-16 particles as a function of particle density, ρ_s, and shaking frequency. Solid lines fitted using Equation 3.2. Experimental conditions as described in Section 2.6.1. Operating conditions: 24-SRW, $d_s = 0.0125\ m$ $V_f = 2.0\ ml$, $S_f = 0.5\%$ v/v. Particle characteristics as described in Table 3.1.

ticle types, XAD-16 and IB-150, both reach pseudo-steady state conditions with >90% particle suspension. The IB-150 particles, despite being the lighter of the pair, are seen to require higher shaking frequencies to attain >90% suspension in the fluid phase.

To explain this it is important to consider the forces which are involved in particle suspension processes. The onset of suspension is reached once the vertical component of the drag force on a single particle is just smaller than its effective weight (Shamlou, 1993). The effective weight of a single particle is governed by Equation 3.3.

$$F_E = \left(\frac{\pi}{6}\right) \Delta\rho {d_p}^3 g, \tag{3.3}$$

where F_E is the effective weight, $\Delta\rho$ is the solid-liquid density difference, d_p is the particle diameter and g is the acceleration due to gravity. The drag force is generated by the liquid phase as it flows past the solid particles and is governed by the Equation 3.4 (Shamlou, 1993).

$$F_D = C_D \left(\frac{1}{2}\rho {U_{js}}^2\right) \left(\frac{\pi}{4}{d_p}^2\right), \tag{3.4}$$

where F_D is the drag force, C_D is the particle drag coefficient, ρ is the liquid density, U_{js} is the axial component of the local velocity near the base of the well and d_p is the particle diameter. Thus, the criterion for the onset of suspension of a single particle can be expressed by the relationship given in Equation 3.5 (Shamlou, 1993).

$$\frac{\left(\frac{\pi}{6}\right) \Delta\rho {d_p}^3 g}{C_D \left(\frac{1}{2}\rho {U_{js}}^2\right) \left(\frac{\pi}{4}{d_p}^2\right)} > 1. \tag{3.5}$$

Given Equation 3.5, it becomes apparent that although particle density is important suspension also relies upon the particle diameter and the drag coefficient. Therefore, as indicated in Table 1, the significantly smaller IB-150 particles are likely to require

higher shaking frequencies (faster liquid velocities) to generate a sufficient drag force in order to compensate for their smaller size, which is confirmed by Figure 3.4

Figure 3.5 illustrates the influence exerted by fill volume on the number of particles suspended at different shaking frequencies. Although the range of fill volumes examined is small, but they correspond to typically used values (Barrett et al., 2010). It is clear that although there is small variation in kinetics of suspension, the steady state conditions are not influenced by variation in fill volume by any significant degree.

Although it was not possible to quantify the influence of well geometry on steady state particle suspension as it was not possible to change this variable without changing liquid height (representing fill volume), qualitative comparison of cases that offered relatively similar ratios between the two (d_w/h_L) showed that near-full ($> 90\%$) suspension occurred at lower shaking frequencies in 24-DSW than in 24-SRW (see Figure B.3) while 96-DSW required significantly higher shaking frequencies at similar shaking diameters. It has been suggested by Micheletti et al. (2006) that the corners in a square well can act similar to baffles in stirred tank bioreactors, promoting higher mixing performance. This is similar to influence of baffling on oxygen transfer rates (Funke et al., 2009; Hermann et al., 2003).

3.5 Relationship Between Fluid Hydrodynamics and Particle Suspension

Results in Sections 3.3 and 3.4 have shown that the factors which influence the rate and extent of particle suspension under pseudo-steady state conditions in shaken microwells are similar to those influencing particle suspension in stirred tank reactors (Zwietering,

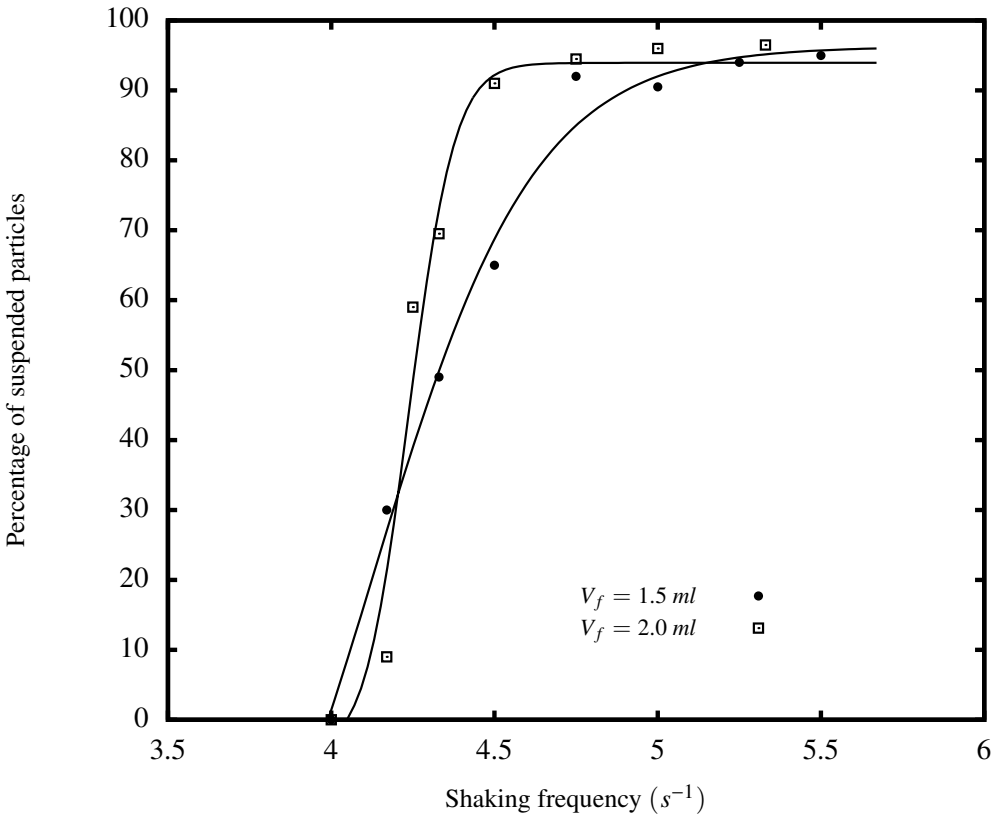

Figure 3.5: Steady state suspension of XAD-16 particles as a function of fill volume, V_f, and shaking frequency. Solid lines fitted using Equation 3.2. Experimental conditions as described in Section 2.6.1. Operating conditions: XAD-16, 24-SRW, $d_s = 0.0125\ m$ $S_f = 0.5\%$ v/v. Particle characteristics as described in Table 3.1.

1958). The primary, or most significant factors include well geometry, particle density, shaking frequency and shaking diameter. Less significant or secondary factors include total fill volume and solid volume fraction at least over the ranges investigated. Figure 3.6 presents a flow pattern map that attempts to summarise fluid flow and XAD-16 particle suspension in a 24-SRW as a function of orbital shaking diameter and microwell Reynolds Number. This identifies different particular particle suspension regimes and the operating boundaries for microwell experimentation where full particle suspension (defined here as >90%) is achieved within 15 s.

Data points in Figure 3.6 represent the calculated Reynolds Numbers for conditions studied at each orbital shaking diameter. The solid lines are based on observation of high speed video footage and the quantified level of pseudo-steady state particle suspension. These represent clearly identifiable transitions in both fluid flow and particle suspension behaviour. As can be seen in Figure 3.6 there exists a relatively narrow operating window in which full suspension of particles can be achieved and where it appears feasible to study the kinetics of immobilised enzyme bioconversions (Woodley and Titchener-Hooker, 1996). For each orbital shaking diameter these favourable suspension conditions occur close to the upper boundary where breakage of the free liquid surface and splashing occurs. Similar flow pattern maps can be drawn for different microwell geometries and for particles of different density. In general these indicate that the available operating window for immobilised bioconversion studies decreases with increasing particle density and for lower volume microwells.

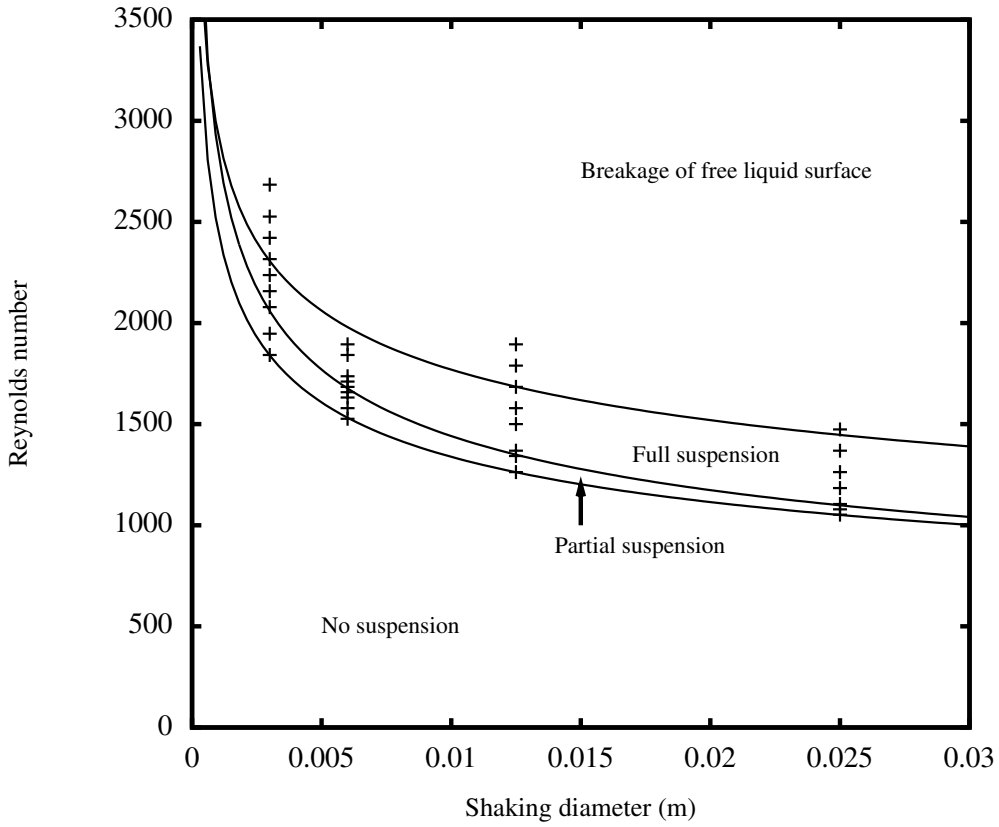

Figure 3.6: Flow pattern map of steady state XAD-16 particle suspension as a function of Reynolds number and shaking diameter. Solid lines represent transition between different suspension regimes based on quantitative analysis of high speed video images. Experimental conditions as described in Section 2.6.1. Operating conditions: XAD-16, 24-SRW, $V_f = 2.0\ ml$, $S_f = 0.5\%$ v/v. Particle characteristics as described in Table 3.1.

3.6 Modeling and Prediction of Particle Suspension

While Figure 3.6 provides a graphical indication of suitable microwell operating conditions it would be useful to be able to predict a priori conditions where >90% particle suspension can be achieved. This would facilitate the rapid establishment of shaking conditions for the study of different immobilised enzyme preparations as described later in Section 3.7. Based on the experimental results shown in Figures 3.1 to 3.6, a wide range of parameters will determine the quality of particle suspension. These include microwell diameter (d_w), liquid height (representing fill volume) (h_L), orbital shaking diameter (d_s), shaking frequency (N_s), particle diameter (d_p), particle density (ρ_p), liquid density (ρ), kinematic viscosity (ν), solid to liquid volume fraction (S_f) as well as the acceleration due to gravity (g), which represents the force acting against particle suspension. From these ten parameters, a set of seven dimensionless groups can be formed that allows for independent variation of these parameters during experiments. According to Zwietering (1958) graphical analysis of the experimental data should lead to the discovery of a relation similar to the one given in Equation 3.6.

$$N = K_1 {d_w}^a {d_s}^b {d_p}^c {S_f}^e \tag{3.6}$$

for constant d_w to h_L ratios. Substituting the dimensionless groups related to each parameter into the above equation and rearranging leads to the following relationship, N_{90} (derivation outlined in Appendix B), which predicts the minimum shaking frequency required to achieve >90% suspension.

$$N_{90} = S {d_p}^{0.25} \nu^{0.14} \left(g \frac{\Delta\rho}{\rho} \right)^{0.43} {d_s}^{-0.96} {S_f}^{-0.03}, \tag{3.7}$$

where

$$S = \frac{N {d_s}^{0.96} {S_f}^{0.03}}{{d_p}^{0.25} \nu^{0.14} \left(g\frac{\Delta\rho}{\rho}\right)^{0.43}}. \tag{3.8}$$

The values of S for all the experimental conditions studied in this work ($n = 213$) were calculated and plotted logarithmically against the ratio of well diameter d_w to orbital shaking diameter d_s. Figure 3.7 shows these correlations which have been divided between low density range and high density range particles in order to improve the accuracy of predictions. The accuracy of the N_{90} predictions using Equation 3.7 and S values taken from Figure 3.7 is confirmed in Figure 3.8. This plots measured shaking frequencies at which >90% particle suspension was achieved against the predicted values. Using S values for the two different particle density ranges the error in the predicted values was ±17%. This increased to ±70% when S values covering the whole particle density range were used. Given that it is straightforward to measure the density of immobilised enzyme preparations and new immobilisation resins it is considered that Figure 3.7 represents the most useful and accurate form of the correlation. The tendency to over predict the required shaking frequency should ensure complete particle suspension is achieved in the majority of applications.

3.7 Influence of Particle Suspension and Dispersion on Immobilised Transketolase Kinetics

A number of authors have previously reported on the kinetics of soluble enzymes in microwell systems (Fernley et al., 2007; Ferreira-Torres et al., 2005; Fraisse et al., 2002). Industrial applications using soluble enzymes have a number of disadvantages related to their poor stability and difficulty of recovery and reuse (Kirill et al., 2009; Pecher and Arnold, 2009; Ruben et al., 2007). The immobilisation of enzymes on the types of

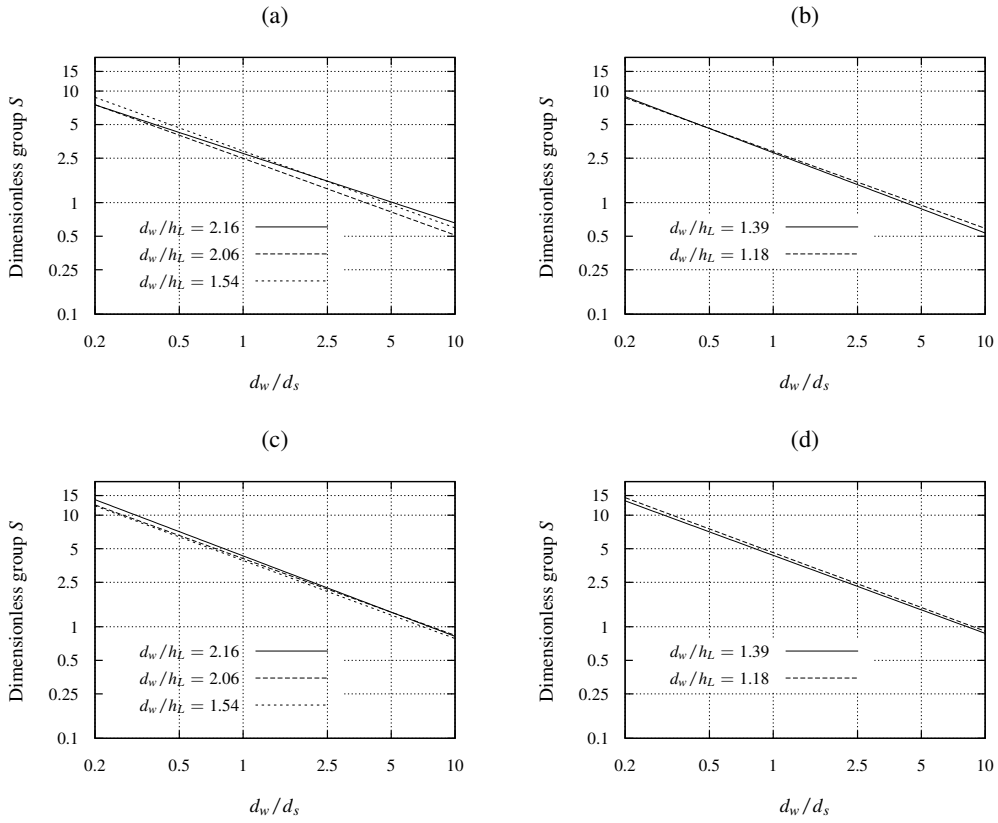

Figure 3.7: Correlation of measured particle suspension conditions with the ratio of microwell to shaking diameter (d_w/d_s). Lines fitted by linear regression to the data calculated from Equation 3.8 for (a, b) high density particles , $\rho_p \geq 1.2 \times 10^3\ kgm^{-3}$ for (a) low and (b) high fill volumes and (c, d) low density particles, $0.8 \times 10^3\ kgm^{-3} < \rho_p < 1.2 \times 10^3\ kgm^{-3}$ for (c) low and (d) high fill volumes.

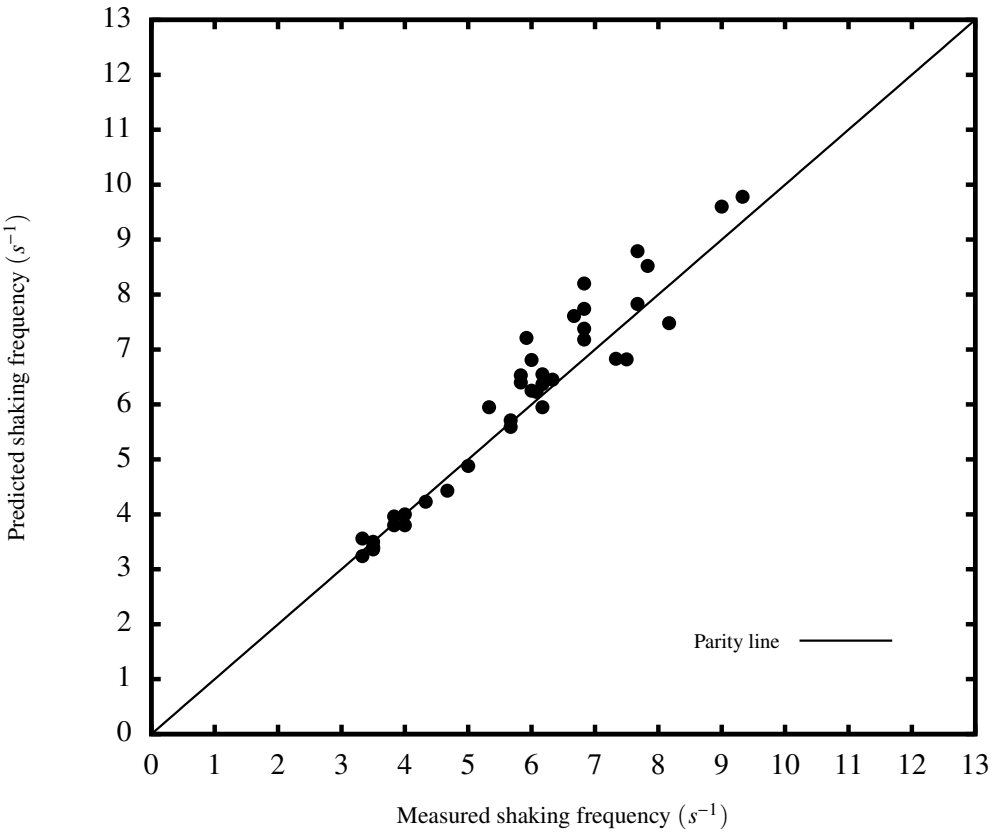

Figure 3.8: Parity plot of measured and predicted shaking frequencies required to ensure >90% steady state particle suspension. Predictions based on Equation 3.7 for various particles and experimental conditions.

solid support studied here generally provides a rapid and convenient way to overcome these process limitations (Mateo et al., 2007). The optimisation of immobilisation and bioconversion conditions is normally a lengthy experimental process, however, and so parallel microwell studies have the potential to reduce early stage process development times.

Accurate quantification of immobilised enzyme kinetics in shaken microwell systems will be necessary if the data obtained is to be used for bioprocess design purposes (Chen et al., 2009). In terms of the engineering environment in the microwells this is expected to require full suspension of the immobilised enzyme particles within a flow field where any external mass transfer limitations on reaction rate are minimised (Barros et al., 1998; Kheirolomoom et al., 2002). In order to illustrate the significance of this point the rate of L-erythrulose synthesis from glycolaldehyde and β-hydroxypyruvate using immobilised transketolase was measured (Matosevic et al., 2010). Transketolase catalyses asymmetric carbon-carbon bond formation from a range of achiral substrates and has been shown to be a useful reaction for accessing a variety of chiral synthons (André et al., 1998; Zimmermann et al., 1999). Two sets of experiments were performed. The first examined the influence of either complete or poor suspension of TK immobilised on IB-150 beads on the measured bioconversion kinetics. In this case full suspension (>95%) was achieved at a shaking frequency of 5.33 s^{-1} and a shaking diameter of 0.0125 m. Poor suspension conditions (<5%) were achieved, at the same d_s, by reducing the shaking frequency to 4.33 s^{-1}. The second experiment aimed to compare the measured bioconversion kinetics under complete suspension conditions (>95% in each case) but achieved by operation either at high shaking diameter ($N = 5.33\ s^{-1}$, $d_s = 0.0125\ m$) or high shaking frequency ($N_s = 7.33\ s^{-1}$, $d_s = 0.003\ m$).

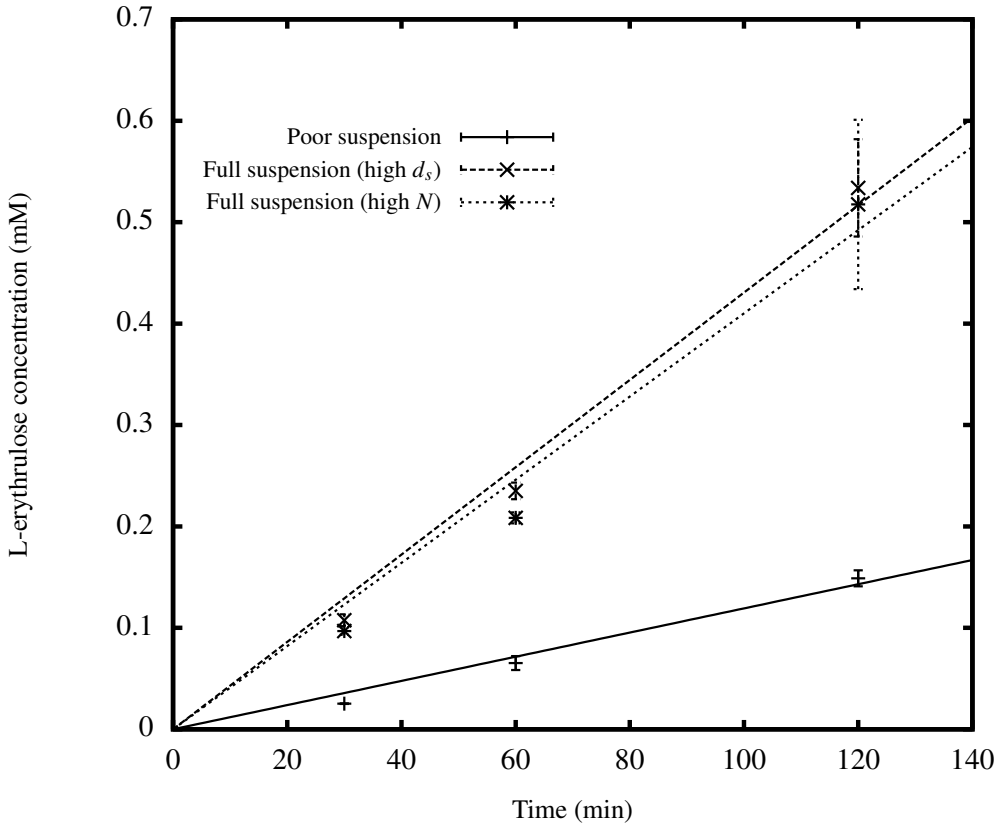

Figure 3.9: Influence of steady state particle suspension conditions on the measured kinetics of L-erythrulose synthesis by transketolase immobilised on IB-150 beads. Immobilisation procedure as described in Section 2.9.1.2 and bioconversion kinetics determined as described in Section 2.10.1. Solid lines fitted by linear regression. Error bars represent one standard deviation about the mean (three samples). Operating conditions: 24-DSW, $N_s = 4.33$ or $5.33\ s^{-1}$ and $d_s = 0.0125\ m$, $N_s = 7.33\ s^{-1}$ and $d_s = 0.003\ m$.

Figure 3.9 compares the initial rates of L-erythrulose synthesis under the various conditions. These results confirm the need for complete particle suspension (>95%) and adequate fluid flow conditions in order to reliably measure immobilised TK bioconversion kinetics. Figure 3.9 also shows that under complete suspension conditions the measured bioconversion rate does not depend upon how particle suspension is achieved, i.e. by increases in either N_s or d_s. The lines in Figure 3.9 were fitted by linear regression and represent the apparent initial rate of reaction. In the case of full suspension conditions these rates were found to be 0.0025 $\pm$0.0003 $mMmin^{-1}$ (at high d_s) and 0.0023 $\pm$0.0002 $mMmin^{-1}$ (at high N_s). Based on a student's t-test these were not found to be statistically different ($p = 0.05$). Both bioconversion rates were significantly higher, however, than the value of 0.0015 $\pm$0.0002 $mMmin^{-1}$ measured for the same IB-150 immobilised TK preparation under partial suspension conditions.

3.8 Summary

The aim of this chapter was to develop predictive correlations describing particle suspension in shaken bioreactors and to show how the quality of suspension influences the qualification of immobilised enzyme kinetics. In order to meet this aim a high speed video and image analysis technique was first established (Figure 3.1) so as to be able to relate the measured particle suspension to key parameters such as shaking frequency (Figure 3.2), shaking diameter (Figure 3.3) and particle density (Figure 3.4). Based on these original insights into particle suspension in shaken microwell systems a correlation was developed (Equation 3.7) based on analogy with Zwietering's correlation (Equation 1.11). This enabled accurate prediction of the suspension frequency to within $\pm$17%.

Finally, based on these findings, it was shown that the nature of the particle suspension has significant impact on the measured rate of an immobilised enzyme bio-

conversion. These results have important implications for the use of shaken microwell methods for the early stage evaluation of immobilised enzyme bioconversion processes. In particular, as shown in Figure 3.9, kinetic measurements made under poor suspension conditions can give highly inaccurate (almost two-folds difference in initial reaction rate) estimates of the overall bioconversion rate.

As described in Section 1.1.1 miniature stirred bioreactors represent an alternative bioreactor geometry used in early phase bioprocess development. Solid-liquid suspension in these bioreactor formats is described in Chapter 4.

Chapter 4

Solids Suspension in Small Scale Stirred Bioreactors

4.1 Introduction and Aims

As mentioned in Section 1.1.1, miniature stirred tank bioreactors offer an alternative to shaken microwell systems for early stage bioprocess development. One necessary factor in order to be able to do this is to understand these devices from an engineering perspective. Although they are better understood in comparison with shaken microwell systems with regards to some engineering aspects such as steady state gas-liquid mass transfer coefficient (k_La) measurements (Reuss et al., 1986) and power consumption characteristics (van't Riet and Tramper, 1991), there still remain many unexplored characteristics. One such area is the suspension of solids in such devices. Zwietering (1958) studied the suspension of solids in stirred tank bioreactor and correlated the results in Equation 1.11, however the range of bioreactor geometries used in that study did not include miniature scales (< 0.5 L).

The aim of this chapter is to determine the suitability of Equation 1.11 for predicting solids suspension in small scale and miniature stirred bioreactors and to show how the quality of suspension influences the quantification of immobilised enzyme kinetics. The specific objectives include:

- Identification of typical miniature and small scale stirred bioreactor geometries and visual observation and recording of the suspension process at various combinations of operating conditions such as bioreactor geometry, impeller diameter and particle density.
- Creation of an image analysis routine for automated quantification of this visual data in order to determine whether particles are suspended or not.
- Comparison of the results with predictions made using Zwietering's correlation.
- Computational modelling of fluid flow in the chosen geometries for further comparative studies.
- Quantification of the influence of suspension quality on the kinetics of an immobilised enzyme bioconversion.

Protex $6L^2$ was the enzyme chosen for the purpose of biocatalyst kinetics determination. It was preferred to transketolase because it is commercially available in immobilised form. Using transketolase would have meant purifying and immobilising a large amount of enzyme required particularly in the 5.0 L laboratory scale stirred bioreactor, while the large amount of HPA required would have made it prohibitively expensive to carry out the necessary number of experiments.

4.2 Selection of Particles, Bioreactors and Operating Conditions

4.2.1 Particle Selection

As describe in Section 3.2 a range of particles with different physical properties were selected for study (Table 3.1). The solids volume fraction, S_f, was varied at a different range than in the microwell studies between 2.5% and 5% v/v.

4.2.2 Bioreactor Selection

The primary criteria for bioreactor selection was that they should be geometrically similar to those conventionally used in laboratories and be agitated by a similar Rushton turbine impeller. This was dictated by the desire to obtain quantitative and scalable data from each bioreactor. It was also important for the bioreactors to be, in the case of miniature bioreactor, of a size used in early stage bioprocess development. Being of that size, it means the miniature bioreactor is outside the range of bioreactors ($2.9\ L < V < 170\ L$) used by Zwietering and therefore require further study while the laboratory bioreactor should have been chosen as to be within the range used by Zwietering (1958).

Although a Rushton turbine is classed as a radial flow impeller and, hence, not an ideal solution for particle suspension, it was nevertheless chosen as for this study due to its commonality in various operations across the chemical and biochemical industries, but also due to time limitations. These limitations meant that fabrication of a different impeller design at two different scales would have been impossible. Given this, a glass vessel with a nominal volume of 0.17 L was removed from a parallel miniature biore-

actor (Gill et al., 2008a) and utilised for this project in place of the miniature stirred tank bioreactor. The magnetic stirrer was also modified by removing the magnetic plate so it could be used with direct drive overhead stirrer motor. The same baffles were retained for this study. For the laboratory bioreactor a glass vessel of nominal volume of 5.0 L was chosen and a suitably sized Rushton turbine impeller and a set of baffles were built specifically for this study. See Figure 2.2.

4.3 Visualisation and Quantification of Just Suspension Conditions

A MATLAB routine was developed for the accurate quantification of particle suspension via automated analysis of the experimental video images. The principle of the routine is described in Section 2.7.1 and the routine itself is given in Appendix A. Initial experiments were performed in the 5.0 L laboratory stirred tank. Representative images from the high speed video camera and the outputs from the MATLAB analysis are shown in Figure 4.1. The particles used were XAD-16, suspended at a stirrer frequency of 4.17 s^{-1}. The total fill volume, V_f was 3.5 L and the solid volume fraction, S_f, was 5% v/v.

The images in Figure 4.1 show the development of particle suspension from the outset of mixing to $t \approx 6$ s. At the outset, all particles are submerged ($\rho = 1.092$ gml^{-1}) and located on the base of the vessel. This is observed in the form of a white disk. Approximately 1.7 s after commencing agitation, the particles start to lift from the bottom of the tank in regions close to baffles. This behaviour is expected as baffles induce extra drag around the vessel periphery (Kresta and Wood, 1991). By 3.6 s after

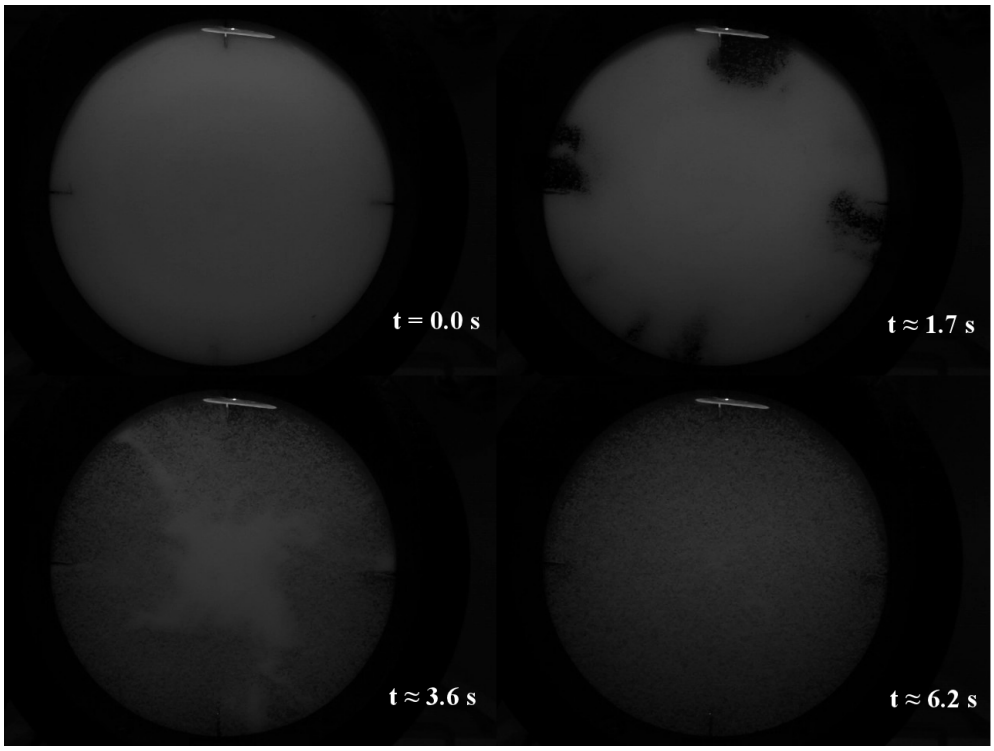

Figure 4.1: Representative video images showing the extent of particle suspension at different times from the start of mixing. Experiments performed and images acquired as described in Section 2.6.2. Operating conditions: XAD-16, $N_s = 4.17s^{-1}$, $V_f = 3.5\ L$ and $S_f = 5\%$ v/v. Particle characteristics as described in Table 3.1.

the start of mixing, the majority of the particles have been lifted off the bottom of the tank. The particles are fully suspended by 6.2 s after the start of the mixing procedure and a pseudo equilibrium state is reached.

As described in Section 2.7.2, a MATLAB routine was established to quantify the state of suspension. The experimental results were quantifies by comparing consecutive frames from each test. For the purpose of this study, consecutive frames were taken to be exactly 1 s apart. This would allow for an accurate comparison to be carried out with predicted results based on Zwietering's correlation. Zwietering (1958) considers the presence of stationary particles on the tank's floor for any period longer than 2 s to mean that the suspension is incomplete.

As described in Section 2.7.2, from each frame, eight separate interrogation areas were selected and compared to their corresponding area on the next frame. Figure 4.2 illustrates a representative sample from an experiment carried out in a miniature bioreactor with a nominal volume of 0.170 L and indicates the position of the interrogation areas chosen. The two columns on the right exhibit the difference between two frames, 1 s apart, over the marked areas of the frames. The left column shows the state of the particles at $t = t_1$ and the right column does the same at $t = t_1 + 1$ s. Although during the analysis the original images were used without any enhancements, for the purpose of illustration here the contrast has been increased so that the differences can be more readily recognised between the two frames.

As described in Section 2.7.2, the two consecutive frames were compared by looking at their intensity values pixel by pixel. The difference was then quantified using a relationship expressed by Equation 4.1.

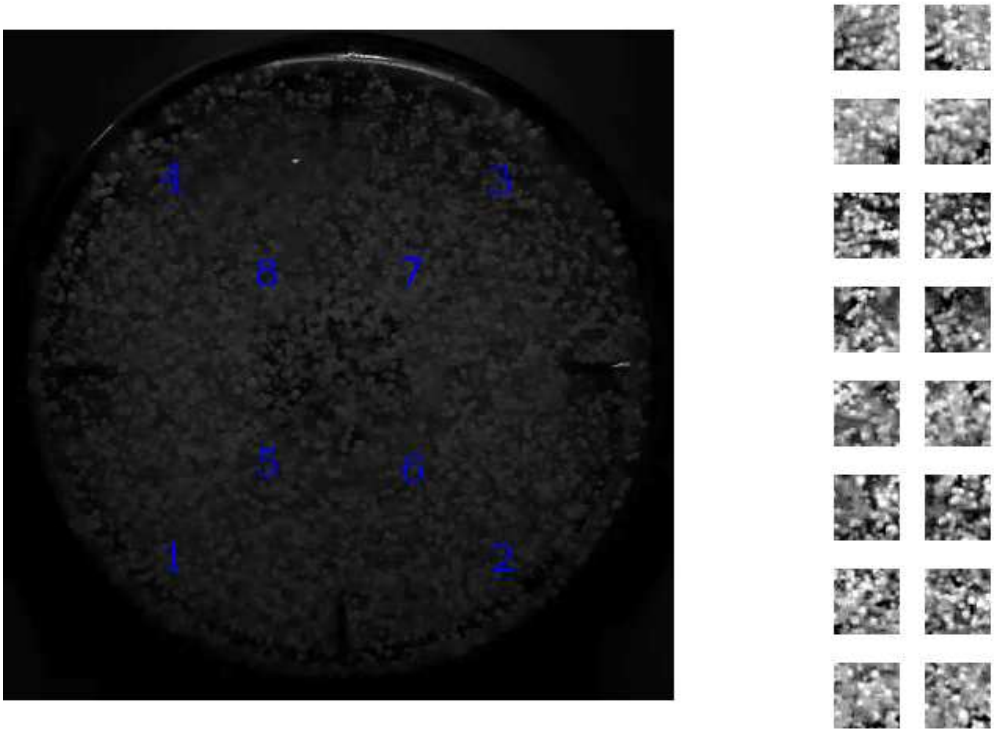

Figure 4.2: A representative image marking the areas over which consecutive frames were automatically compared. The two columns on the right show images from the interrogation areas in greater detail. For the left column, $t = t_1$ and the right column, $t = t_1 + 1\ s$. From top to bottom, areas 1 to 8. Experiments performed as described in Section 2.6.2 and images analysed as described in Section 2.7.2. Operating conditions: XAD-16, $N_s = 6.67\ s^{-1}$, $V_f = 0.170\ L$ and $S_f = 2.5\%$ v/v. Particle characteristics as described in Table 3.1.

$$D_{value} = \frac{\sqrt{\sum (A_{ij} - B_{ij})^2}}{\sqrt{\sum {B_{ij}}^2}}, \tag{4.1}$$

where D_{value} is the dimensionless difference, A is the intensity matrix for the first image, B is the intensity matrix for the second image, i is the number of rows and j is the number of columns in those matrices. Running the example given in Figure 4.2 through the MATLAB routine, the D_{value} for each interrogation area is given in Table 4.1.

Table 4.1: Difference between pairs of consecutive frames for the interrogation areas shown in Figure 4.2. Values expressed in the form of a dimensionless number, D_{value}, calculated as described in Section 4.3

Interrogation Area	D_{value}
1	0.37
2	0.35
3	0.35
4	0.37
5	0.28
6	0.36
7	0.36
8	0.32

This comparison is then repeated for all the frames recorded through an experiment in order to get a more representative result over a longer time, roughly equal to 25 s, by finding the average for D_{value} over time for each of the eight interrogation areas in each frame. These eight different values can then be averaged to get a single value corresponding to the overall difference between two consecutive frames. With further experiments performed as described in Section 2.6.2 at different mixing frequencies, it

is possible to plot this data as shown in Figures 4.3 and 4.4.

Figure 4.3 illustrates the typical change in D_{value} for a set of experiments performed in the miniature bioreactor using XAD-16 particles. The top graph corresponds to those experiments which were carried out with 2.5% v/v solid volume fraction, while the bottom graph belongs to 5% v/v solid volume fraction experiments. Figure 4.4 shows the same data for experiments carried out in the laboratory bioreactor using XAD-16 particles, with the top graph depicting the experiments performed at 2.5% v/v solid volume fraction and the bottom graph showing the data for the set of experiments performed at 5% v/v solid volume fraction. In all cases, a steep rise is observed at lower stirring frequencies which gradually flattens as stirring frequency increases, reaching a plateau towards the end of their respective range.

The exact mixing frequency required to achieve full suspension was determined by calculating the difference between the calculated D_{value} at each stirring frequency. The stirring frequency for which this difference with the following frequency was found to be $< 1\%$ was accepted as the full suspension frequency.

4.4 Comparison with Zweitering's Correlation

Zwietering's correlation is the main means for predicting the minimum mixing frequency necessary for achieving a full suspension in a stirred tank reactor. The different tank geometries used in his original study fell within the range of 2.9 L and 170 L (Zwietering, 1958). Although the laboratory scale bioreactor employed in this project is just within that range, the miniature scale bioreactor sits significantly outside of it. Given this, it is important to undertake a comparative study between the experimentally found minimum stirring frequencies for full suspension from this study and the

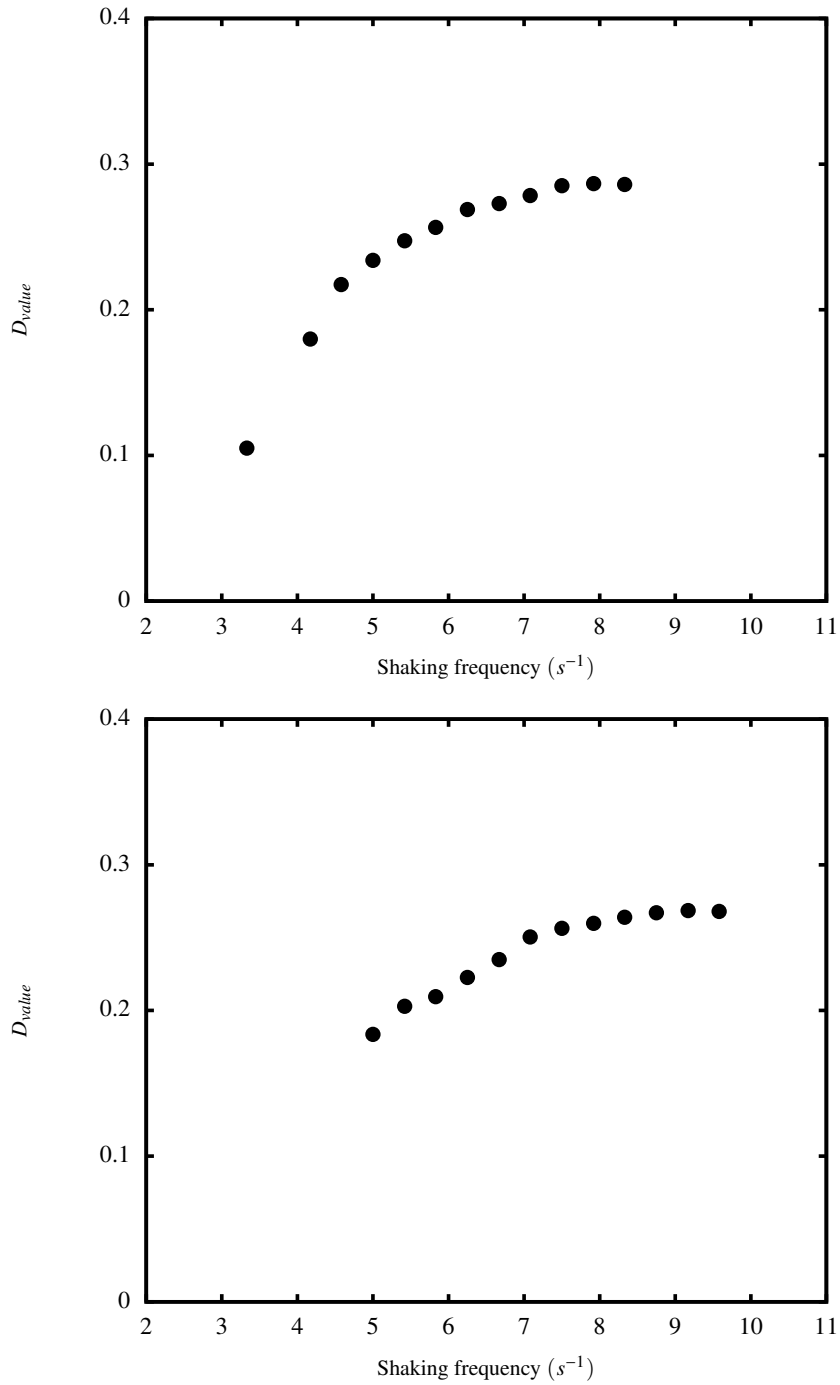

Figure 4.3: Variation of calculated D_{value} with respect to stirring frequency for experiments performed in a miniature bioreactor. Operating conditions: XAD-16, $V_f = 0.170$ L, $S_f = 2.5\%$ v/v at the top and $S_f = 5.0\%$ v/v. Experiments performed as described in Section 2.6.2 and D_{value} calculated as described in Section 4.3. Particle characteristics as described in Table 3.1.

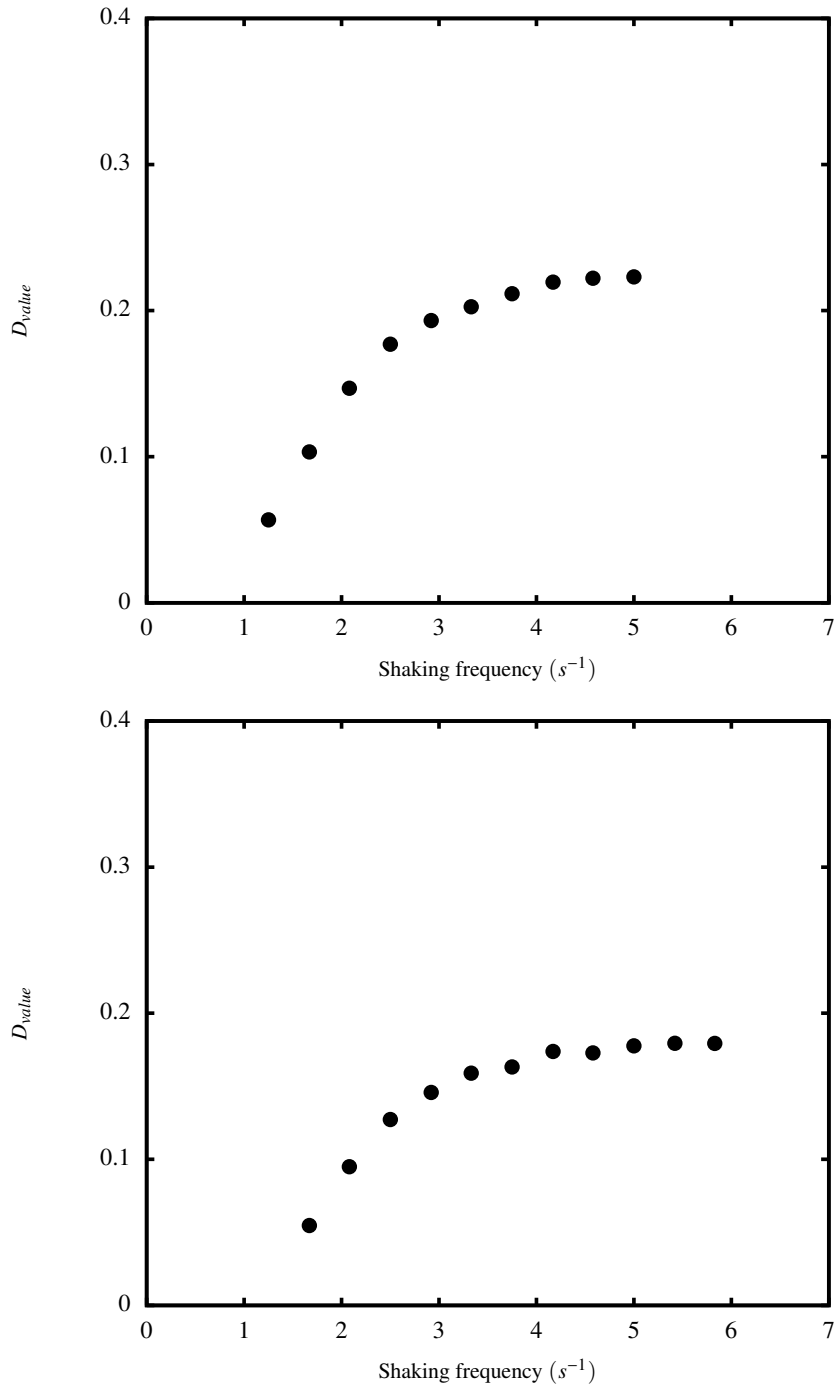

Figure 4.4: Variation of calculated D_{value} with respect to stirring frequency for experiments performed in a laboratory scale bioreactor. Operating conditions: XAD-16, $V_f = 3.5\ L$, $S_f = 2.5\%$ v/v at the top and $S_f = 5.0\%$ v/v. Experiments performed as described in Section 2.6.2 and D_{value} calculated as described in Section 4.3. Particle characteristics as described in Table 3.1.

predictive values given by Zwietering's correlation in identical scenarios. Figure 4.5 and Table 4.2 show the U_{js} found by experiments and also the predicted values calculated with Zwietering's correlation for all the various experimental conditions.

Table 4.2: Experimental and predicted values for minimum stirring frequency required for full suspension. Experimental values determined as described in Section 4.3. Predicted values calculated using Equation 1.11

Experimental Conditions (particle, tank, S_f)	**Experimental** U_{js} s^{-1}	**Predicted** U_{js} s^{-1}	% **Difference**
IB-150, 5.0 L, 2.5%	5.83	6.18	6.1
IB-150, 5.0 L, 5.0%	6.67	6.78	1.6
IB-150, 0.17 L, 2.5%	19.17	14.57	24.0
IB-150, 0.17 L, 5.0%	20.00	15.93	20.3
XAD-7, 5.0 L, 2.5%	6.67	10.03	50.5
XAD-7, 5.0 L, 5.0%	7.92	10.98	38.6
XAD-7, 0.17 L, 2.5%	19.17	23.58	23.1
XAD-7, 0.17 L, 5.0%	20.83	25.82	23.9
XAD-16, 5.0 L, 2.5%	4.58	5.52	20.5
XAD-16, 5.0 L, 5.0%	5.42	6.05	11.6
XAD-16, 0.17 L, 2.5%	7.50	12.98	73.2
XAD-16, 0.17 L, 5.0%	8.75	14.22	62.5

Figure 4.5 shows a parity plot between experimental and predicted U_{js} values for the two different bioreactor volumes investigated. A close study of these results show that Zwietering's correlation is, statistically speaking, equally unsuitable for predicting suspension in the laboratory scale and the miniature scale reactors. Although this is expected in the case of the miniature reactor, it being outside the volumetric range of reactors studied by Zwietering (1958) by a significant margin, the same cannot be said of the laboratory reactor. One suitable hypothesis for this phenomena is the difference

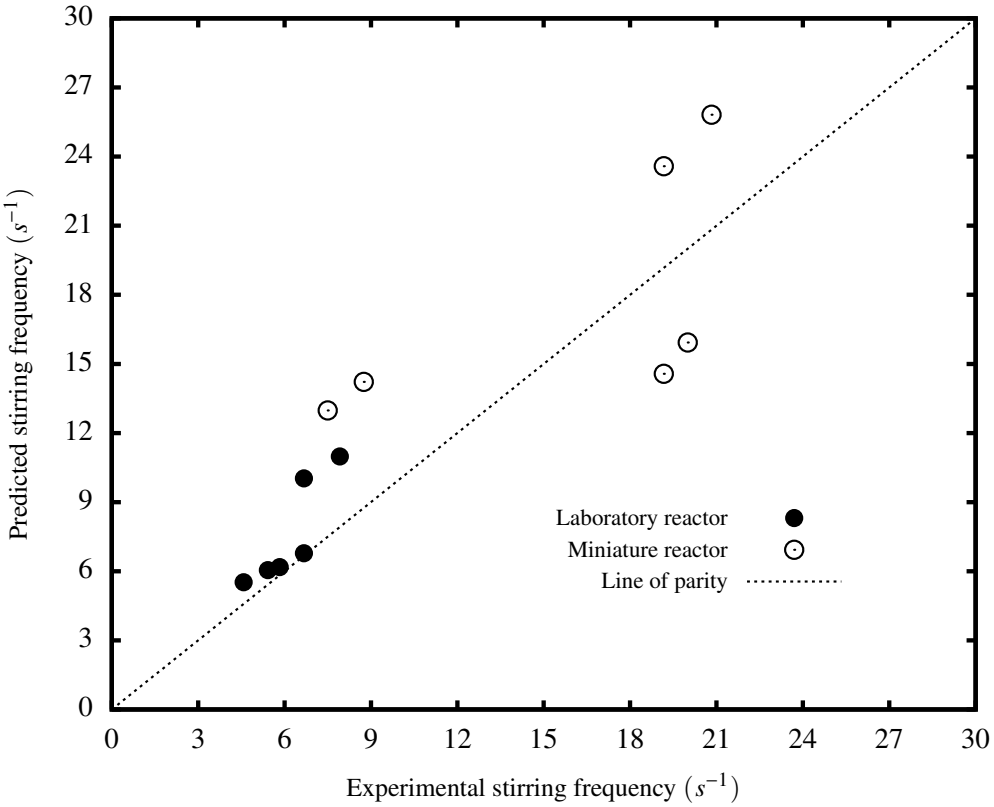

Figure 4.5: Parity plot between experimentally established U_{js} and predicted U_{js} using Zwietering's correlation. Data shown for laboratory scale and miniature miniature stirred tank reactors. Values taken from Table 4.2.

in impeller power consumption, especially in the case of the miniature reactor. The Rushton turbine used by Zwietering had an N_p value of 6.2. The miniature turbine impeller used in this study, has an unconventional design with relatively thick turbine blades. Geometric parameters such as the disk and the blade thickness are known to influence an impeller's measured Power Number (Bujalski et al., 1987). The Power Number of both Rushton impellers will be experimentally measured in Chapter 5.

4.5 Computational Simulation of Fluid Flow in Stirred Tank Bioreactors

In this section, the means through which the experimental results gathered for the previous sections can be compared to the data generated by computational simulation of the flow properties inside the two different size stirred tank reactors operated under various conditions will be provided. Such comparison will cover the two different reactor geometries used so far in this study and will aim to bolster the findings described in Section 4.3 regarding the quality of solid suspension in both of these vessels. CFD simulations of single-phase fluid flow field were performed as described in Section 2.8. Determining the local fluid velocities will make calculating the drag force responsible for lifting solid particles off the bottom of the tank possible. Also, in order to proceed to complex multi-phase CFD calculations, it is important to obtain predictive results for a single phase system.

For cases in which the flow was laminar, the normal configuration of the Navier-Stokes equations, given in Equations 2.3 and 2.4 were solved. For the turbulent cases though solving the exact Navier-Stokes equations is not possible (Aubin et al., 2004) and they were replaced by the Reynolds-averaged Navier-Stokes equations given by

Equations 2.5 and 2.6. The turbulent model used was the standard $k-\epsilon$ model as this has been shown to be in good agreement with experimental data when studying the flow produced by a Rushton turbine impeller (Jaworski et al., 1997).

The velocity field, given in Figure 4.6, shows two separate circulation loops above and below the impeller as expected for a Rushton turbine (Guha et al., 2007; Lamberto et al., 2001). The circulation loop below the turbine has higher energy levels than the circulation loop above the turbine which is in agreement with previously reported experimental findings using computer automated radioactive particle tracking (Guha et al., 2008). Looking at the bottom of the tank, it is worth noting that the flow in this region which is responsible for lifting the particles into suspension has a significant vertical component which gets stronger as the flow moves closer to the centre of the reactor. The other important factor is the presence of strong radial velocity under the impeller and close to bottom of the reactor. This is again confirmed by previous experimental results which show simultaneous radial and axial velocities.

The imbalance in energy levels between the lower and upper circulation loops are further confirmed by the data presented in Figure 4.7 All the data in this graph have been normalised. The position of each point along the radius of the reactor is given as a fraction of the total radius (r/R), where $R = 0.082\ m$, the height at which the points are positioned relative to the reactor's bottom surface are given as fractions of its diameter (z/d_v), where $d_v = 0.164\ m$ and the magnitude of the local velocity at each point is given as a fraction of the magnitude of the impeller tip velocity (u_r/U_t), where $U_t = 1.334\ ms^{-1}$.

Figure 4.7 shows the magnitude of the local velocity at different points across the ra-

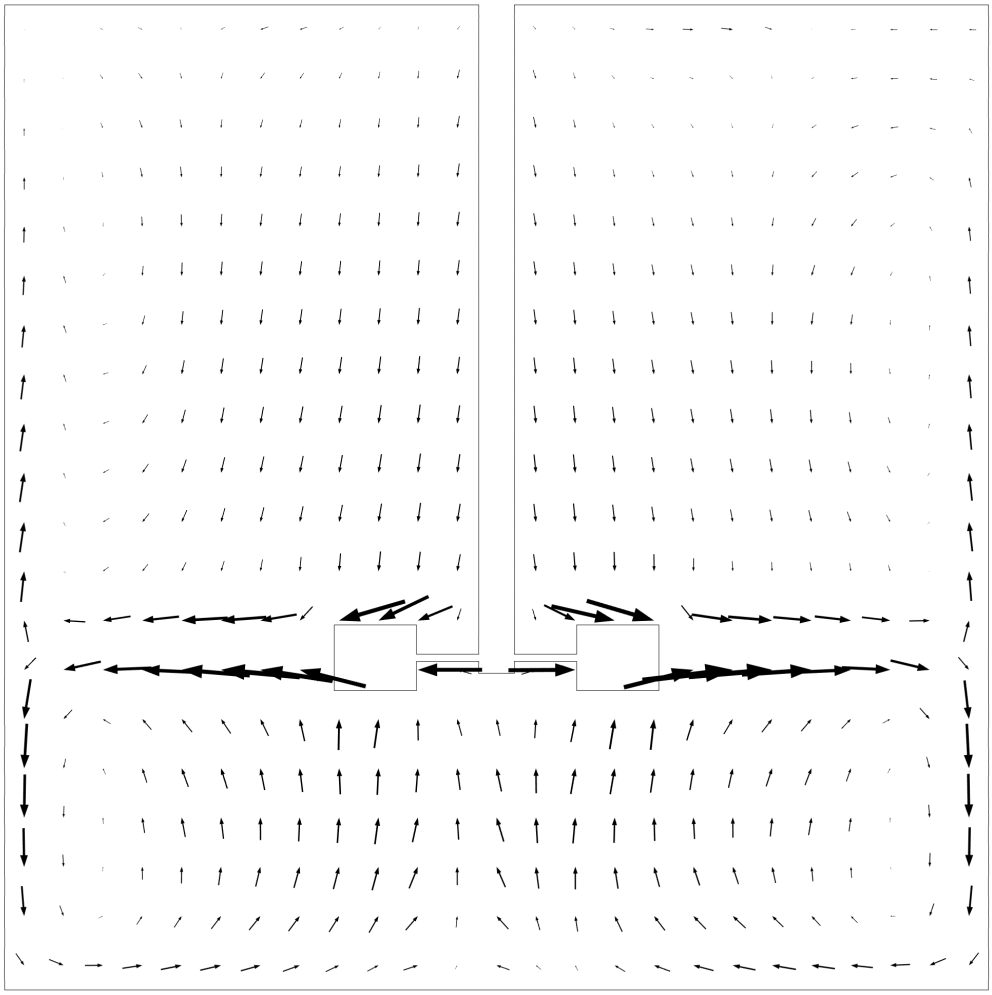

Figure 4.6: Simulation of the overall flow pattern inside the 5.0 L laboratory reactor for a single phase fluid, showing vertical profile of velocity vectors through centre of reactor. CFD performed as described in Section 2.8. Simulation conditions: $Re = 22400$ and water as the working fluid.

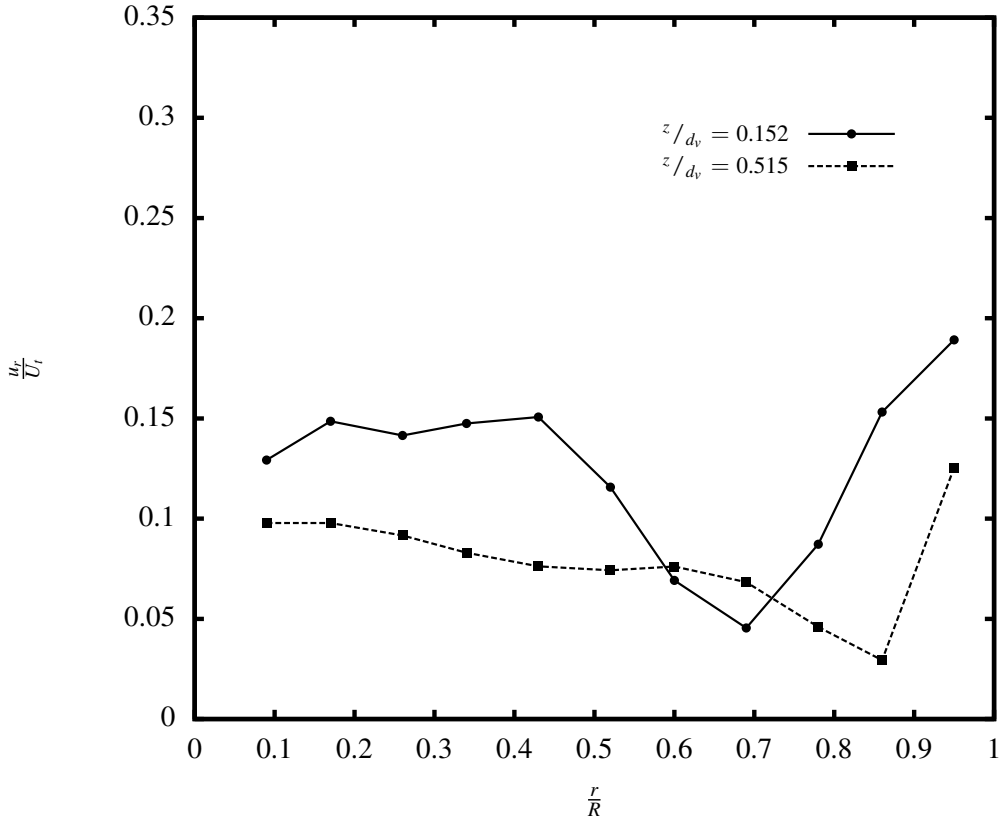

Figure 4.7: Local fluid velocity predictions at different points along the reactor radius. Values calculate at equal distances above and below the impeller. All values normalised against bioreactor radius, R and impeller tip velocity, U_t. CFD performed as described in Section 2.8. Simulation conditions: $d_v = 0.164\ m$, $U_t = 1.334\ ms^{-1}$, $R = 0.082\ m$, $Re = 22400$ and water as the working fluid.

dius of the tank at two different heights; one set cuts across the lower loop, $z/d_v = 0.152$, while the other cuts across the upper loop, $z/d_v = 0.515$. They are both placed at equal distance from the impeller's central plane. Moving away from the central axis of the reactor, the velocity magnitude is gradually reduced as the position moves closer to the centre of the circulation loop and is increased again approaching the reactor wall. Looking at the points placed below the impeller, they show both greater velocity magnitude and greater variation compared to the points placed above the impeller. The graph also confirms the closer vicinity of the upper circulation loop to the wall in relation to the lower circulation loop as the drop in velocity magnitude occurs further along the radius and closer to the wall.

Following on from the experimental work carried out in previous sections, two different conditions were computationally modelled for comparative studies. A single-phase model, using water properties, was simulated inside a domain matching the geometrical properties of the laboratory scale, 5.0 L reactor used in this study. Two different mixing frequencies were simulated; 6.67 s^{-1}, for which $U_t = 1.334\ ms^{-1}$, representing the upper mixing frequency which was shown to be capable of suspending a variety of particles with different physical properties, and 0.83 s^{-1}, for which $U_t = 0.142\ ms^{-1}$, representing the lower mixing frequency which was found to be inadequate for fully suspending any of the particles used through this project.

Figures 4.8 and 4.9 compare the velocity magnitude on four different axial locations, from the bottom of the tank, at different points along the tank radius. The four different heights are $z_1 = 0.005\ m$, $z_2 = 0.015\ m$, $z_s = 0.025\ m$ and $z_4 = 0.035\ m$ from the bottom surface of the tank. They are once again presented as fractions of the tank diameter, which translate into, $z_1/d_v = 0.031$, $z_2/d_v = 0.091$, $z_3/d_v = 0.152$ and

$z_4/d_v = 0.213$ respectively.

In Figure 4.8, the top graph compares the velocity magnitude given by the two simulations at $z_1/d_v = 0.031$. This is significant as it falls very close to the base of the tank where particles would be resting in the absence of any agitation and will not lift into suspension if the liquid flow is not adequate. It can be seen that the higher mixing frequency results in an overall significantly higher values in this region and the resulting velocity field will probably have a higher vertical component, which is directly responsible for generating the necessary lift force for particle suspension. It is at its weakest in the vicinity of the walls, due to friction, and in the region under the impeller. The lower mixing frequency results in lower velocity magnitude across the radial section and produces less variations. The bottom graph compares the velocity magnitude given by the two simulations at $z_2/d_v = 0.091$. Although the difference between the normalised velocity magnitudes are less in this case, the pattern between the two data sets is quite different. While the simulation with the higher U_t value shows a radial velocity profile which is almost uniform, the other simulation shows significant variation across the tank radius and reveals a pattern of change which is very similar to the one exhibited by faster stirring in the top graph; suggesting a weaker loop.

Figure 4.9 illustrates the same set of data for the two remaining cases of $z_3/d_v = 0.152$ and $z_4/d_v = 0.213$. The graph at the top carries the data from an axial position of $z_3/d_v = 0.152$. Again the two sets of data are relatively similar in magnitude once normalised with respect to impeller tip velocity, but the set with the higher U_t is now cutting through the circulation loop seen below the impeller in Figure 4.6, hence the drop in velocity magnitude around half way along the radius. This drop is then recovered in the vicinity of the reactor wall as the discharge from the impeller takes over.

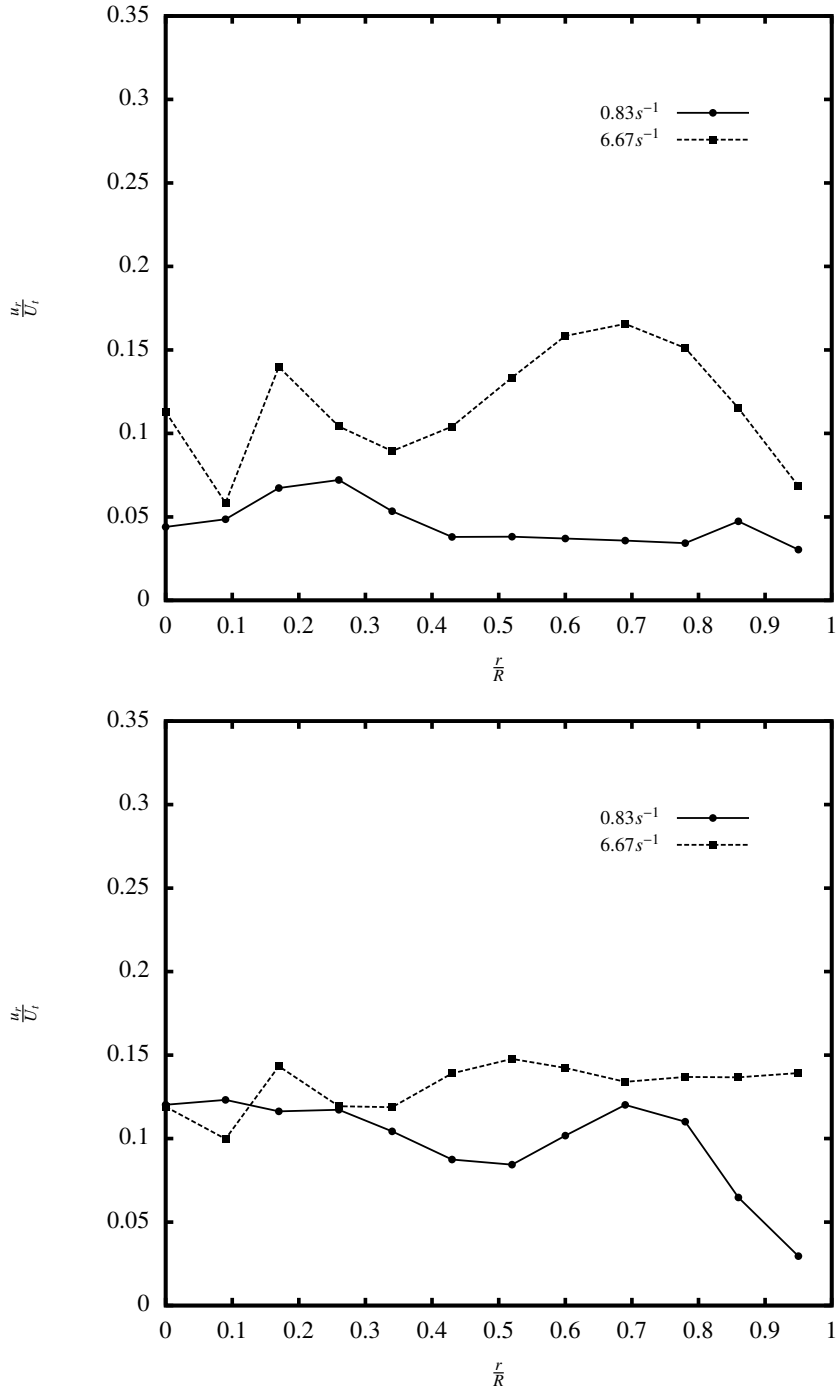

Figure 4.8: Profile of velocity magnitude in different points along the radial direction for axial positions $z_1/d_v = 0.031$ at the top and $z_1/d_v = 0.091$ at the bottom. All values normalised against bioreactor radius, R and impeller tip velocity, U_t. CFD performed as described in Section 2.8. Simulation conditions: $d_v = 0.164\ m$, $R = 0.082\ m$, $Re = 22400$ and water as the working fluid.

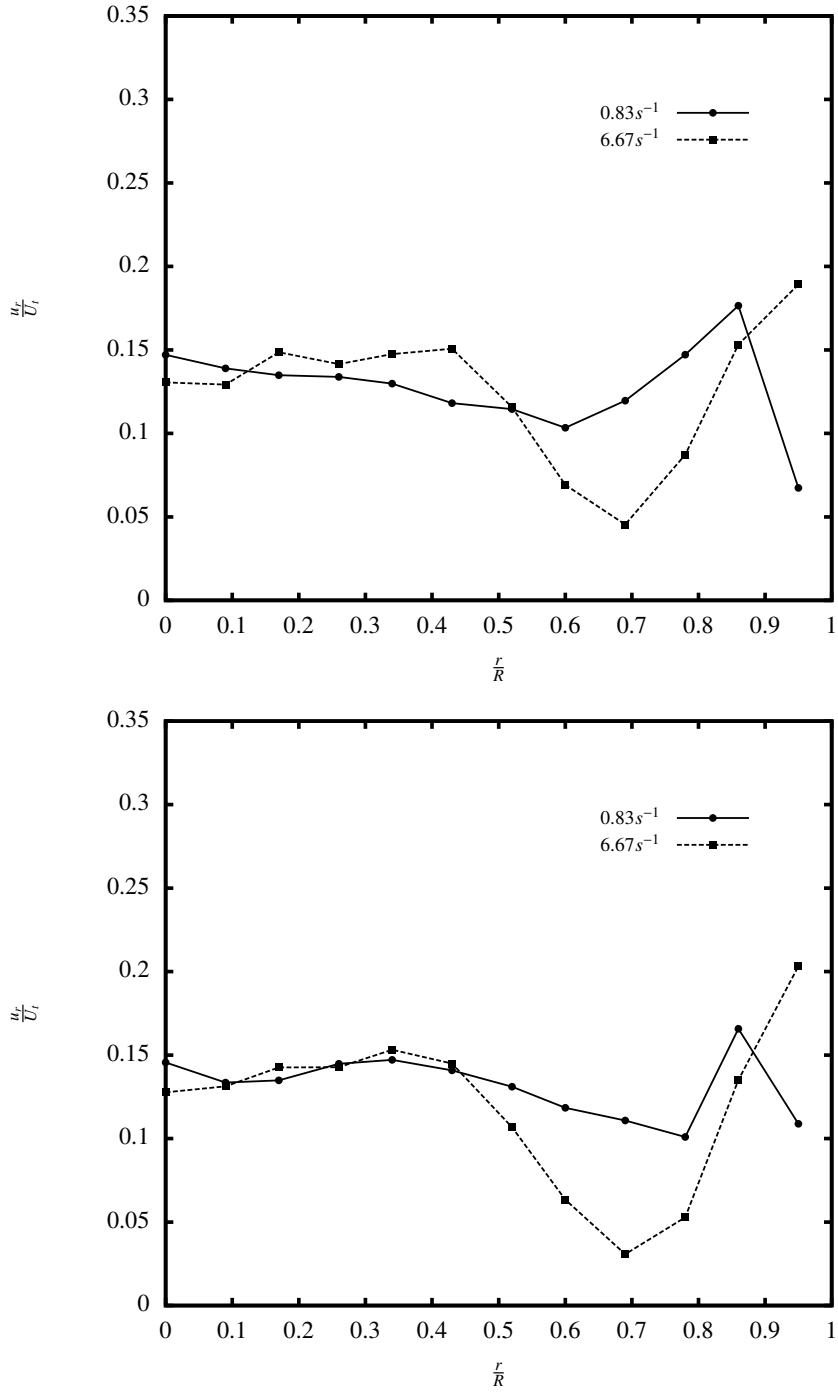

Figure 4.9: Profile of velocity magnitude in different points along the radial direction for axial positions $z_3/d_v = 0.152$ at the top and $z_4/d_v = 0.213$ at the bottom. All values normalised against bioreactor radius, R and impeller tip velocity, U_t. CFD performed as described in Section 2.8. Simulation conditions: $d_v = 0.164\ m$, $R = 0.082\ m$, $Re = 22400$ and water as the working fluid.

The results from the simulation with the lower impeller tip velocity is uniform until the mid point across the reactor radius but after that exhibits a gradual rise in velocity magnitude due to direct impeller discharge, before showing a significant drop close to the wall. The bottom graph shows the results from the axial position $z_4/d_v = 0.213$. This position is very close to the impeller but not quite close enough as to be within the discharge region. The simulation performed at higher stirring frequency shows no significant difference in comparison to the graph on top, apart from slightly lower minimum velocity in the middle of the circulation loop and a slightly higher maximum velocity close to the wall and the impeller discharge region as it moves down in collision with the wall along a parallel path as seen in Figure 4.6. The simulation with the lower U_t also shows strong similarity with the graph on top with a significantly lower drop in velocity magnitude in regions close to wall.

The important factor in suspension of particles in a stirred tank reactor is the axial component of the local velocity close to the bottom of the tank. The onset of suspension is reached once the vertical component of the drag force on a single particle is just smaller than its effective weight (Shamlou, 1993). The effective weight of a single particle is governed by Equation 4.2.

$$F_E = \left(\frac{\pi}{6}\right) \Delta\rho {d_p}^3 g, \tag{4.2}$$

The drag force is generated by the liquid phase as it flows past the solid particles and is governed by Equation 4.3 (Shamlou, 1993).

$$F_D = C_D \left(\frac{1}{2}\rho {U_{js}}^2\right) \left(\frac{\pi}{4}{d_p}^2\right), \tag{4.3}$$

Therefore a particle can be suspended when $F_D > F_E$.

Figure 4.10 shows the axial component of the velocity at $z/d_v = 0.031$. Two different simulations were carried out in a domain representing the miniature, 0.170 L reactor. The two simulations differed in the applied stirring frequency. One was carried out at a frequency of 21.67 s^{-1} and the other one was carried out at a frequency of 5 s^{-1}. The agitation rate was gradually ramped up using a step function over a 5 s period as to match the actual stirrer used during experiments.

Figure 4.11 shows the axial component of velocity at different points across the tank radius with respect to time, matching the conditions presented in Figure 4.10. Using the data presented in Figure 4.11 in conjuncture with Equations 4.2 and 4.3, it would be possible to calculate the axial drag force exerted on individual particles and hence quantify whether or not they'll be lifted off the bottom of the tank at various times during these two simulations. It is known that in a mechanically agitated solid-liquid solution, the solid phase flows upward in a region under the impeller. This is one of a number of characteristic flow patterns generated with radial flow impellers (Guha et al., 2008), thus it is worth concentrating on this region alone.

4.6 Influence of Particle Suspension on Immobilised Protex 6L^2 Kinetics

As previously mentioned in Section 3.7, applications commonly encountered across the industry which depend on soluble enzymes have a number of disadvantages related to their poor stability and recovery for reuse (Kirill et al., 2009; Pecher and Arnold, 2009; Ruben et al., 2007). Accurate quantification of immobilised enzyme kinetics will depend on reduction of external mass transfer limitations (Barrett et al., 2010;

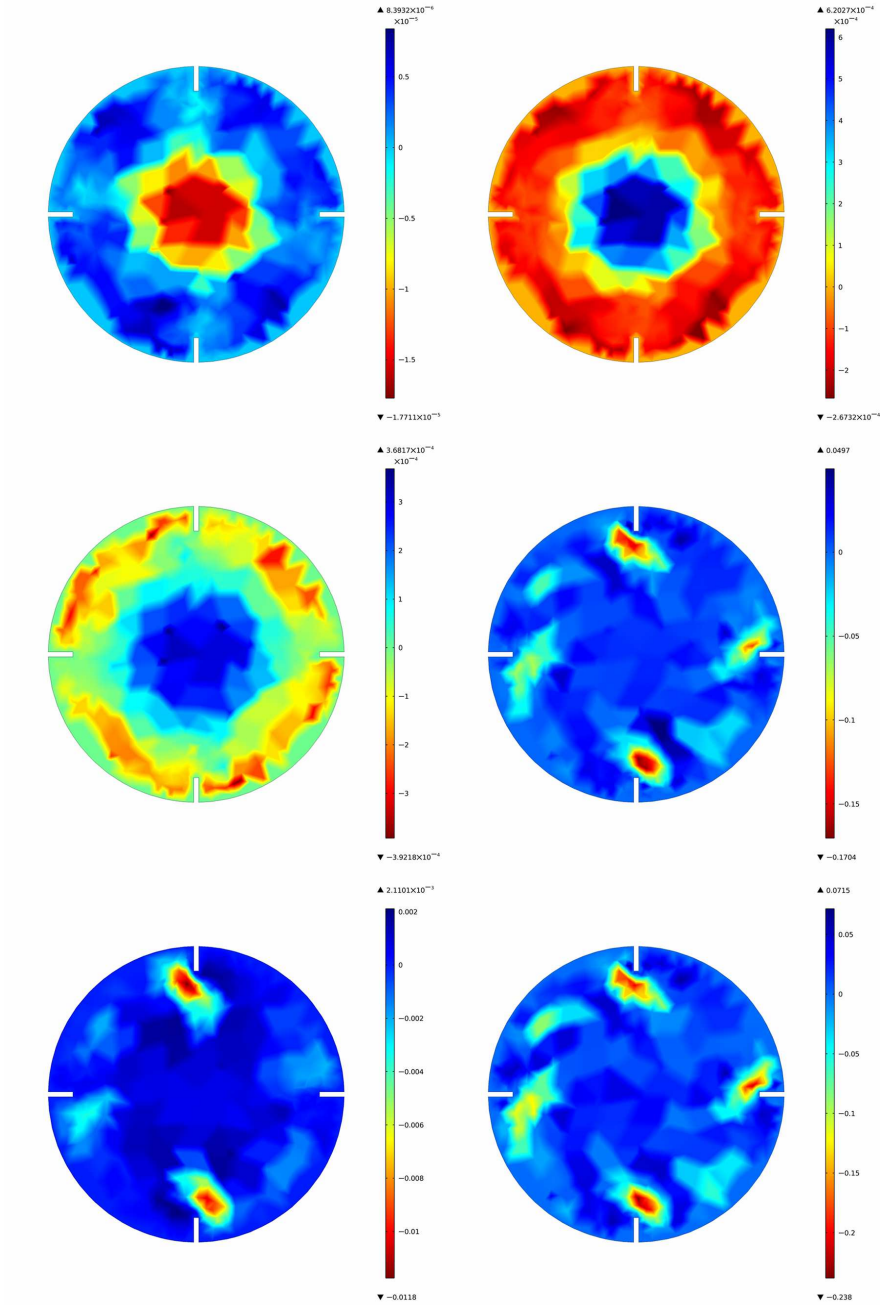

Figure 4.10: Axial component of the velocity at $z/d_v = 0.031$ in a miniature bioreactor with respect to time for different stirring frequencies. Left column, from top to bottom: $t = 1\ s$, $t = 3\ s$ and $t = 5\ s$ at a stirring frequency of 5 s^{-1}. Right column, from top to bottom: $t = 1\ s$, $t = 3\ s$ and $t = 5\ s$ at a stirring frequency of 21.67 s^{-1}. CFD performed as described in Section 2.8. Simulation conditions: $d_v = 0.06\ m$, $R = 0.03\ m$ and water as the working fluid.

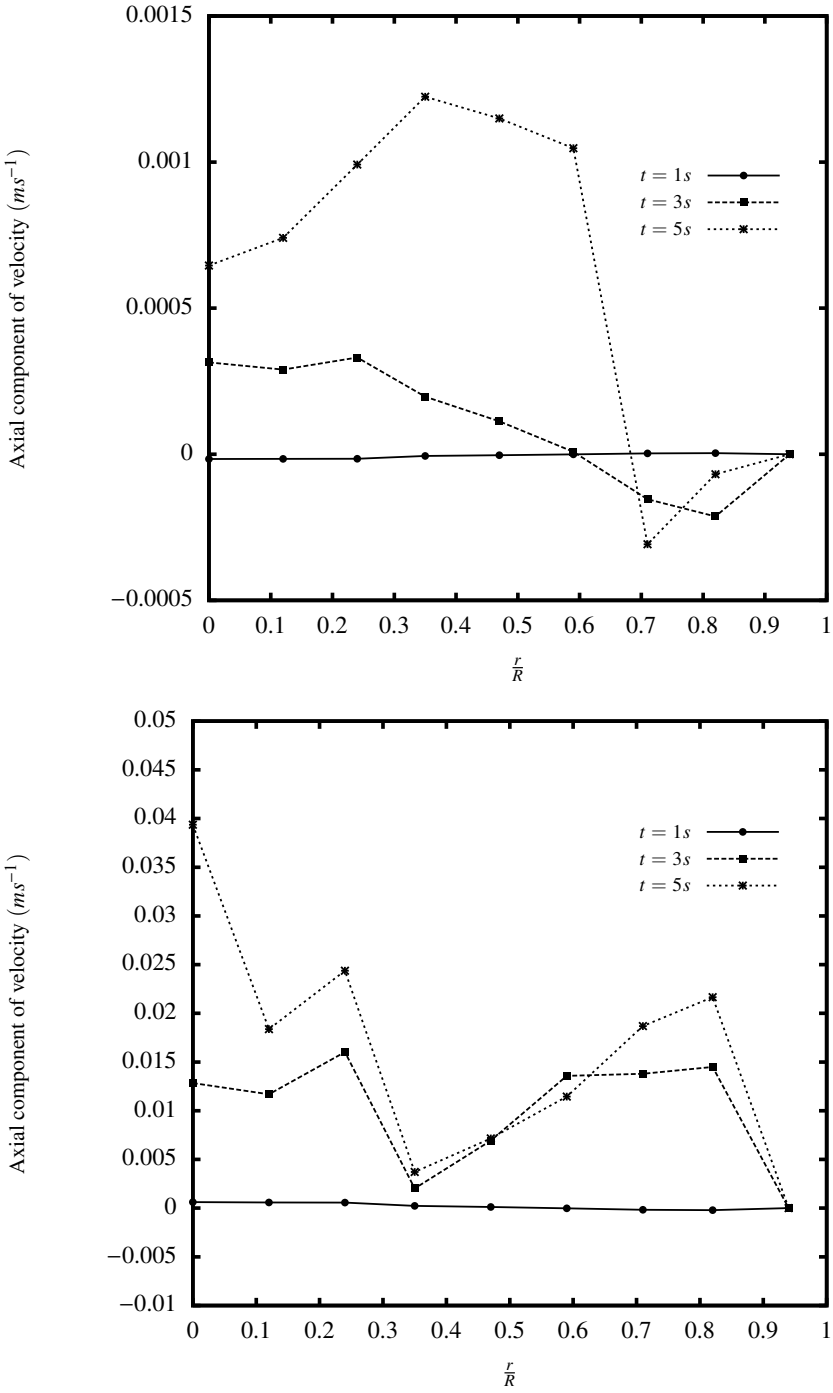

Figure 4.11: Axial component of velocity at different points across radius of a miniature bioreacor at $z/d_v = 0.031$ with respect to time and performed at 5 s^{-1} (top) and 21.67 s^{-1} (bottom). CFD performed as described in Section 2.8. Simulation conditions: $d_v = 0.06\ m$, $R = 0.03\ m$, and water as the working fluid.

Kheirolomoom et al., 2002) and to emphasise the significance of this point the rate of ethyl-(S)-lactate hydrolysis using immobilised Protex $6L^2$ was determined in the two different stirred bioreactor scales and under different suspension conditions. Experiments were performed in pH-stat mode, as described in Section 2.9.2, where the rate of lactic acid formation was monitored via the cumulative addition of the titrant solution consisting of 0.5 M NaOH. Protex $6L^2$ is a protease sourced from *Bacillus licheniformis* and is used extensively in the food industry (Karki et al., 2011; Wu et al., 2009). It was purchased immobilised on IB-150 beads used to study immobilised transketolase kinetics in Chapter 3.

In order to establish what constitutes the initial rate of reaction and the period over which this occurs when lactic acid is produced linearly, an initial experiment was carried out in the miniature, 0.170 L reactor as described in Section 2.9.2 with the addition of NaOH monitored for 50 min. The results are shown in Figure 4.12. The initial blip in titrant addition between 0-50 s is a consequence of the necessary pH adjustment at the start of the reaction. Following this it can be seen that the rate at which NaOH is added is linear until 3000 s and shows no signs of the reaction nearing completion. Given that the hydrolysis rate is constant for the initial 50 min, it was decided that reaction monitoring for 5 min would be sufficient to establish the initial hydrolysis rate in subsequent experiments.

For each reactor size, two sets of experiments were conducted as described in Section 2.9.2 and monitored as described in Section 2.10.2. One set was performed under conditions that the enzyme carriers were fully suspended ($> 95\%$) within the reactor, while the other set produced a poor suspension ($< 5\%$). This meant a mixing frequency of 20 s^{-1} and 3.33 s^{-1} respectively for the miniature scale reactor and 5.83 s^{-1} and

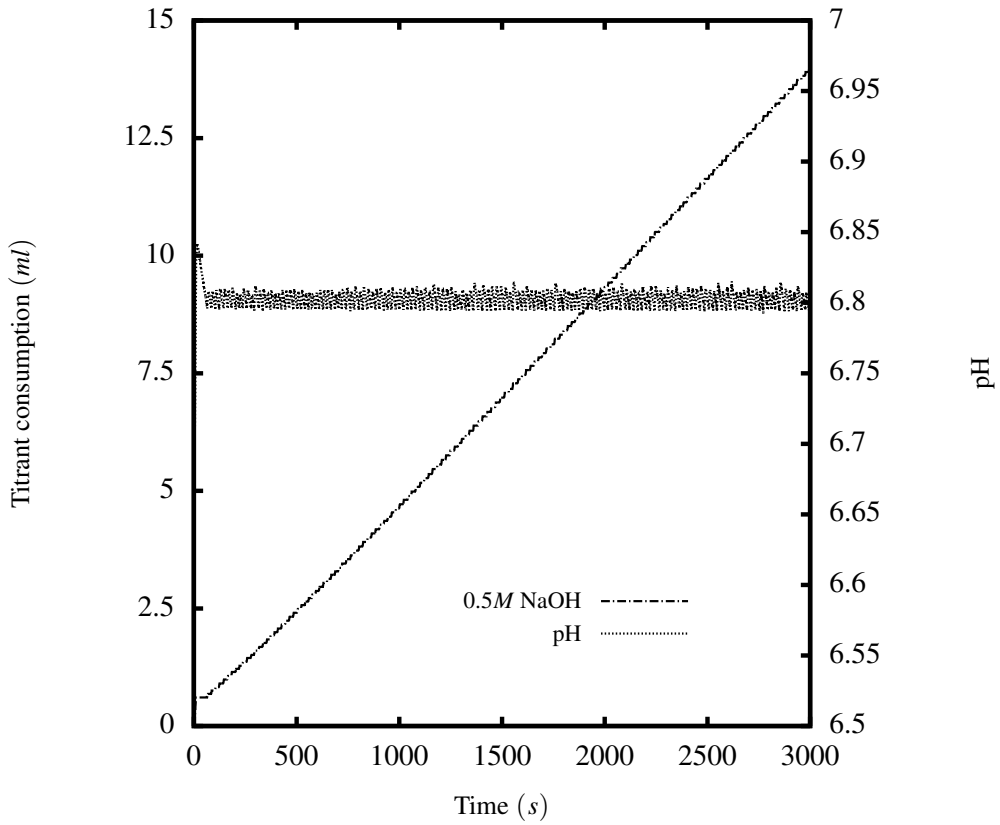

Figure 4.12: Illustration of the measured rate of lactate hydrolysis in the pH-stat. Graph shows cumulative addition of NaOH over a 50 *min* period at a set point of pH 6.8. Reaction mixed at a rate of 20 s^{-1}. Substrate solution prepared as described in Section 2.9.2. Operating conditions for pH-stat operation as described in Section 2.10.2.

1.25 s^{-1} respectively for the laboratory scale reactor.

Figure 4.13 illustrates the rate at which NaOH is added during hydrolysis of lactic acid from ethyl-(S)-lactate inside the miniature scale bioreactor under poor (top) and full (bottom) suspension conditions. The data shows a representative experimental trace from triplicate experiments. The results indicate a roughly two-fold increase in the measured rate of lactic acid production and hence confirm the importance of full suspension for accurate measurement of immobilised enzyme bioconversion kinetics.

Figure 4.14 show the comparable pH-stat data obtained using the laboratory scale reactor under poor (top) and full (bottom) suspension conditions respectively. An almost three-fold increase in the rate of NaOH consumption, once again indicates a significant increase in the initial reaction rate under full suspension conditions.

In terms of the calculated initial reaction rates for the miniature, 0.170 L reactor, the average initial rates were calculated to be 222 ± 10.6 $\mu molg^{-1}min^{-1}$ and 112 ± 6.4 $\mu molg^{-1}min^{-1}$ under full and poor suspension conditions respectively. The reactions carried out inside the laboratory, 5.0 L reactor showed average initial rates of 612 ± 20.3 $\mu molg^{-1}min^{-1}$ and 223 ± 9.6 $\mu molg^{-1}min^{-1}$ under full and poor suspension conditions respectively. At this stage the emphasis of the work was only on illustrating how the nature of the suspension impacts on measured reaction rates. In Chapter 5 the differences in rates between the two different sizes of reactor under full suspension conditions will be explored in more detail.

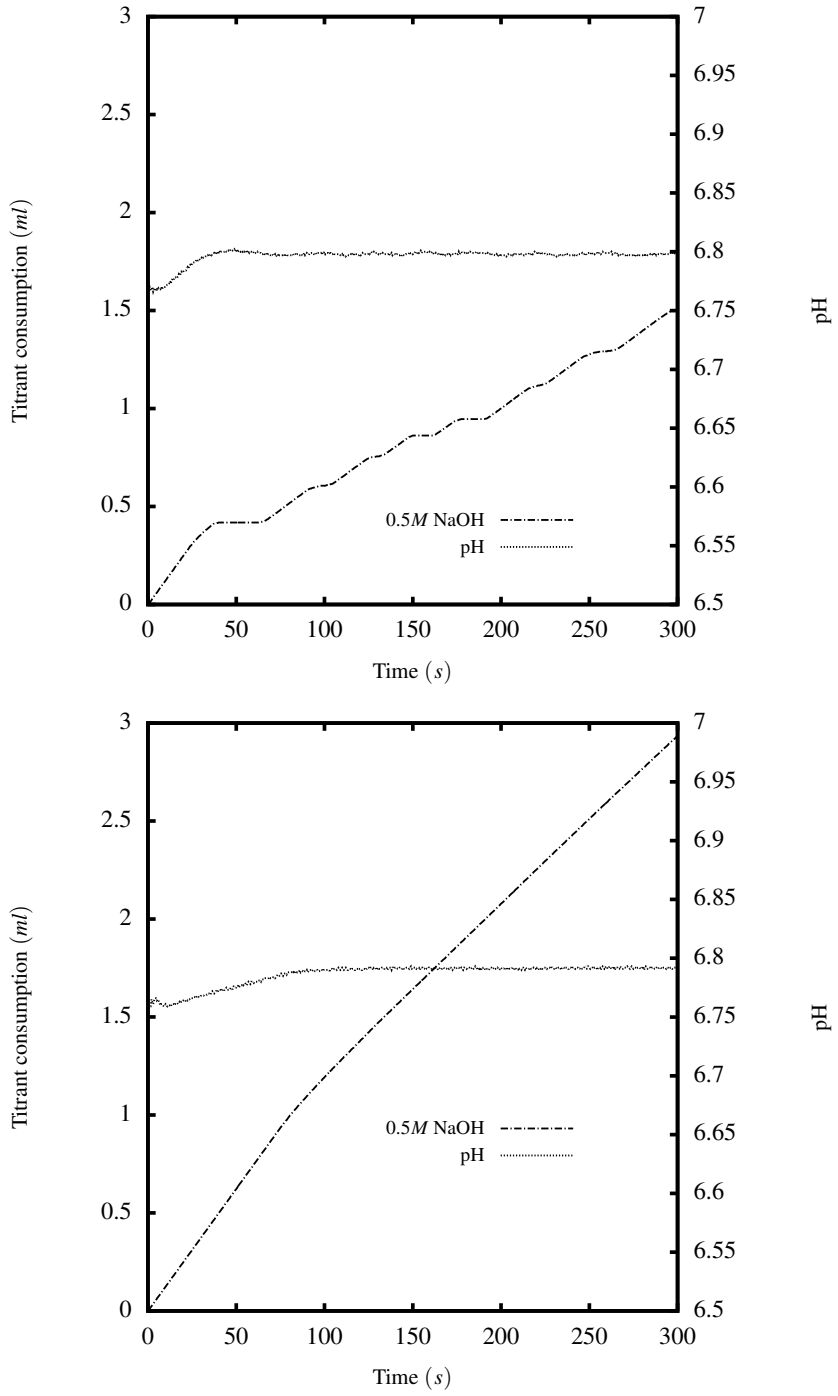

Figure 4.13: Illustration of the measured rate of lactate hydrolysis in the pH-stat. The graph on top shows cumulative addition of NaOH during an immobilised enzyme reaction performed with poor particle suspension, $N_s = 3.33\ s^{-1}$. The bottom graph shows cumulative addition of NaOH during an immobilised enzyme reaction performed with full particle suspension, $N_s = 20\ s^{-1}$. Substrate solution prepared as described in Section 2.9.2. Operating conditions for pH-stat operation as described in Section 2.10.2.

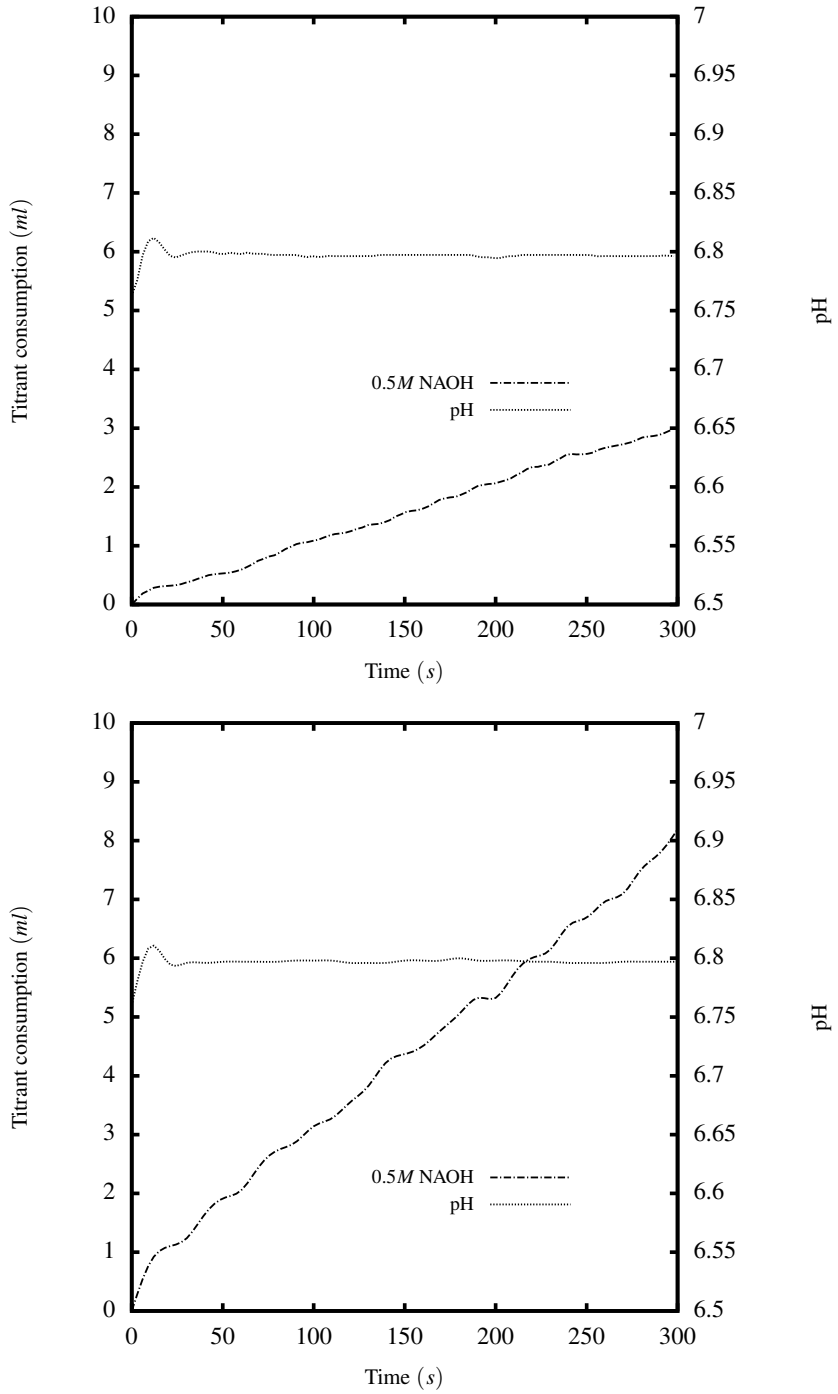

Figure 4.14: Illustration of the measured rate of lactate hydrolysis in the pH-stat. The graph on top shows cumulative addition of NaOH during an immobilised enzyme reaction performed with poor particle suspension, $N_s = 1.25\ s^{-1}$. The bottom graph shows cumulative addition of NaOH during an immobilised enzyme reaction performed with full particle suspension, $N_s = 5.83\ s^{-1}$. Substrate solution prepared as described in Section 2.9.2. Operating conditions for pH-stat operation as described in Section 2.10.2.

4.7 Summary

The aim of this chapter was to determine the suitability of Equation 1.11 for predicting solids suspension in small scale and miniature stirred bioreactors and to show how the quality of suspension influences the quantification of immobilised enzyme kinetics. In order to be able to achieve this aim a high speed video and image analysis technique was first established (Figure 4.2) as a means of quantifying the effects of various parameters including particle density and solid volume fraction and stirring frequency on suspension of solid particles (Figures 4.4 and 4.4). It was shown that the predictions made by Zweitering's correlation don't compare well with experimental results from either the laboratory scale reactor or the miniature scale bioreactor (Figure 4.5). This will be further investigated in Chapter 5.

Numerical simulation of the liquid phase hydrodynamics in stirred bioreactors confirmed the existence of a two circulation loop above and below the impeller (Figure 4.6) and showed that bottom loop has higher energy levels than the loop above the impeller (Figure 4.7). Further simulations performed at different stirring frequencies showed the velocity magnitude to be directly related to U_t at different axial points below the impeller (Figures 4.8 and 4.9) and that the vertical component of the velocity close to the bottom of the tank is increased as U_t is increased (Figure 4.11).

Finally, based on these findings, it was shown that the quality of particle suspension has a large influence on the measured rate of an immobilised enzyme reaction. Poor suspension quality resulted in decreased kinetics of two-folds and three-folds for the reactions performed in miniature and laboratory scale bioreactors respectively as seen in Figures 4.13 and 4.14.

As mentioned in Section 1.1.4, achieving comparable product conversion rates at different scales is paramount to industrialisation of any bioprocess. Finding a suitable scale-up criteria from miniature to laboratory scale bioreactors are described in Chapter 5.

Chapter 5

Immobilised Enzyme Bioconversions at Different Stirred Bioreactor Scales

5.1 Introduction and Aims

In Chapters 3 and 4 the effect which suspension quality has on immobilised enzyme reaction kinetics was examined in both shaken and stirred systems. In both cases adequate suspension was shown to be necessary in order to increase and standardise the measured rate of the reaction. Although the microwell and miniature bioreactor technologies described in Sections 1.1.2 and 1.1.3 are important in their own right, for them to be useful industrially, they have to be shown to be capable of providing reasonably accurate predictions of industrial results treated at different scales. For the solid-liquid systems described in this thesis there is really no standard method for reaction scale-up at present. Scale-up bases are very much dependent on the organisms and processes involved. Some of the most commonly suggested process characteristics suggested to be

kept constant during scale-up include k_La, power consumption per unit volume, oxygen transfer rate, impeller tip speed and mixing time (Hosobuchi and Yoshikawa, 1999; Ju and Chase, 1992; Oosterhuis and Kossen, 1985; Stanbury et al., 2003).

The aim of this chapter then is to explore the use of matched power input per unit volume as a quantitative basis for scale transition between the two stirred tank bioreactors described in Section 2.4.2. In particular, this work will establish the power consumption characteristics of the two turbine impellers and will look at bioconversion kinetics at matched power input per unit volume. The specific objectives include:

- Measurement of the gassed power input of both impellers (Figure 2.3) as a function of mixing frequency.
- Performance of a series of enzyme reactions in different bioreactor scales at matched power consumption per unit volume in order to establish a suitable engineering basis for process scale-up.
- Verification of both the chosen basis for scale-up and comparison of reaction kinetics across different scales.

As in Chapter 4, Protex $6L^2$ was the enzyme chosen for the purpose of biocatalyst kinetics determination. It was preferred to transketolase because it is commercially available in immobilised form. Using transketolase would have meant purifying and immobilising a large amount of enzyme required particularly in the 5.0 L laboratory scale stirred bioreactor.

5.2 Measurement of Power Consumption in Stirred Tank Bioreactors

For the standard and miniature stirred tank bioreactor, it is important to understand its mixing and energy dissipation characteristics (Elias and Joshi, 1997; Mantzouridou et al., 2002). It is known that the impeller power consumption of aerated systems is always lower than that of unaerated systems as the transfer of power from the impeller to the liquid is influenced by aeration. This reduction of power is the result of cavities which are formed behind the impeller blades and the difference in liquid density in gassed and ungassed systems (Sensel et al., 1993). It has been shown that the power requirement of a gassed system is approximately 30-40% of an ungassed system (Oosterhuis and Kossen, 1985).

The typical power ratio used in this scale-up concept is 1 to 2 kWm^{-3} (Abia et al., 1973). While this method has been successfully applied to antibiotic fermentations (Ju and Chase, 1992; Schmidt, 2005), the tendency to overestimate the required power can be problematic (Cui et al., 1996; Mockel et al., 1983).

The results in Figure 5.1 show that the measured power consumption of both turbine impellers rise exponentially with the increase in stirring frequency. This is in agreement with the trend reported by Gill et al. (2008b) It is clear that the larger impeller consumes more power compared to the smaller impeller. In the case of the larger impeller, the maximum power consumption was 1.16 W at a stirring frequency of 450 rpm, while the measured maximum power consumption of the smaller impeller was 0.42 W at a stirring frequency of 2000 rpm.

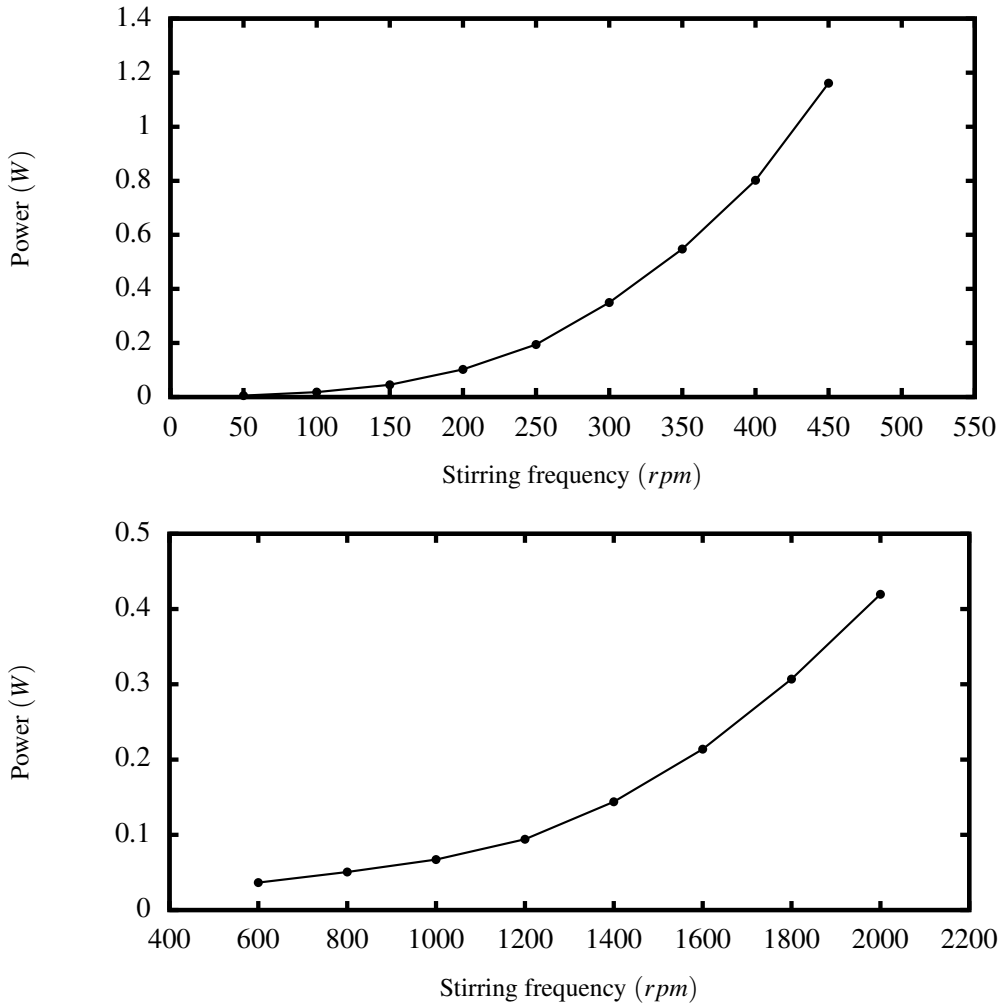

Figure 5.1: Measured power requirements of the (top) large turbine impeller, $d_i = 0.0547\ m$ and (bottom) small turbine impeller, $d_i = 0.02\ m$ over a range of mixing frequencies. Experiments conducted with RO water as described in Sections 2.5.2 and 2.5.1 respectively.

Figure 5.2 shows the relationship between the calculated Power Number, N_p, for both impeller sizes and the corresponding impeller Reynolds number, Re. The N_p values have been calculated by substituting the measured power input data, represented in Figure 5.1, into Equation 5.1.

$$P = N_p \rho N^3 d_i^5, \tag{5.1}$$

where P is the impeller's measured power input, N_p is the Power Number, ρ is the density of the liquid, N_s is the stirring frequency and d_i is the diameter of the turbine impeller. The results shown are for agitation of water. It is visible from Figure 5.2 that, in both instances, N_p tends towards a constant value, as expected, as the impeller Re is increased. For flow conditions assumed to be turbulent ($Re > 10000$), N_p values of 5.7 and 3.5 are achieved respectively for the large and small turbine impellers.

In the case of the large turbine impeller, the measured value of N_p is sufficiently close to that typically reported in literature for a six blade Rushton turbine, however the measured N_p value for the small turbine impeller is lower than this reported value of 6 (Nienow et al., 1994) in the turbulent flow region. However, Bujalski et al. (1987) have reported geometric parameters, such as the thickness of the impeller blades and disk, can have a measurable influence on the Power Number of a Rushton turbine. Also, Rutherford et al. (1996) have concluded that N_p was inversely proportional to the ratio of impeller blade thickness to impeller diameter. The correlation derived by Rutherford et al. (1996) is given as,

$$N_p = 6.57 - 54.771 \frac{b_i}{d_i}, \tag{5.2}$$

where N_p is the Power number, b_i is the impeller blade thickness and d_i is the impeller

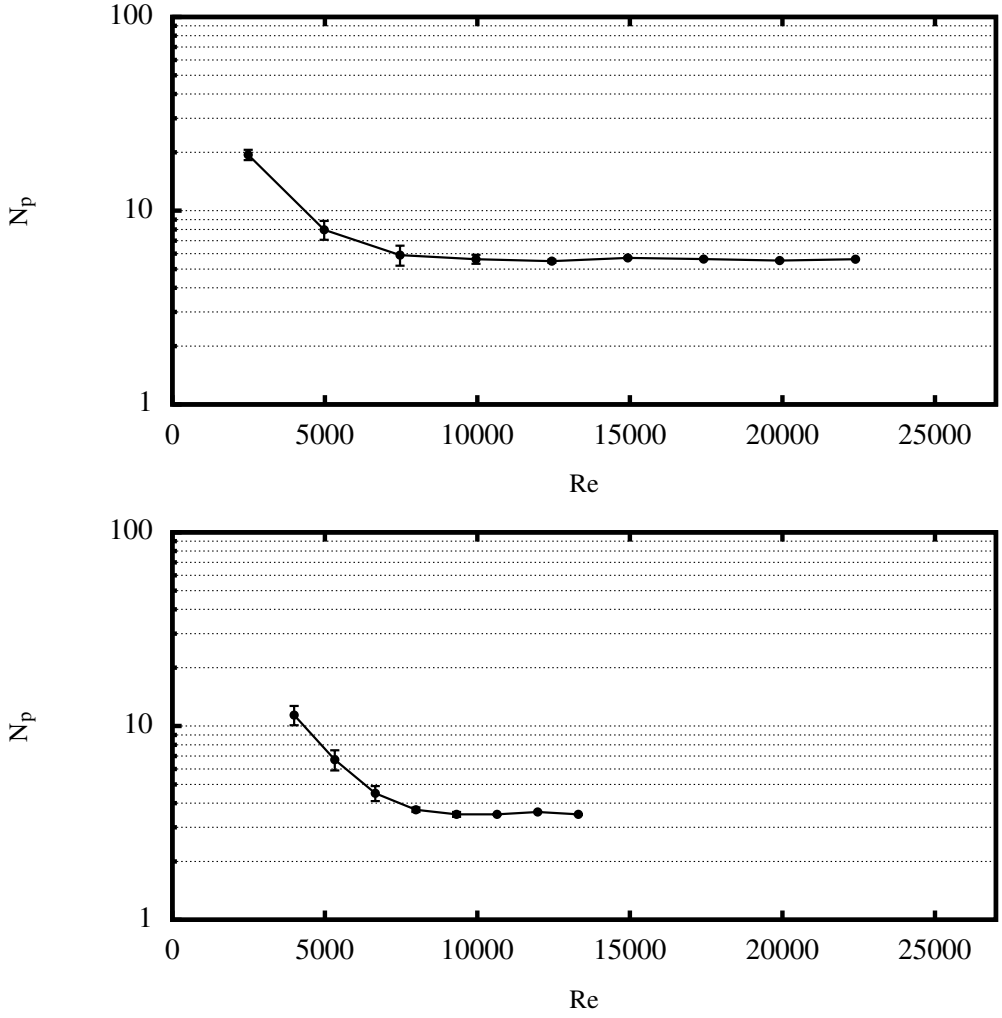

Figure 5.2: Variation of calculated Power Number, N_p, with increasing Reynolds Number in RO water: (top) large impeller; (bottom) small impeller. N_p values calculated from the data presented in Figure 5.1 as described in Section 5.2 and using Equation 5.1. Error bars represent one standard deviation about the mean ($n = 3$).

diameter. Equation 5.2 returns a N_p value of 3.8 for the small turbine impeller used in this study which has a blade thickness ratio of 0.05. Therefore, the experimentally determined Power Number is in good agreement with the predicted value. It also matches the value reported by Gill et al. (2008b). Compared to other small impeller designs this measured N_p falls within the same range which Puskeiler et al. (2005) reported for a magnetically driven bioreactor block ($d_i = 20\ mm, d_i = 14.5\ mm$), who estimated a value of 3.7 based on CFD simulation, and Betts et al. (2006) who predicted a Power Number of 3 for a triple impeller system ($d_i = 23\ mm, d_i = 8.5\ mm$) based on directly measuring the electrical energy input of the agitator motor.

It was hypothesised in Section 4.4 that the large difference between the experimentally established U_{js} and the predicted U_{js} could be explained by the impeller power consumption. To test this hypothesis, the measured Power Number for each impeller was put back into Equation 5.1 and utilised to calculate the corrected U_{js}. These are given in Table 5.1 for comparison.

The results given in Table 5.1 prove that the difference in Power Number does influence the predictions made by Zwietering's correlation, but not in the hypothesised manner. Using the measured Power Number has increased the difference between the measured U_{js} and the predicted U_{js} for every experimental condition bar two: the third and fourth conditions as presented in Table 5.1. Therefore, this hypothesis doesn't hold and some other factors must be responsible for this difference. While the errors seen in the case of the miniature reactor can be safely put down to the volumetric range of reactors used by Zwietering (1958), the errors seen in the case of the laboratory reactor merit further analysis.

Table 5.1: Experimental and predicted values for minimum stirring frequency required for full suspension. Experimental values determined as described in Section 4.3. Predicted values calculated using Equation 5.1, while utilising the measured Power Numbers as described in Section 5.2

Experimental Conditions (particle, tank, S_f)	**Experimental** U_{js} s^{-1}	**Predicted** U_{js} s^{-1}	% **Difference**
IB-150, 5.0 L, 2.5%	5.83	6.36	9.0
IB-150, 5.0 L, 5.0%	6.67	6.97	4.5
IB-150, 0.17 L, 2.5%	19.17	17.63	8.0
IB-150, 0.17 L, 5.0%	20.00	19.27	3.6
XAD-7, 5.0 L, 2.5%	6.67	10.32	54.6
XAD-7, 5.0 L, 5.0%	7.92	11.29	42.6
XAD-7, 0.17 L, 2.5%	19.17	28.53	48.8
XAD-7, 0.17 L, 5.0%	20.83	31.24	50.0
XAD-16, 5.0 L, 2.5%	4.58	5.68	23.9
XAD-16, 5.0 L, 5.0%	5.42	6.22	14.8
XAD-16, 0.17 L, 2.5%	7.50	15.71	109.4
XAD-16, 0.17 L, 5.0%	8.75	17.21	96.6

5.3 Immobilised Protex 6L^2 Bioconversions at Matched P/V

In order to explore scalability of immobilised Protex 6L^2 bioconversion kinetics between the miniature bioreactor and laboratory scale bioreactors, a series of experiments were performed at matched P/V values of 0.74 kWm^{-3}. This value was chosen because the corresponding mixing frequency delivers a fully turbulent flow ($Re > 10000$). Also, in both cases, being even larger than the values used in Chapter 4, the corresponding mixing frequency guarantees a full solid suspension. A 5.0 L vessel, representing the laboratory scale, was fitted with the large turbine impeller characterised in Section

5.2, while a 0.170 L vessel, representing the miniature scale, was fitted with the small turbine impeller.

Using Power number values derived in Section 5.2 and the conditions described in Section 2.9.2, various mixing frequencies and their resultant impeller Reynolds numbers and power to volume ratios were analysed. Figure 5.3 illustrates the results. To ensure the validity of scale-up experiments, it was decided to use conditions in which the difference in P/V was as small as possible and, also, the resultant flow would have been fully turbulent as to minimise any effects arising from inconsistent mass transfer across different experiments. It would have also guaranteed full suspension. Table 5.2 summarises the important parameters and operating conditions necessary for each bioreactor at a single matched P/V value.

Table 5.2: Summary of bioreactor operating conditions used in scale translation experiments at a matched energy dissipation rate of 0.74 kWm^{-3}. Power input calculated using Equation 5.1. Experiments carried out as described in Section 2.9.2.

P/V kWm^{-3}	0.74	
Bioreactor	Miniature	Laboratory
Agitation rate s^{-1}	22.42	9.75
Reynolds Number	10063	32742
Suspended particles %	> 99	> 99
Initial substrate volume ml	165.75	3412.5
Enzyme carrying particles g	0.264	5.452
Percentage of enzyme carrying particles %	20	20

Immobilised Protex 6L[2] reactions were carried out in the two bioreactors as de-

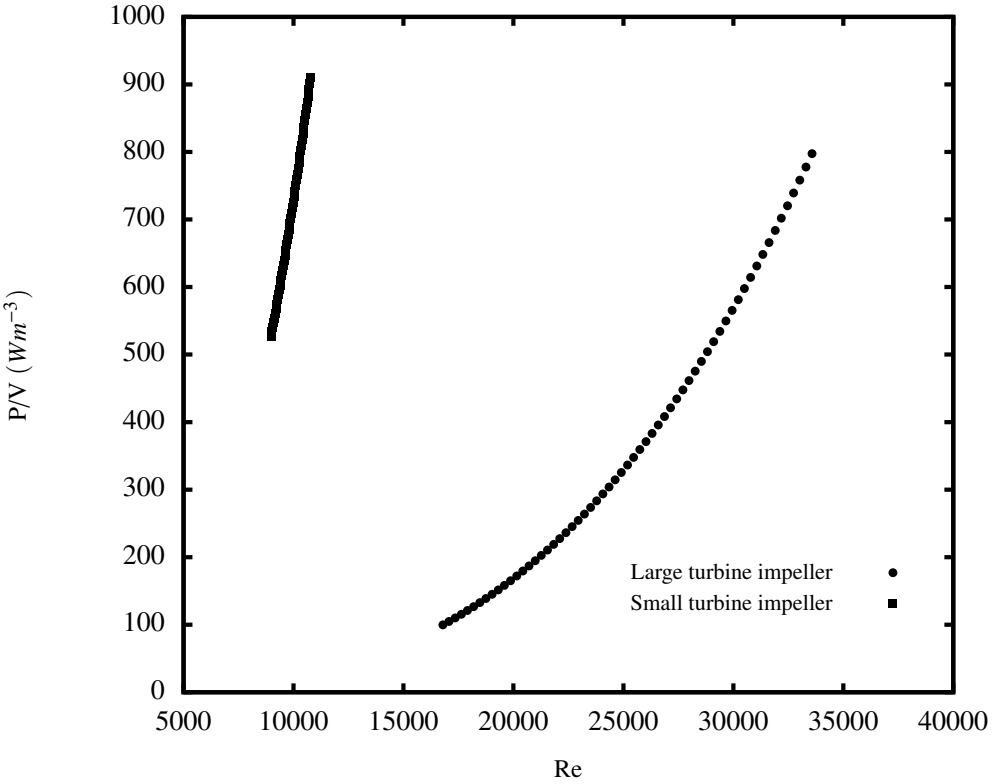

Figure 5.3: Variation of P/V values with Re for the two different bioreactor scales.

scribed in Section 2.9.2 and monitored throughout as described in Section 2.10.2 in order to generate the data required for further quantification analysis.

5.4 Quantification of Scale-up Possibilities of Immobilised Protex 6L[2]

Figure 5.4 illustrates typical data generated in the pH-stat, representing a reaction carried out in the laboratory scale bioreactor at a stirring frequency of 9.75 s^{-1} and as described in Section 2.9.2. After an initial injection of 0.5 M NaOH to adjust the pH at the predefined value of 6.8, the titrant delivery rate is adjusted as to keep the pH value of the reaction constant. This requires the dosing unit to be refilled, accounting for the drop in the pH value and the flat titrant delivery curve at around the 160 s mark. The titrant delivery rate differs before and after this refill. To account for this difference, the titrant delivery rage was average across the whole experiment.

The reaction rate was quantified as described in Section 2.10.2 using the relationship given in Equation 5.3.

$$S_a = \frac{T_c \times T_m \times 1000}{M_e}, \tag{5.3}$$

where, S_a is the specific enzyme activity, T_c is the rate of titrant consumption, T_m is the concentration of titrant and M_e is the mass of enzyme carriers used to run reaction. For the three reactions carried out in the laboratory scale bioreactor, this yielded an average value of 702 ± 27 $\mu molg^{-1}min^{-1}$. See Table 5.3 for the rate of reaction for each individual experiment.

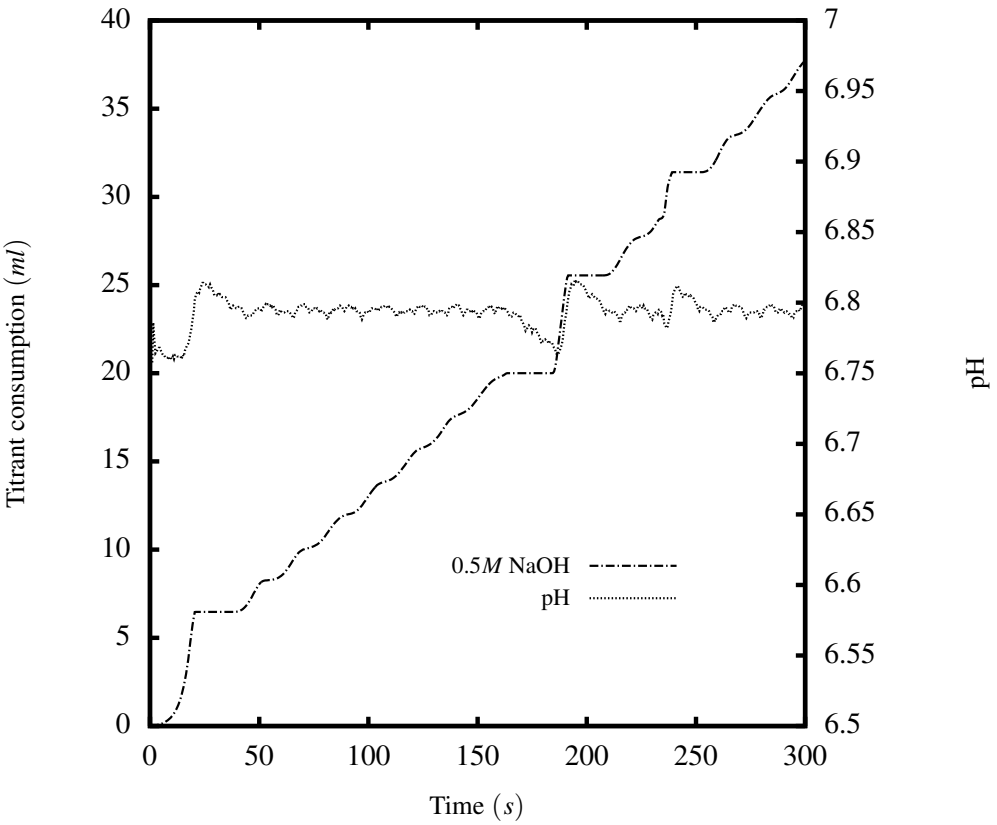

Figure 5.4: Typical pH-stat trace for measurement of the initial rate of immobilised Protex 6L[2] reaction at pH 6.8. Experimental conditions as described in Section 2.9.2. Reaction carried out at a stirring frequency of 9.75 s^{-1} in a laboratory scale bioreactor and monitored as described in Section 2.10.2.

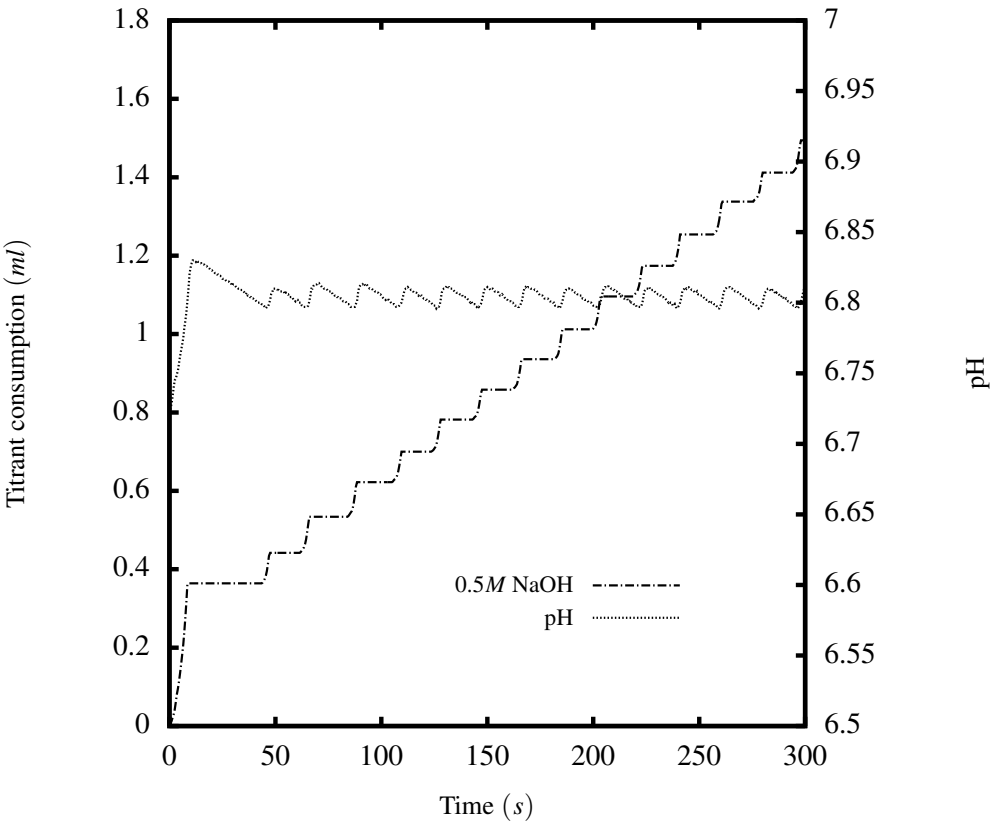

Figure 5.5: Typical pH-stat trace for measurement of the initial rate of immobilised Protex 6L[2] reaction at pH 6.8. Experimental conditions as described in Section 2.9.2. Reaction carried out at a stirring frequency of 22.42 s^{-1} in a miniature scale bioreactor and monitored as described in Section 2.10.2.

Figure 5.5 shows typical data generated during a reaction carried out in the miniature scale bioreactor at a mixing frequency of 22.42 s^{-1} and as described in Section 2.9.2. Similar to the reaction carried out in the laboratory scale bioreactor, there is an initial injection of 0.5 M NaOH in order to adjust the pH at the predefined value of 6.8. The titrant delivery rate is then adjusted to keep the pH value of the reaction constant until the reaction is carried out for a total of 5 min. Using the relationship given by Eq. 5.3, it was possible to calculate an average reaction rate of 576 ± 30 $\mu molg^{-1}min^{-1}$. See Table 5.3 for the rate of reaction for each individual experiment.

Table 5.3: Summary of individual reaction rates carried out in order to quantify scale translation possibilities. Experiments carried out as explained in Section 2.9.2 and monitored as described in Section 2.10.2.

Experiment	**Rate of reaction** $\mu molg^{-1}min^{-1}$	
	Miniature bioreactor	Laboratory bioreactor
A	565.9	691.9
B	550.0	731.9
C	607.8	681.6

The two average rates generally show good agreement, with the miniature bioreactor value being 18% lower. While the two experiments were performed at matched P/V values and full suspension, achieving these conditions necessarily meant different Re for each case. In laboratory bioreactor Re was very high and the flow fully turbulent, however the miniature bioreactor was only operated at a Re value just beyond the turbulent flow threshold. Although sufficient to fully suspend the solid phase, this could mean that external mass transfer limitations remained in place, explaining the

slightly slower bioconversion rate observed in the miniature bioreactor.

5.5 Summary

The aim of this chapter was to explore the use of matched power input per unit volume as a quantitative basis for scale transition between miniature and laboratory scale stirred tank bioreactors. In order to meet this aim the power characteristics of the turbine impellers used in this study were established (Figure 5.2) so as to be able to determine the scale transition requirements.

Based on these conditions, it was shown that matched power input per unit volume is a suitable engineering basis for bioprocess scale-up (Figures 5.4 and 5.5). The average reaction rates at miniature and laboratory scales showed generally acceptable agreement with each other (only 18% difference), despite the inevitable and large disparity in impeller Reynolds Number between miniature and laboratory scales.

Chapter 6 will conclude this study and identify the paths through which the experiments reported in this thesis can be improved and point at other directions in which the work can be taken.

Chapter 6

Conclusions and Future Work

6.1 Conclusions

In this study a number of small scale bioreactor formats have been characterised and evaluated for the study of immobilised enzyme kinetics. While the main aim has been to establish a fundamental understanding of particle suspension in these miniaturised systems (Section 1.1.2.1) the study underpins their use in early stage and high throughput biocatalytic process development (Section 1.1.5).

Shaken systems offer the opportunity for highly parallel and automated studies using only millilitre quantities of material (Section 1.1.2.1). They were therefore the initial focus of this study since currently there is no reported literature on particle suspension in shaken microwells. Here a new correlation was developed for predicting the minimum necessary shaking frequency for suspension of a range of solid particles, as given in Table 3.1, in three different microwell geometries; 24-SRW, 24-DSW and 96-DSW (Figure 2.1). At first, the effect of various factors such as well geometry, particle diameter, particle density and shaking diameter were investigated (Section 3.4). These experiments were recorded by means of high speed video equipment and the state of the suspension accurately quantified via a computational code written in MATLAB

(Appendix A). The way these different factors influence suspension and kinetics of suspension were demonstrated in Figures 3.3, 3.4 and 3.5 Finally, these results were used to form a correlation by employing dimensional analysis. The correlation itself is presented in Figure 3.7 and its accuracy tested and shown in Figure 3.8. In practical terms this would help other researchers and industry and academia to be able to predict full suspension conditions for study of different immobilised enzyme preparations.

In order to investigate and emphasise the influence that the quality of suspension has on biochemical reactions, a number of experiments were designed to synthesise L-erythrulose from glycolaldehyde and β-hydroxypyruvate acid using immobilised transketolase at different states of suspension (Section 2.9.1.2). The results, presented in Figure 3.9, confirmed that a high quality suspension, irrespective of whether it is achieved by high shaking frequency or high shaking diameter, yields constant estimates of the initial rate of reaction. Kinetics determination under poor suspension conditions led to an almost two-fold decrease in the initial reaction rate. This is important when considering the collection of quantitative kinetic data for use in bioconversion process design.

Miniature stirred bioreactor technologies are now also finding application in early stage bioprocess development. Consequently these bioreactor geometries were also studied with regard to immobilised enzyme bioconversions. Zwietering's correlation, as developed for larger scale stirred bioreactors (Section 1.1.3.1) is commonly used in various applications involving stirred tank reactors in order to predict the minimum impeller frequency required to achieve full suspension of the solid phase. It's suitability for applications carried out in stirred tank reactors outside the original volumetric range used by Zwietering was investigated here in Chapter 4 for the first time.

Experiments in a miniature scale (0.17 L) and a laboratory scale (3.5 L) working volume stirred tank reactor initially studied the effect of various parameters such as particle density, reactor geometry and solid volume fraction on particle suspension. The kinetics of suspension process were again monitored by employing high speed video equipment. The state of suspension throughout each experiment was then quantified using a further computational code developed with MATLAB (Appendix A). Influence of stirring frequency on particle suspension are presented in Figures 4.3 and 4.4. The quantified results were then compared to predicted values derived using Zwietering's correlation, as shown in Figure 4.5 and Table 4.2. They showed a large deviation between experimental and predicted suspension frequencies in the miniature reactor which has a volumetric capacity outside the range used by Zwietering. The results from the laboratory scale reactor were generally in good agreement with predicted values.

To help provide insight into the particle suspension data the behaviour of the liquid phase was numerically modelled in the two differently sized stirred tank reactors. Using CFD (Section 4.5), flow conditions, especially at the base of the vessel, were simulated over a range of stirring frequencies and the results compared. It was found that, as shown in Figure 4.7, at equal distance above or below the impeller, the magnitude of velocity across the tank radius is higher below the impeller than above it. The effect of impeller frequency on magnitude of local velocity was investigated at different distances below the impeller. The results, shown in Figure 4.8 and 4.9 show a significant increase in velocity at greater distances away from the impeller at higher Impeller frequencies. The axial component of the velocity, being the main driving force in a suspension process, was then compared and the results, shown in Figure 4.10 and 4.11, confirmed a significant rise at higher impeller frequencies. Higher axial velocities near the base

of the tank, where the particles would rest, mean higher drag forces exerted on those particles and therefore the possibility of suspension would be higher.

As with the shaken microwell systems the influence that the state and quality of suspension has on bioconversion reactions carried out in stirred tank reactors was then investigated. The model system studied involved the hydrolysis of ethyl-(S)-lactate to lactic acid using immobilised Protex $6L^2$ (Section 2.9.2). As with the microwell systems these experiments showed, as given in Figures 4.13 and 4.14, an increase in product conversion rate as the quality of suspension increased. Reactions carried out in the miniature bioreactor showed two-folds increase under full suspension conditions while reactions performed in the laboratory bioreactor under full suspension conditions registered a three-fold increase compared to reactions carried out under poor suspension conditions.

Finally, the use of constant power input per unit volume was explored as a basis for predictive scale translation between the miniature and laboratory scale stirred tank reactors. In order to facilitate this the power input characteristics of two differently sized Rushton turbine impellers were experimentally measured using an air-bearing technique (Section 2.5). The calculated Power Numbers for the small and large Rushton turbine impellers used were 3.5 and 5.7 respectively. The small turbine had a lower Power Number due to its thick blades. These Power Numbers were then used to investigate reaction scale-up possibilities from a miniature reactor to a conventional laboratory reactor using matched power input. The measured reaction rates at a matched power input of 0.74 kWm^{-3} are shown in Table 5.3 and generally indicate a good agreement between the two different scales. The slightly lower rates measured in the miniature stirred bioreactor were attributed to the lower Reynolds number used and the influence

this would have on the rate of substrate transfer to the immobilised enzyme due to external mass transfer limitations.

6.2 Future Work

Overall this study has successfully established a number of new and fundamental insights into solid suspension in small scale bioreactors and the influence suspension conditions have on the kinetics of immobilised enzyme bioconversions. In particular the work has successfully established a predictive correlation for suspension of solid particles in shaken microwell reactors (Equation 3.7), numerical modelling of the liquid phase in a stirred tank reactor (Section 4.5) and has examined scale-up possibilities between two stirred tank reactor sizes. There are, however, a number of ways in which the experiments reported can be improved and other directions in which the work can be taken. These are summarised below.

- The experiments carried out in Chapter 3 in order to establish the experimental data required for forming a mathematical correlation can be further expanded in order to increase its applicability. The biggest improvement can be made by expanding the range of particle densities and sizes used. Although the current range covers many particles used in various processes, there are other forms of particles, such as higher density glass beads that fall outside the range investigated.

- The correlation given in Equation 3.7 can be made more accurate by using more sophisticated experimental techniques such as particle image velocimetry (PIV) to track particle position during mixing process and determine the onset of suspension (Choi et al., 2002).

- Numerical prediction of particle suspension can be further improved by solving

multi-phase flow regimes with a dispersed solid phase (Derksen, 2003; Montante et al., 2001) as opposed to only investigating the liquid phase. This can then be directly compared with experiments carried out as described in this thesis.

- The scale translation experiments could be expanded to also include reactions carried out in microwell reactors in order to form a more complete picture from discovery stage to laboratory experiments and pilot/production. This would entail measuring/simulating power input characteristics into shaken microwells.

- A range of scale translation criteria could be examined including matched mixing time and k_La (for oxygen requiring bioconversions) while using different micro-organisms forming more rigorous scale-up protocols.

- The generic applicability of the microwell/miniature stirred tank reactor technologies for enzyme kinetics determination could be demonstrated by exploring a wider range of bioconversion reactions. Particularly timely examples might include study of transaminase catalysed bioconversions (Koszelewski et al., 2008; Smith et al., 2010) or the study of oxidative bioconversion processes such as chyclohexanone monooxygenase (CHMO) reactions (Baboo et al., 2012).

References

S Abia, A E Humphrey, and N Millis. *Biochemical engineering*. Academic Press, New York, 2nd edition, 1973. 49, 50, 150

C André, J Bolte, and C Demuynck. Synthesis of 4-deoxy-D-fructose and enzymatic affinity study. *Tetrahedron-Asymmetr*, 9:3737–3739, 1998. 93, 112

J A Asenjo and J C Merchuk, editors. *Bioreactor System Design*. Marcell Dekker, Inc., New York, 1994. 37, 38, 40, 41, 44

J Aubin, D F Fletcher, and C Xuereb. Modeling turbulent flow in stirred tanks with CFD: the influence of the modelling approach, turbulence model and numerical scheme. *Exp. Therm. Fluid Sci.*, 28:431–445, 2004. 129

L M Babé and C S Craik. Viral proteases: Evolution of diverse structural motifs to optimize function. *Cell*, 91:427–430, 1997. 64

J Baboo, J Galman, G J Lye, Hailes H, and M Michelettii. An automated microscale platform for evaluation and optimisation of oxidative bioconversion processes. *Biotechnol. Prog.*, 28(2):392–405, 2012. 168

A J Barrett, N D Rawlings, and J F Woessner. *Handbook of proteolytic enzymes*. Academic Press, New York, 1998. 64

T A Barrett, A Wu, H Zhang, M S Levy, and G J Lye. Microwell engineering characterization for mammalian cell culture process development. *Biotechnol. Bioeng.*, 105 (2):260–275, 2010. 104, 138

R J Barros, E Wehtje, and P Adlercreutz. Mass transfer studies on immobilised α-chymotrypsin biocatalysts prepared by deposition for use in organic medium. *Biotechnol. Bioeng.*, 59:364–373, 1998. 112

J I Betts, S D Doig, and F Baganz. Characterisation and application of a miniature 10 mL stirred tank bioreactor, showing scale-down equivalence with a conventional 7 L reactor. *Biotechnol. Prog.*, 22:681–688, 2006. 154

P Bonvillani, M P Ferrari, E M Ducrós, and J A Orejas. Theoretical and experimental study of the effects of scale-up on mixing time for a stirred tank. *Brazilian J. Chem. Eng.*, 23:1–7, 2006. 50

S P Brocklebank, R K Mitra, J M Woodley, and M D Lilly. Carbon-carbon bond synthesis: preparation and use of immobilised transketolase. *Enzyme Engineering XIII*, 799:729–736, 1996. 12, 57, 61, 62, 63

S P Brocklebank, J M Woodley, and M D Lilly. Immobilised transketolase for carbon-carbon bond synthesis: biocatalyst stability. *J. Mol. Catal. B: Enzym.*, 7:223–231, 1999. 52, 93

K Brocklehurst, A B Watts, M Patel, and E W Thomas. *Comprehensive biological catalysis*, volume 1, page 381. Academic Press, New York, 1998. 65

J Büchs, U Maier, C Milbradt, and B Zoels. Power consumption in shaking flasks on rotary shaking machines: I. power consumption measurement in unbaffled flasks at low liquid viscosity. *Biotechnol. Bioeng.*, 68:589–593, 2000. 36

W Bujalski, A W Nienow, S Chatwin, and M Cook. The dependency on scale of power numbers of Rushton turbines. *Chem. Eng. Sci.*, 42:317–326, 1987. 129, 152

C Carpio, P González, J Ruales, and F Batista-Viera. Bone-bound enzymes for food industry application. *Food Chem.*, 68:403–409, 2000. 51

S W Cavalieri, K E Neet, and H Z Sable. Enzymes of pentose biosynthesis. The quaternarystructure reacting form of transketolase from baker's yeast. *Arch. Biochem. Biophys.*, 171:527–532, 1975. 59

B H Chen, M Micheletti, F Baganz, J M Woodley, and G J Lye. An efficient approach to bioconversion kinetic model generation based on automated microscale experimentation integrated with model driven experimental design. *Chem. Eng. Sci.*, 64: 403–409, 2009. 95, 96, 112

H M Choi, T Kurihara, H Monji, and G Matsui. Measurement of particle/bubble motion and turbulence around it by hybrid PIV. *Flow Meas. Instrum.*, 12:421–428, 2002. 167

Y Q Cui, R G J M van der Lans, and K Ch A M Luyben. Local power uptake in gas-liquid systems with single and multiple Rushton turbines. *Chem. Eng. Sci.*, 51: 2631–2636, 1996. 50, 150

J J Derksen. Numerical simulation of solids suspension in a stirred tank. *AIChE J.*, 49:2700–2714, 2003. 168

Diaz and F Acevedo. Scale-up strategy for bioreactors with Newtonian and non-Newtonian broths. *Bioprocess Eng.*, 21:21–23, 1999. 46

J DiMasi, R Hansen, and H Grabowski. The price of inovation: new estimates of drug development costs. *J. Health Econ.*, 22:151–185, 2003. 31, 67

S D Doig, S C R Pickering, G J Lye, and F Baganz. Modelling surface aeration rates in shaken microtiter plates using dimensionless groups. *Chem. Eng. Sci.*, 60:2741–2750, 2005. 34, 92, 100

P M Doran. *Bioprocess Engineering Principles*. Academic Press, New York, 5th edition, 2000. 46

W A Duetz and B Witholt. Effectiveness of orbital shaking for aeration of suspended cultures in square-deepwell microtiter plates. *Biochem. Eng. J.*, 7:113–115, 2001. 34

W A Duetz, L Rüedi, R Hermann, K O'Connor, J Büchs, and B Witholt. Methods for intense aeration, growth, storage and replicatio of bacterial strains in microtiter plates. *Appl. Environ. Microbiol.*, 66:2641–2646, 2000. 32

C B Elias and J B Joshi. Role of hydrodynamic shear on activity and structure of proteins. *Adv. Biochem. Eng. Biot.*, 59:47–71, 1997. 150

I Elmahdi, F Baganz, K Dixon, T Harrop, D Sugden, and G J Lye. ph control in microwell fermentations of *s. erythraea* CA340: influence in biomass growth kinetics and erythromycin biosynthesis. *Biochem. Eng. J.*, 16:299–310, 2004. 32

S Emi and Y Murase. Protease immobilization onto copoly (ethylene/acrylic acid) fibre. *J. Appl. Polym. Sci.*, 41:2753–2767, 1990. 65

R Fernandez-Lafuente, P Armisén, P Sabuquillo, G Fernández-Lorente, and J M Guisán. Immobilization of lipases by selective adsorption on hydrophobic supports. *Chem. Phys. Lipids*, 93:185–197, 1998. 57

R T Fernley, P Iliades, and I Macreadie. A rapid assay for dihydropteroate synthase activity suitable for identification of inhibitors. *Anal. Biochem.*, 360:227–234, 2007. 109

C Ferreira-Torres, M Micheletti, and G J Lye. Microscale process evaluation of recombinant biocatalyst libraries: application to Bayer-Villiger monooxygenase catalysed lactone synthesis. *Bioprocess. Biosyst. Eng.*, 28:83–93, 2005. 32, 109

A Fersht. *Structure and Mechanism in Protein Science*. W H Freeman and Company, 1998. 64, 65

A R Fersht. Acyl-transfer reactions of amides and esters with alcohols and thiols. A reference system for the serine and cysteine proteinases. Concerning the N protonation of amides and amide-imidate equilibria. *J. Am. Chem. Soc.*, 93(14):3504–3515, 1971. 65

L Fraisse, M C Bonnet, J P de Farcy, C Agut, D Dersigny, and A Bayol. A colorimetric 96-well microtiter plate assay for the determination of urate oxidase activity and its kinetic parameters. *Anal. Biochem.*, 309:173–179, 2002. 109

M Funke, S Diederichs, F Kensy, C Müller, and J Büchs. The baffled microtiter plate: Increased oxygen transfer and improved online monitoring in small scale fermentations. *Biotechnol. Bioeng.*, 103:1118–1128, 2009. 104

N K Gill, M Appleton, F Baganz, and G J Lye. Design and characterisation of a miniature stirred bioreactor system for parallel microbial fermentations. *Biochem. Eng. J.*, 39:164–176, 2008a. 119

N K Gill, M Appleton, F Baganz, and G J Lye. Quantification of power consumption and oxygen transfer characteristics of a stirred miniature bioreactor for predictive fermentation scale-up. *Biotechnol. Bioeng.*, 100:1144–1155, 2008b. 150, 154

D Guha, P A Ramachandran, and M P Dudukovic. Flow field of suspended solids in a stirred tank reactor by Lagrangian tracking. *Chem. Eng. Sci.*, 62:6143–6154, 2007. 130

D Guha, P A Ramachandran, M P Dudukovic, and J J Derksen. Evaluation of large eddy simulation and Euler-Euler CFD models for solids flow dynamics in a stirred tank reactor. *AIChE J.*, 54:766–778, 2008. 45, 130, 138

U Hanefeld, L Gardossi, and E Magner. Understanding enzyme immobilisation. *Chem. Soc. Rev.*, 38:453–468, 2008. 54

H Hartmanna, J J Derksena, C Montavonb, J Pearsonb, Hamillb I S, and H E A van den Akkera. Assessment of large eddy and RANS stirred tank simulations by means of LDA. *Chem. Eng. Sci*, 59:2419–2432, 2004. 44

T Hayashi and Y Ikada. Protease immobilization onto porous chitosan beads. *J. Appl. Polym. Sci.*, 42:85–92, 1991. 67

H-J Henzler. Verfahrenstechnische auslecrunasunterlacren für rührbehälter als fermenter. *Chem. Ing. Tech.*, 54:461–476, 1982. 40

R Hermann, M Lehmann, and J Büchs. Characterisation of gas-liquid mass transfer phenomena in microtiter plates. *Biotechnol. Bioeng.*, 81:178–186, 2003. 33, 92, 100, 104

E Hibbert, F Baganz, H Hailes, J War, G J Lye, J Woodley, and P A Dalby. Directed evolution of biocatalytic processes. *Biomol. Eng.*, 22:11–19, 2005. 32

H Horvath. Gustav Mie and the scattering and absorption oflight by particles: Historic developments and basics. *J. Quant. Spectrosc. Radiat. Transfer.*, 110:787–799, 2009. 70

M Hosobuchi and H Yoshikawa. *Manual of industrial microbiology and biotechnology.* ASM Press, Washington, D.C., 2nd edition, 1999. 48, 149

A Hughmark. Power requirements and interfacial area in gas-liquid turbine agitated systems. *Ind. Eng. Chem. Proc. D. D.*, 19:638–641, 1980. 50

N Jackson, J M Liddell, and G J Lye. An automated microscale technique for the quantitative and parallel analysis of microfiltration operations. *J. Membr. Sci.*, 276: 31–41, 2006. 33

Z Jaworski, K N Dyster, I P T Moore, A W Nienow, and M L Wyszynski. The use of angle resolved LDA data to compare two different turbulence models applied to sliding mesh CFD flow simulations in a stirred tank. *Récent Progès en Génie des Procédés*, 11:187–194, 1997. 130

M Jenne and M Reuss. A critical assessment on the use of $k - \epsilon$ turbulence models forsimulation of the turbulent liquid flow induced by a Rushton-turbine in baffed stirred-tank reactors. *Chem. Eng. Sci.*, 54:3921–3941, 1999. 44

R E Johnston and M W Thring. *Pilot plants, models and scale-up methods.* McGraw Hill, New York, 1957. 47

R M Jones, A D Harvey III, and S Acharya. Two-equation turbulence modelling for impeller stirred tanks. *J. Fuilds Eng.*, 123:640–648, 2001. 44

L K Ju and G G Chase. Improved scale-up strategies of bioreactors. *Bioproc. Eng.*, 8: 49–53, 1992. 45, 48, 49, 149, 150

H Junker. Scale-up methodologies for *Escherichia coli* and yeast fermentation processes. *J. Biosci. Bioeng.*, 97:347–364, 2004. 49

A I Kallenberg, F van Ranwijk, and R A Sheldon. Immobilization of penicillin G acylase: the key to optimum performance. *Adv. Synth. Catal.*, 347:905–926, 2005. 93

B Karki, D Maurer, and S Jung. Efficiency of pretreatments for optimal enzymatic saccharification of soybean fiber. *Bioresource Technol.*, 102:6522–6528, 2011. 141

G R Kasat, A R Khopkar, V V Ranade, and A B Pandit. CFD simulation of liquid-phase mixing in solid–liquid stirred reactor. *Chem. Eng. Sci.*, 63:3877–3885, 2008. 45

E Katchalski-Katzir. Immobilized enzymes learning from past successes and failures. *Trends Biotechnol.*, 11:471–478, 1993. 52

A Kheirolomoom, F Khorasheh, and H Fazelinia. Influence of external mass transfer limitation on apparant kinetic parameters of penicilin g acylase immobilised on nonporous ultrafin silica particles. *J. Biosci. Bioeng.*, 93:125–129, 2002. 112, 141

K Kipke. Erosiver verschlei von rürorganen. *Chem. Ing. Tech.*, 52:658–659, 1980. 41

R Kirill, H Schultze, M Bot, U Bornscheuer, and J Büchs. Enzyme test bench, a high-throughput enzyme characterization technique including the long-term stability. *Biotechnol. Bioeng.*, 103:305–322, 2009. 109, 138

Y Kostov, P Harms, L Randers-Eichhorn, and G Rao. Low-cost microbioreactor for high-throughput bioprocessing. *Biotechnol. Bioeng.*, 71:346–352, 2001. 32

D Koszelewski, I Lavandera, D Clay, and D Rozzell. Asymmetric synthesis of optically pure pharmacologically relevant amines employing ω-Transaminases. *Adv. Synth. Catal.*, 350:2761–2766, 2008. 168

V Kourilov and M Steinitz. Magnetic-bead enzyme-linked immunosorbent assay verifies adsorption of ligand and epitope accessibility. *Anal. Biochem.*, 311:166–170, 2002. 93

B Krajewska. Application of chitin- and chitosan-based materials for enzyme immobilizations: a review. *Enzyme Microb. Tech.*, 35:126–139, 2004. 51

S M Kresta and P E Wood. Prediction of the three-dimensional turbulent flow in stirred tanks. *AIChE J.*, 37:448–460, 1991. 119

T Kubitzki, T Noll, and S Lütz. Immobilisation of bovine enterokinase and application of the immobilised enzyme in fusion protein cleavage. *Bioprocess. Biosyst. Eng.*, 31: 173–182, 2008. 56, 57

D J Lamberto, M M Alvarez, and F J Muzzio. Computational analysis of regular and chaotic mixing in a stirred tank reactor. *Chem. Eng. Sci.*, 56:4887–4899, 2001. 130

J C W Lan, G E Hamilton, and A Lyddiatt. Physical and biochemical characterization of a simple intermediate between fluidized and expanded bed contactors. *Bioseparation*, 8:43–51, 1999. 94

G Larsson, M Tornkvist, E S Wernersson, C Traigardh, H Noorman, and S O Enfors. Substrate gradients in bioreactors: origin and consequences. *Bioproc. Eng.*, 14:281–289, 1996. 50

A Liese, K Seelback, and C Wandrey. *Industrial biotransformations*. Wiley-VCH, 2nd edition, 2006. 51

Y Lindqvist, G Schneider, U Ermler, and M Sundström. Three-dimensional structure of transketolase, a thiamine diphosphate dependent enzyme, at 2.5 A resolution. *EMBO J.*, 11(7):2372–2379, 1992. 12, 59, 60

H T Luong and B Volesky. Mechanical power requirements of gas-liquid agitated systems. *AIChE J.*, 25:893–895, 1979. 50

G J Lye, P A Shamlou, F Baganz, P A Dalby, and J M Woodley. Accelerated design of bioconversion process using automated microscale processing techniques. *Trends. Biotechnol.*, 21:29–37, 2003. 31, 67, 94

F Mantzouridou, T Roukas, and P Kotzekidou. Effect of the aeration rate and agitation speed on β-carotene production and morphology of *Blakeslea trispora* in a stirred tank reactor: mathematical modelling. *Biochem. Eng. J.*, 10:123–135, 2002. 150

M Marques, C Carvalho, M Claudino, J Cabral, and P Fernandes. On the feasibility of the microscale approach for a multistep biotransformation: sitosterol side chain cleavage. *J. Chem. Technol. Biotechnol.*, 82:856–863, 2007. 32

M P C Marques, J M S Carbal, and P Fernandes. High throughput in biotechnology: From shake-flasks to fully instrumented microfermentors. *Recent Pat. Biotechnol.*, 3:124–140, 2009. 31, 67

C Mateo, J M Palomo, G Fernandez-Lorente, J M Guisan, and R Fernandez-Lafuente. Improvement of enzyme activity, stability and selectivity via immobilization techniques. *Enzyme Microb. Tech.*, 40:1451–1463, 2007. 51, 52, 57, 112

S Matosevic, G J Lye, and F Baganz. Design and characterization of a prototype enzyme microreactor: quantification of immobilised transketolase kinetics. *Biotechnol. Prog.*, 26:118–126, 2010. 112

F Mavituna. *Computer and information science application in bioprocess engineering*, chapter Strategies for bioreaactor scale-up. Kluwer Academic, 1996. 50

C B Mazza, K Rege, C Breneman, N Sukumar, J Dordick, and S Cramer. High-throughput screening and quantitative structure-efficiency relationship models of potential displacer molecules. *Biotechnol. Bioeng.*, 80:60–72, 2002. 33

J Michel and S A Miller. Power requirements of gas-liquid agitated systems. *AIChE J.*, 8:262–266, 1962. 50

M Micheletti and G J Lye. Microscale bioprocess optimisation. *Curr. Opin. Biotechnol.*, 17:231–245, 2006. 30, 31, 32, 67

M Micheletti, T A Barrett, S D Doig, F Baganz, M S Levy, J M Woodley, and G J Lye. Fluid mixing in shaken bioreactors: implications for scale-up predictions from microlitre scale microbial and mammalian cell cultures. *Chem. Eng. Sci.*, 61:2939–2949, 2006. 67, 94, 104

I Migneault, C Dartiguenave, M J Bertrand, and K C Waldron. Glutaraldehyde: behavior in aqueous solution, reaction with proteins, and application to enzyme cross-linking. *BioTechniques*, 37:790–802, 2004. 57

M Minier and G Goma. Ethanol production by extraction fermentation. *Biotechnol. Bioeng.*, 24:1565–1579, 1982. 95

R K Mitra and J M Woodley. A useful assay for transketolase in assymetric syntheses. *Biotechnol. Tech.*, 10:167–172, 1996. 90

H O Mockel, H Weissgärber, and K Börner. Der leistungseintrag in belüfeten rührsystemen mit niedrigviskosen median. *Chem. Techn.*, 35:344–347, 1983. 50, 150

G Montante, G Micale, F Magelli, and A Brucato. Experiments and CFD predictions of solid sarticle sistribution in a sessel agitated with four pitched blade turbines. *Chem. Eng. Res. Des.*, 79:1005,1010, 2001. 168

A W Nienow. Suspension of solid particles in turbine agitated baffled vessels. *Chem. Eng. Sci.*, 23:1453–1459, 1968. 42

A W Nienow and D Miles. A dynamometer for the accurate measurement of mixing torque. *J. Sci. Instrum. 2*, 2:994–995, 1969. 74

A W Nienow, G Hunt, and B C Buckland. A fluid dynamic study of the retrofitting of large agitated bioreactors: Turbulent flow. *Biotechnol. Bioeng.*, 44:1177–1185, 1994. 152

J Y Oldshue. *Chemical engineering: concepts and reviews*, volume 1: Mixing of liquids by mechanical agitation. Garden and Breach Science, 1985. 46

M G Oosterhuis and N W F Kossen. *Biotechnology*, volume 2. Verlagsgesellschaft, Berlin, 1985. 47, 48, 149, 150

P Pecher and U Arnold. The effect of additional disulfide bonds on the stability and folding of ribonuclease A. *Biophys. Chem.*, 141:21–28, 2009. 109, 138

C Peter, Y Suzuki, and Büchs J. Hydrodynamical stress in shake flasks: correlation for the maximum local energy. *Biotechnol. Bioeng.*, 93:1164–1176, 2006. 35

R Puskeiler, K Kaufmann, and D Weuster-Botz. Development, parallelisation, and automation of a gas inducing millilitre-scale bioreactor for high-throughput bioprocess design (HTBD). *Biotechnol. Bioeng.*, 89:512–523, 2005. 154

R Raab, K Tyo, and G Stephanopoulos. Metabolic engineering. *Adv. Biochem. Eng. Biotechnol.*, 100:1–17, 2006. 32

K Rege, A Ladiwala, N Tugcu, C Breneman, and S Cramer. Parallel screening of selective and high-affinity displacers for proteins in ion-exchange systems. *J. Chromatogr. A.*, 1033:19–28, 2004. 33

M Reuss. Oxygen transfer and mixing: scale-up implications. In *Biotechnology*. Wiley-VCH Verlag GmbH, Weinheim, 2nd edition, 1993. 38

M Reuss, S Frhlich, B Kramer, K Messerschmidt, and G Pommerening. Coupling of microbial kinetics and oxygen transfer for analysis and optimization of gluconic acid production with Aspergillus niger. *Bioprocess Eng.*, 1(2):79–91, 1986. 40, 116

T Reynolds, M Boychyn, T Sanderson, M Bulmer, and J More. Scale-down of continuous filtration for rapid bioprocess design: recovery and dewatering of protein precipitate suspension. *Biotechnol. Bioeng.*, 83:454–464, 2003. 33

J M T Ruben, J P Aucamp, R George, and P A Dalby. Structural stability of *e.coli* transketolase to urea denaturation. *Enzyme Microb. Technol.*, 41:653–662, 2007. 109, 138

K Rutherford, S M S Mahmoudi, K C Lee, and M Yianneskis. The influence of Rushton impeller blade thickness on the mixing characteristics of stirred vessels. *Trans. IChemE*, 74(Part A):369–378, 1996. 152

S Schmalzriedt and M Ruess. Application of computational fluid dynamics to simulations of mixing and biotechnolgical conversion processes in stirred tank bioreactors. In *Proceedings of the 9th European Conference on Mixing*, Paris, March 1999. 43

F R Schmidt. Optimization and scale up of industrial fermentation processes. *Appl. Microbiol. Biotechnol.*, 68:425–435, 2005. 23, 46, 49, 50, 150

M E Sensel, K J Myers, and J B Fasano. Gas dispersion at high aeration rates in low to moderately viscous newtonian liquids. *AIChE Symposium Series 293*, 89:76, 1993. 49, 150

P A Shamlou. *Processing of Solid-Liquid Suspension*, chapter 10, page 228. Butterworth-Heinermann Ltd, Oxford, 1993. 41, 42, 103, 137

S Shin, M S Hong, and J Lee. Oxygen transfer correlation in high cell density culture of recombinant *E.coli*. *Biotechnol. Techn.*, 10:679–682, 1996. 50

S K Singh, I D Clarke, M Terasaki, V E Bonn, C Hawkins, J Squire, and P B Dirks. Identification of cancer stem cell in human brain tumors. *Cancer Res.*, 63:5821–5828, 2003. 94

M E B Smith, B H Chen, E G Hibbert, U Kaulmann, K Smithies, J L Galmant, F Baganz, P A Dalby, H C Hailes, G J Lye, J M Ward, J M Woodley, and M Micheletti. A multidisciplinary approach toward the rapid and preparative-scale biocatalytic synthesis of chiral amino alcohols: A concise Transketolase-/ω-Transaminase-mediated synthesis of (2S,3S)-2-Aminopentane-1,3-diol. *Org. Process Res. Dev.*, 14:99–107, 2010. 168

F Stanbury, A Whitaker, and S J Hall. *Principles of fermentation technology*. Butterworth-Heinermann Ltd, Oxford, 2nd edition, 2003. 46, 47, 48, 50, 149

A Steiff, R Poggemann, and P-M Weinspach. Wärmeübergang in rührkesseln mit mehrphasigen systemen. *Chem. Ing. Tech.*, 52:492–503, 1980. 41

D Subbarao and V K Taneja. Three phase suspension in agitated vessels. *Proc. 3rd Eur. Conf. Mixing*, 1:229–240, 1979. 42

A Togatorop, R Mann, and D F Schofield. An application of CFD to inert and reactive tracer mixing in a natch stirred vessel. *Aiche. Symposium Series*, 299:19, 1994. 43

X D Tong and Y Sun. Ndfeb alloy-densified agarose gel for expanded bed adsorption of proteins. *J. Chromatogr. A.*, 943:63–75, 2002. 94

H S Toogood, I N Talor, R C Brown, S J C Taylor, R McCague, and J A Littlechild. Immobilisation of the thermostable l-aminoacylase from thermococcus litoralis to

generate a reusable industrial biocatalyst. *Biocatal. Biotransfor.*, 20(4):241–249, 2002. 56, 57, 58

E Topoglidis, T Lutz, R L Willis, C J Barnett, A E G Cass, and J R Durrant. Protein adsorption on nanoporous tio_2 films: a novel approach to studying photoinduced protein/electrode transfer reactions. *Faraday Discuss.*, 116:35–46, 2000. 56

K van't Riet. Review of measuring methods and results in non-viscous gas-liquid mass transfer in stirred vessels. *Ind. Eng. Chem. Process D. D.*, 18(3):357–364, 1979. 40

K van't Riet and H Tramper. *Basic Bioreactor Design*. Marcell Dekker Inc., New York, 1991. 37, 38, 41, 116

S Vishvanath, D Bhattacharyya, W Huang, and L G Bachas. Site-directed and random enzyme immobilization on functionalized membranes: kinetic studies and models. *J. Membrane Sci.*, 108:1–13, 1995. 52

C Wang, C L Cooney, A I Demian, P Dunhill, A E Humphrey, and M D Lilly. *Fermentation and enzyme technology*. Wiley and Sons, New York, 1979. 49

J Wang and J A Carlisle. Covalent immobilization of glucose oxidase on conducting ultrananocrystalline diamond thin films. *Diam. Relat. Mater.*, 15:279–284, 2006. 57

J M Woodley and N J Titchener-Hooker. The use of windows of operation as a bioprocess design tool. *Bioprocess Eng.*, 14:263–268, 1996. 106

J M Woodley, R K Mitra, and M D Lilly. Carbon-carbon bond synthesis: reactor design and operation for transketolase-catalysed biotransformations. *Enzyme Engineering XIII*, 799:434–445, 1995. 63, 93

J Wu, L A Johnson, and S Jung. Demulsification of oil-rich emulsion from enzyme-assisted aqueous extraction of extruded soybean flakes. *Bioresource Technol.*, 100: 527–733, 2009. 64, 141

D Yamamoto, K Matsumoto, H Ohishi, T Ishida, M Inoue, K Kitamuta, and H Mizuno. Refined x-ray structure of papain.E-64-c complex at 2.1-A resolution. *J. Biol. Chem.*, 266:14771–14777, 1991. 12, 66

H Zhang, S Lamping, and P A Shamlou. Numerical simulation of mixing in a micro-well scale bioreactor by computational fluid dynamics. *Chem. Res. Chinese U.*, 18: 113–116, 2002. 34

F T Zimmermann, A Schneider, U Schörken, G A Sprenger, and W-D Fessner. Efficient multi-enzymatic synthesis of D-xylulose 5-phosphate. *Tetrahedron-Asymmetr*, 10: 1643–1646, 1999. 93, 112

T H N Zwietering. Suspending of solid particles in liquid by agitators. *Chem. Eng. Sci.*, 8:244–253, 1958. 42, 104, 108, 116, 118, 121, 124, 127, 154, 193, 194

Appendix A

Verbatim MATLAB Code

A.1 MATLAB Code Used in Chapter 3

```
clc

clear all

cd E:\335RPM

files = dir;

b=0

Count=zeros(length(files),2);

for i=3:2:length(files)


    I1 = imread(files(i).name);

    I2 = imcrop(I1 ,[111 435 505 560]);

    J = imnoise(I2,'gaussian',0,0.0000001);

    K = wiener2(J,[25 25]);

    L = imsubtract(J,K);

    I3 = im2double(L);
```

```
c=0;
I4=im2double(I3);

x=40;
y=40;
radius=3;
value=120/255;
M=zeros(x,y);
xc = int16(x/2);
yc = int16(y/2);

x = int16(0);
y = int16(radius);
d = int16(1 - radius);

M(xc, yc+y) = value;
M(xc, yc-y) = value;
M(xc+y, yc) = value;
M(xc-y, yc) = value;

while ( x < y - 1 )
    x = x + 1;
    if ( d < 0 )
        d = d + x + x + 1;
    else
        y = y - 1;
```

```
        a = x - y + 1;
        d = d + a + a;
    end
    M( x+xc,  y+yc) = value;
    M( y+xc,  x+yc) = value;
    M( y+xc, -x+yc) = value;
    M( x+xc, -y+yc) = value;
    M(-x+xc, -y+yc) = value;
    M(-y+xc, -x+yc) = value;
    M(-y+xc,  x+yc) = value;
    M(-x+xc,  y+yc) = value;
end

I5=imfilter(I4,M, 'conv','circular', 'same');

bw=im2bw(I5, graythresh(I5));

bw=bwareaopen(bw,50);

L=bwlabel(bw);
s=regionprops(L, 'PixelIdxList');
max_values=zeros(numel(s),1);

for k=1:numel(s)
    max_value(k)=max(I5(s(k).PixelIdxList));
end
```

```
bright_objects=find(max_value > 0.5);
I6=ismember(L, bright_objects);

I7=im2double(I6);
I8=edge(I7);
I9 = imfill(I8,'holes');

[B,L] = bwboundaries(I9,'noholes');

imshow(label2rgb(L, @jet, [.5 .5 .5]))
hold on
for k = 1:length(B)
     boundary = B{k};
     plot(boundary(:,2), boundary(:,1), 'w', 'LineWidth', 2)
end

stats = regionprops(L,'Area','Centroid');

downthreshold = 0.94;
upthreshold = 1.05;

for k = 1:length(B)

    boundary = B{k};
```

```
    delta_sq = diff(boundary).^2;
    perimeter = sum(sqrt(sum(delta_sq,2)));

    area = stats(k).Area;

    metric = 4*pi*area/perimeter^2;
    stats(k).Metric = metric;

    metric_string = sprintf('%2.2f',metric);

    if upthreshold > metric && metric > downthreshold
        c=c+1;
        centroid = stats(k).Centroid;
        plot(centroid(1),centroid(2),'ko');
    end

    text(boundary(1,2)-35,boundary(1,1)+13,metric_string,...
     'Color','y','FontSize',7,'FontWeight','bold');
end

title(['Metrics closer to 1 indicate that ',...
    'the object is approximately round']);
Count(i-2,1)=i-2;
Count(i-2,2)=c;
b=b+1
```

```
end
```

A.2 MATLAB Code Used in Chapter 4

```
clc
clear all
cd /media/STR/XAD-16(small2.5)/300RPM/MVI_0049
files = dir;
count = zeros((length(files)-1),8);
b = 0;
c = 1;


for i = 3:49:length(files);


    if i >= (length(files)-50)
        break
    elseif i <= (length(files)-50)
        I1 = imread (files(i).name);
        I2 = imcrop (I1, [144 187 42 42]);
        I3 = rgb2gray (I2);
        I4 = imcrop (I1, [333 406 42 42]);
        I5 = rgb2gray (I4);
        I6 = imcrop (I1, [510 220 42 42]);
        I7 = rgb2gray (I6);
        I8 = imcrop (I1, [321 35 42 42]);
        I9 = rgb2gray (I8);
```

```
I10 = imcrop (I1, [280 290 42 42]);
I11 = rgb2gray (I10);
I12 = imcrop (I1, [406 290 42 42]);
I13 = rgb2gray (I12);
I14 = imcrop (I1, [384 147 42 42]);
I15 = rgb2gray (I14);
I16 = imcrop (I1, [228 162 42 42]);
I17 = rgb2gray (I16);
J1 = imread (files(i+50).name);
J2 = imcrop (J1, [144 187 42 42]);
J3 = rgb2gray (J2);
J4 = imcrop (J1, [333 406 42 42]);
J5 = rgb2gray (J4);
J6 = imcrop (J1, [510 220 42 42]);
J7 = rgb2gray (J6);
J8 = imcrop (J1, [321 35 42 42]);
J9 = rgb2gray (J8);
J10 = imcrop (J1, [280 290 42 42]);
J11 = rgb2gray (J10);
J12 = imcrop (J1, [406 290 42 42]);
J13 = rgb2gray (J12);
J14 = imcrop (J1, [384 147 42 42]);
J15 = rgb2gray (J14);
J16 = imcrop (J1, [228 162 42 42]);
J17 = rgb2gray (J16);
```

```
        D1 = sqrt(sum((I3(:) - J3(:)).^2)) / sqrt(sum(J3(:).^2));
        D2 = sqrt(sum((I5(:) - J5(:)).^2)) / sqrt(sum(J5(:).^2));
        D3 = sqrt(sum((I7(:) - J7(:)).^2)) / sqrt(sum(J7(:).^2));
        D4 = sqrt(sum((I9(:) - J9(:)).^2)) / sqrt(sum(J9(:).^2));
        D5 = sqrt(sum((I11(:) - J11(:)).^2)) / sqrt(sum(J11(:).^2));
        D6 = sqrt(sum((I13(:) - J13(:)).^2)) / sqrt(sum(J13(:).^2));
        D7 = sqrt(sum((I15(:) - J15(:)).^2)) / sqrt(sum(J15(:).^2));
        D8 = sqrt(sum((I17(:) - J17(:)).^2)) / sqrt(sum(J17(:).^2));

        count(c,1) = D1;
        count(c,2) = D2;
        count(c,3) = D3;
        count(c,4) = D4;
        count(c,5) = D5;
        count(c,6) = D6;
        count(c,7) = D7;
        count(c,8) = D8;
        b = 0;
        c = c + 1;
    end
end
```

Appendix B

Derivation of N_{90} Correlation

Using the work carried out by Zwietering (1958) as an analogy, the physical parameters given in Table B.1 will determine whether the solid particles will be in suspension or not.

Table B.1: Physical parameters deterministic in suspension of solid particles.

Parameter	**Unit**
Well diameter, d_w	m
Liquid height, h_L	m
Shaking diameter, d_s	m
Shaking frequency, N_s	s^{-1}
Particle diameter, d_p	m
Particle density, ρ_s	kgm^{-3}
Liquid density, ρ	kgm^{-3}
Kinematic viscosity, ν	m^2s^{-1}
Solid fraction, S_f	%
Acceleration due to gravity, g	ms^{-1}

Zwietering suggests seven dimensionless groups, which in this case are

$$d_w \sqrt[3]{\frac{g}{\nu^2}} \quad h_L \sqrt[3]{\frac{g}{\nu^2}} \quad d_s \sqrt[3]{\frac{g}{\nu^2}} \quad d_p \sqrt[3]{\frac{g}{\nu^2}} \quad N_s \sqrt[3]{\frac{g}{\nu^2}} \quad S_f.$$

In each experiment, these groups can be varied independently without changing the values of ν and g. According to Zwietering they are related to each other by the relationship given in Equation B.1.

$$N_s = K_1 {d_w}^a {d_s}^b {d_p}^c {S_f}^e \quad \text{for constant} \quad \frac{d_w}{h_L} \tag{B.1}$$

Therefore, the general relationship between the dimensionless groups will be of the form given in Equation B.2, however, as explained in Section 3.4, it was not possible to adhere to constant d_w/h_L criteria and cases approximately similar to each other were used instead.

$$N_s \sqrt[3]{\frac{g}{\nu^2}} = K_2 \left[d_w \sqrt[3]{\frac{g}{\nu^2}} \right]^a \left[d_s \sqrt[3]{\frac{g}{\nu^2}} \right]^b \left[d_p \sqrt[3]{\frac{g}{\nu^2}} \right]^c {S_f}^e$$

$$= K_2 {d_w}^a \left(\frac{g}{\nu^2} \right)^{a/3} {d_s}^b \left(\frac{g}{\nu^2} \right)^{b/3} {d_p}^c \left(\frac{g}{\nu^2} \right)^{c/3} {S_f}^e \tag{B.2}$$

It is important to emphasise that according to further experiments performed by Zwietering with liquids of different viscosity, the effect of density, whether that of the solid phase or that of the liquid phase, is similar to the effect of gravity, meaning it shares the same exponent and can be added to the relationship later.

Following Zwietering's method, Equation B.2 can be rearranged.

$$N_s = K_2 \left(\frac{d_w}{d_s}\right)^a {d_w}^f {d_p}^c {S_f}^e \nu^{\frac{1+2f+2c}{3}} g^{\frac{2+f+c}{3}} \quad \text{where} \quad f = a + b$$

substituting $c = 0.248$ and $e = -0.028$ (see Figures B.1 and B.2)

$$\therefore N_s = K_2 \left(\frac{d_w}{d_s}\right)^a {d_w}^f {d_p}^{0.248} {S_f}^{-0.028} \nu^{\frac{2f+1.496}{3}} g^{\frac{f+2.248}{3}}$$

substituting $f = -0.957$ (see Figures B.3 and B.4)

$$\therefore N_s = K_2 \left(\frac{d_w}{d_s}\right)^a {d_w}^{-0.957} {d_p}^{0.248} {S_f}^{-0.028} \nu^{0.14} g^{0.43}$$

$$\therefore K_2 \left(\frac{d_w}{d_s}\right)^a = \frac{N_s}{{d_w}^{-0.957} {d_p}^{0.248} {S_f}^{-0.028} \nu^{0.14} g^{0.43}}$$

$$\therefore S = \frac{N_s}{{d_w}^{-0.957} {d_p}^{0.248} {S_f}^{-0.028} \nu^{0.14} g \frac{\Delta\rho}{\rho}^{0.43}} \quad \text{for constant} \quad \frac{d_w}{h_L} \tag{B.3}$$

Rearranging Equation B.3 is the final step to deriving a mathematical formulation for N_{90} correlation, given in Equation B.4.

$$N_{90} = S {d_p}^{0.25} \nu^{0.14} \left(g\frac{\Delta\rho}{\rho}\right)^{0.43} {d_s}^{-0.96} {S_f}^{-0.03} \tag{B.4}$$

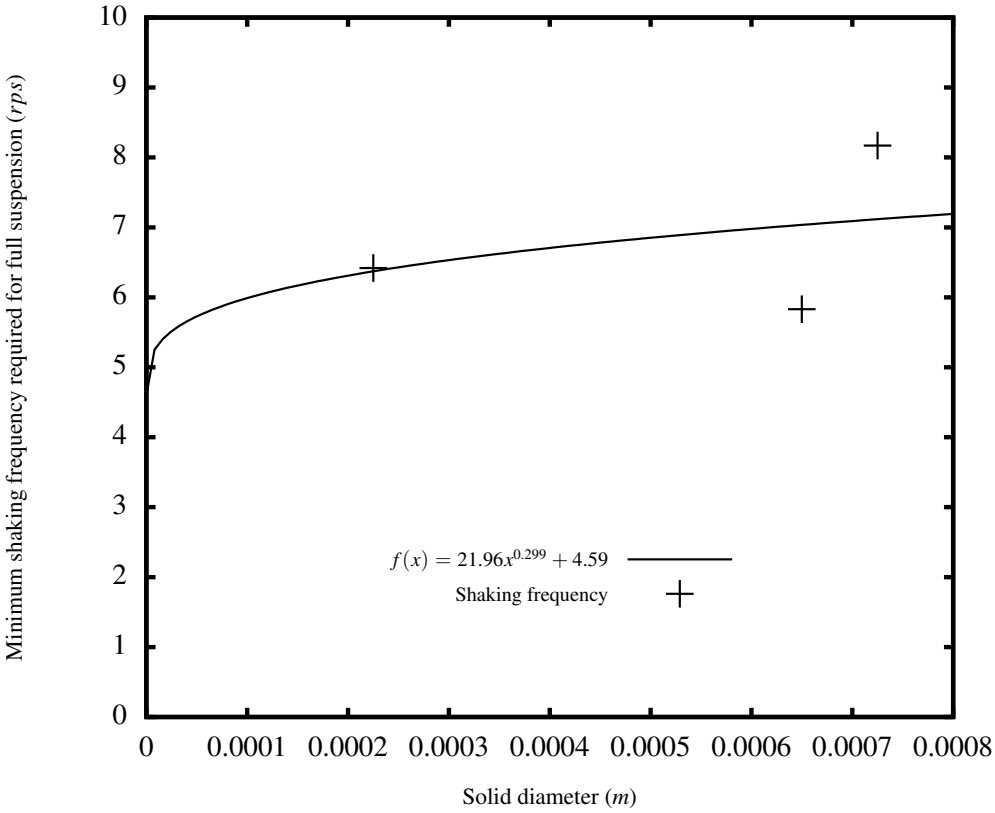

Figure B.1: Typical example of variation in shaking frequency with respect to solid diameter, d_p. c is calculated by averaging the exponent of x across all experiments. Experiments performed as described in Section 2.6.1. Operating conditions: $d_w/h_L = 1.54$, $d_s = 0.006\ m$ and $S_f = 0.5\%$ v/v.

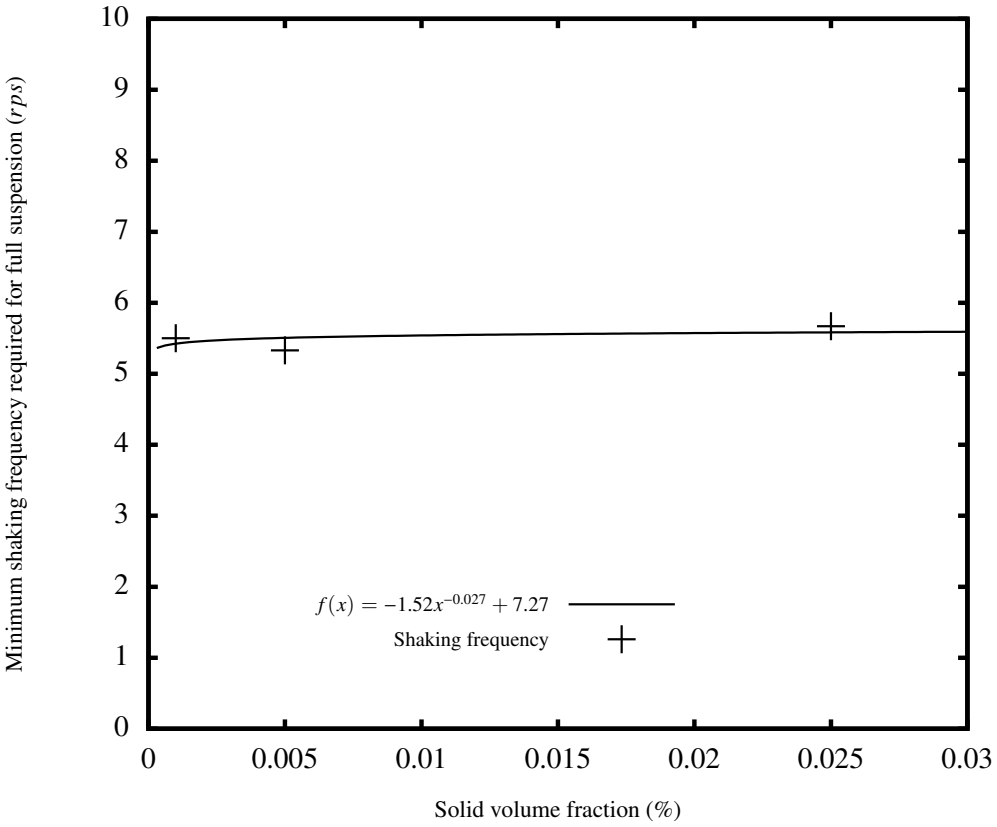

Figure B.2: Typical example of variation in shaking frequency with respect to solid volume fraction, S_f. e is calculated by averaging the exponent of x across all experiments. Experiments performed as described in Section 2.6.1. Operating conditions: XAD-7, $d_w/h_L = 1.39$ and $d_w = 0.0125\ m$.

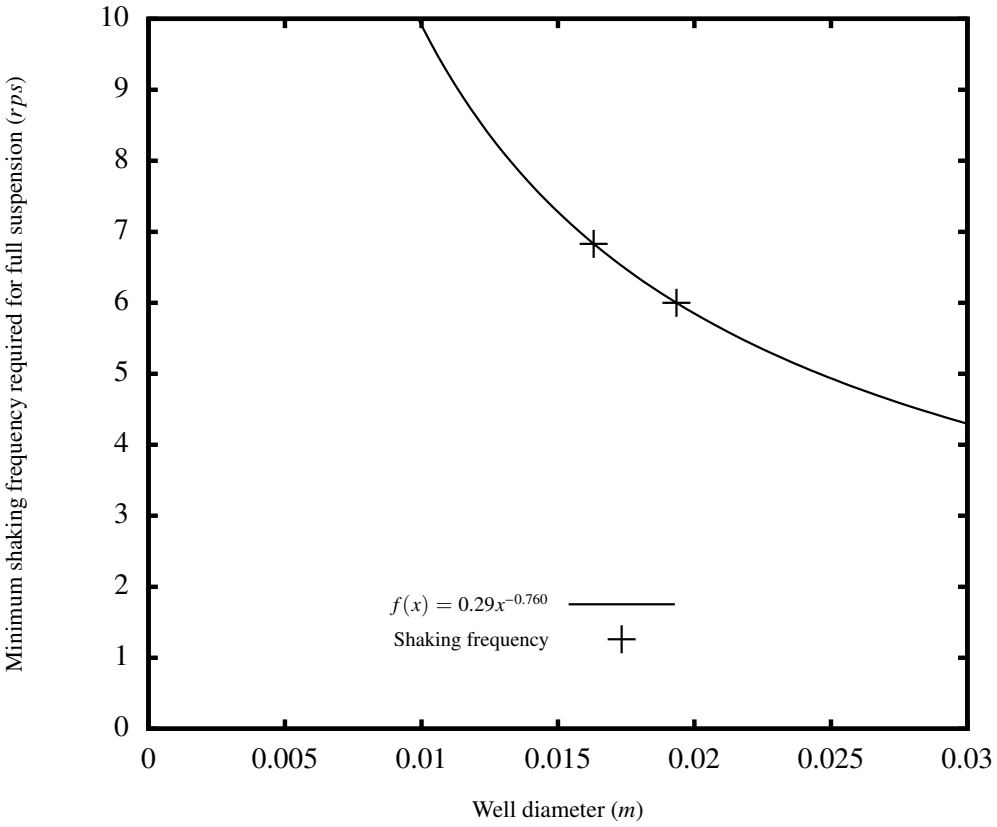

Figure B.3: Typical example of variation in shaking frequency with respect to well diameter, d_w. a is calculated by averaging the exponent of x across all experiments. Experiments performed as described in Section 2.6.1. Operating conditions: XAD-16, $d_w/h_L = 2.16$ and 2.16, $d_s = 0.003\ m$ and $S_f = 0.1\%$ v/v.

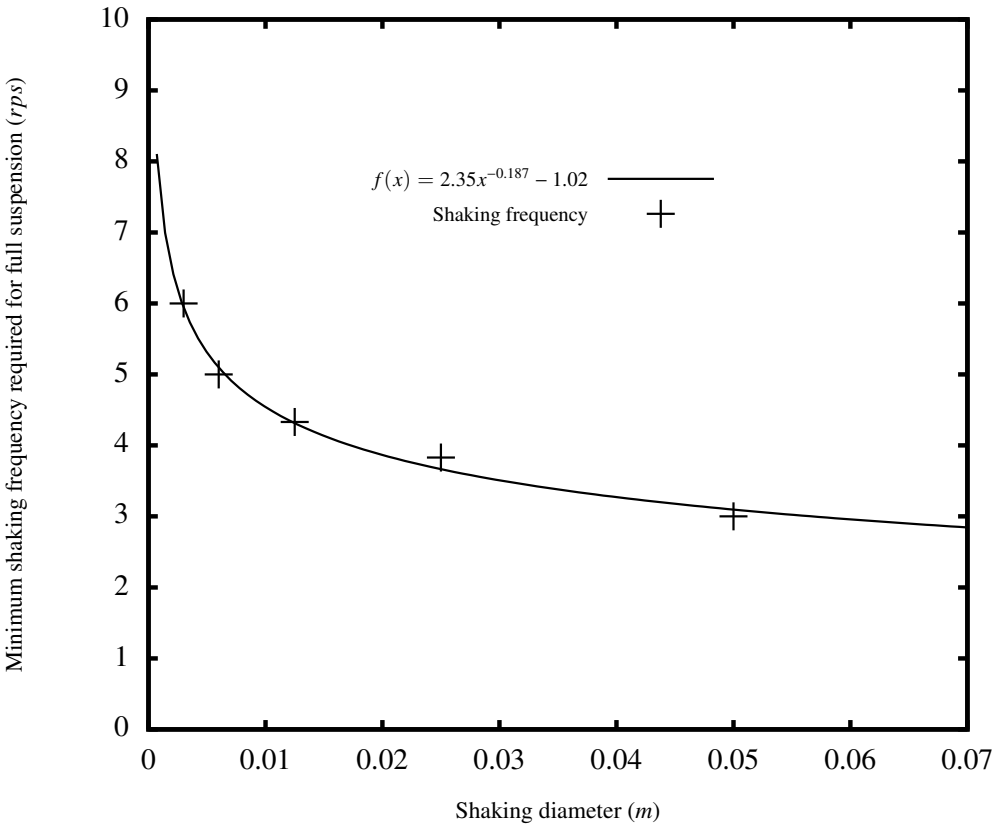

Figure B.4: Typical example of variation in shaking frequency with respect to shaking diameter, d_s. b is calculated by averaging the exponent of x across all experiments. Experiments performed as described in Section 2.6.1. Operating conditions: XAD-16, $d_w/h_L = 2.06$ and $S_f = 2.5\%$ v/v.

Appendix C

HPLC Calibration Curve

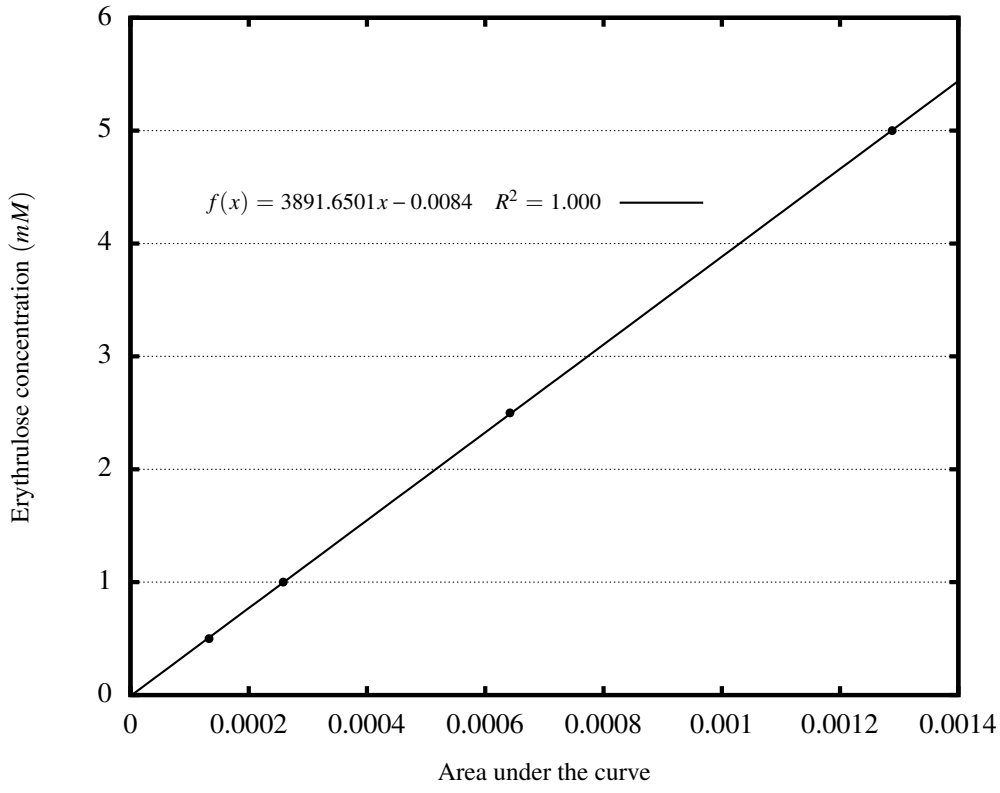

Figure C.1: HPLC calibration curve used in HPLC analysis throughout this thesis.